LOW CYCLE FATIGUE UNDER MULTIAXIAL STRESS CONDITIONS FROM STRUCTURAL ASPECTS

A thesis in

Architectural Engineering

by

Koji Mizuhata

Submitted for the degree of

Doctor of Engineering

March, 1969

ACKNOWLEDGEMENTS

The author is deeply indebted to Professor Takuji Kobori at Kyoto University for his continuing guidance and encouragement. Also, the author wishes to express his sincere gratitude to the late Professor Dr. Joseph Marin, Former Head of Engineering Mechanics Department at the Pennsylvania State University, and Professor Dr. Kiyoshi Ban, Former Dean of the Faculty of Engineering at Kobe University, and Professor Dr. Yoshihisa Gyoten and other colleagues at Kobe University for their giving the opportunity to perform this investigation.

TABLE OF CONTENTS

LIST OF TABLES

LIST OF FIGURES

Page

LIST OF PHOTOGRAPHS

LIST OF SYMBOLS

$A=\frac{\Delta\gamma_{xy}}{\Delta\varepsilon_x}$: Ratio between uniaxial and shear strains

C, C': Material constants

C_t, C_s, C_{oct}: Material constants for tension, shear, and octahedral shear, respectively

D: Die Set Movement

D_m: Damage by mean strain

D_r: Damage by alternating strain

dn: Fractional number of cycles at a certain strain level

$d\varepsilon_{eq}$: Incremental equivalent strain amplitude

E: Young's modulus

$f(\varepsilon_{eq})$: Probability density function of ε_{eq}

G: Shear modulus

h: Thickness of a specimen

$k=\frac{N_1}{N_0}$: Ratio between the number of peak values and the number of mean crossings

k_t, k_s, k_{oct}: Strength coefficients for tension, shear, and octahedral shear, respectively

L: Gage length

M_t: Twisting moment

M_u: Ultimate twisting moment

M_y: Yield twisting moment

N: Number of cycles to fracture

N_i: Number of cycles to fracture at a certain strain level, i

N_t: Total number of cycles to fracture

N_o: Number of mean crossings per second

N_1: Number of peak values per second

n_i: Number of cycles at a certain strain level, i

n_t, n_s, n_{oct}: Strain-hardening exponents for tension, shear and octahedral shear, respectively

R_L: Ratio of minimum strain to maximum strain

r: Radius of the thin-walled cylinder

S: Variable

s_1, s_2, s_3: Parameters

t: Time

t': Time when the stress or strain range is maximum

V_i: Input voltage

V_0: Output voltage

W: Total strain hysteresis energy

w: Width

α, α': Material constants

α_t, α_s, α_{oct}: Material constants for tension, shear, and octahedral shear, respectively

γ: Shear strain

γ_f: Fracture shear strain

γ_{oct}: Octahedral shear strain

$\gamma_{oct,f}$: Fracture octahedral shear strain

γ_{xy}, γ_{yz}, γ_{xz}: Shear strains on planes perpendicular to the x, y, and z axes and parallel to the y, z, and x axes, respectively

ΔD: Range of die set movement

ΔL: Elongation

Δp: Peak value minus mean value

$\Delta\gamma \max|_{1/4\sim 3/4}$: Shear strain range for the first cycle

$\Delta\gamma_{oct}$: Octahedral shear strain range

$\Delta\gamma_p$: Plastic shear strain range

$\Delta\gamma_{xy}$: Shear strain range

$\Delta\delta$: True axial strain range

$\Delta\varepsilon$ max: Maximum principal strain range

$\Delta\varepsilon_p$: Plastic axial strain range

$\Delta\varepsilon_{pe}|_{1/4\sim3/4}$: Equivalent plastic strain range for the first cycle

$\Delta\varepsilon_x$: Conventional axial strain range

$\Delta\theta$: Twisting angle range

$\Delta\sigma_x$: Conventional axial stress range

$\Delta\sigma'_x$: True axial stress range

$\Delta\tau_{oct}$: Octahedral shear stress range

$\Delta\tau_{xy}$: Shear stress range

δ: True axial strain

δ_f: Fracture true axial strain

ε: Conventional strain

ε_e: Elastic strain

ε_{eq}: Equivalent strain

ε_{eqf}: Fracture equivalent strain

$\varepsilon_{eq.}$ max: Maximum equivalent strain

$\varepsilon_{eq.}$ min: Minimum equivalent strain

ε_f: Fracture conventional strain

ε_1, ε_2, ε_3: Principal strains

ε_{1f}, ε_{2f}, ε_{3f}: Fracture principal strains

ε_p: Plastic axial strain

ε_{tl}: Total strain

ε_x, ε_y, ε_z: Normal strains in x, y, and z directions

θ: Angle of twist

θ_f: Fracture angle of twist

ν: Poisson's ratio

σ: Conventional stress

σ': True stress

σ_e: Elastic limit stress

σ_1, σ_2, σ_3: Principal stresses

σ_u: Ultimate stress

σ_x, σ_y, σ_z: Normal stresses in x, y, and z directions, respectively

σ_y: Yield stress

τ: Shear stress

τ_{oct}: Octahedral shear stress

τ_u: Ultimate shear stress

τ_{xy}, τ_{yz}, τ_{xz}: Shear stresses on planes perpendicular to the x, y and z axes and parallel to the y, z, and x axes, respectively

τ_y: Yield shear stress

Φ: Power spectral density

ϕ: Phase difference between axial and torsional loads

φ: Phase difference between input and output voltages

$\Psi=\varepsilon_2/\varepsilon_1$: Ratio of principal stresses

ω: Circular frequency of cyclic load

CHAPTER I INTRODUCTION

§1.1 General Statement of the Problem

Low cycle fatigue is defined to be the fatigue in which the number of cycles to fracture is from 1/4 to 10000, and discriminated from the high cycle fatigue in which the number of cycles to fracture is more than 10^4.

The fatigue problem, as a part of mechanics, originated in 19th century. Until about 1950, however, it was mainly concerned to obtain the endurance limit and stress was a criterion. Recently, atomic piles and aircrafts have become to be used in high temperature and the thermal fatigue problem has been highlighted and followed by the low cycle fatigue problem because of analytical similarity. In the thermal fatigue problem, elongation and contraction caused by temperature change is constrained and the fluctuating stress appears. Therefore, strain becomes meaningful as a variable. Also, in low cycle fatigue, since materials go beyond the yield point and get into the plastic region, it may be more appropriate to control strain instead of stress.

In the high cycle fatigue problem, materials remain in the elastic range where there is no difference between stress control and strain control because the stress-strain relation is linear.

In the case of building structures, members often break due to comparatively few cycles of large fluctuating load, when dynamic loads, such as earthquakes and typhoons, are applied. Hence, the low cycle fatigue problem has been notified. In members of a space frame with unbalanced mass and stiffness, combined axial and torsional cyclic load may be often applied.

The fatigue problem may be treated in the following stages according to the scale of models:

(1) Atomic Scale

(2) Crystallographic Scale

(3) Strength of Material Scale

(4) Structural Member

(5) Assembled Structural Model or Full Scale Model

Although the studies on fatigue have done in all the above stages, it is not possible to explain completely the behavior in one stage from those in other stages. In this study, the stage (3) has been considered.

Fatigue problems are divided into the uniaxial and the multiaxial ones according to the directions of stresses or strains applied on the specimen. In the case of the stress control test, it is easy to discriminate these two conditions, while in the case of the strain control test, it is not, because, even for the uniaxial load, lateral expansion or contraction exists. Hence, in the case of the strain control test, also, the uniaxial and the multiaxial conditions are disciminated according to the state that load is applied in the uni-direction or the multi-direction.

In this study, the biaxial low cycle fatigue where the combined axial and torsional deformations are applied synchronously and nonsychronously on the thin-walled cylinder made of aluminum alloy 7075-T6 is dealt with theoretically and experimentally. This material belongs to semi-ductile materials.

In the experiment, a testing machine utilizing the electro hydraulic servo-mechanism has been constructed and used. Hydraulic pressure is controlled by the electric input signal. The axial force is generated by a linear actuator and the torsional force by a rotary actuator.

Experimental results have been compared with the results in the previous studies.

§1.2 Scope of the Thesis

In CHAPTER I, the introductory comment is given

In CHAPTER II, the studies on low cycle fatigue are reviewed.

In CHAPTER III, construction, adjustment, and calibration of the testing machine are described and, also, the plan and the method of the experiment are explained.

In CHAPTER IV, the experimental results in CHAPTER III are analyzed and compared with the results in the previous studies and discussed.

In CHAPTER V, it is stated how to correlate the low cycle fatigue problem with the dynamic behavior of building structures due to earthquake.

In CHAPTER VI, the summary and conclusions of this study are written and further studies in the future are suggested.

CHAPTER II REVIEW OF THE STUDIES ON LOW CYCLE FATIGUE

§2.1 Introduction

The fatigue problem has been being treated in the elastic range since long time ago. Resently, it becomes necessary to know the behavior of material in the plastic range subjected to large stresses or strains because severe conditions are applied due to recent technological development. The terminology "Low Cycle Fatigue" was first used in Ref.[1]. In low cycle fatigue, both the stress and the strain control tests are possible if material breaks in the small number of cycles to fracture. Actually, in early ages of low cycle fatigue studies cyclic loads were applied as on pressure vessel steel. On the other hand, as stated in CHAPTER I, thermal fatigue was treated as the strain controlled fatigue and furthermore, in the plastic range, strain can be controlled easilier than stress. In addition, material behaviors are more stable during strain cycling than during stress cycling [9]. For these reasons, the strain controlled test are usually used in the low cycle fatigue studies.

Manson [2] first proposed the following relationship in the uniaxial test;

$$\Delta\varepsilon_p N^{\alpha}=C \tag{2.1}$$

where $\Delta\varepsilon_p$ is the plastic strain range, N the number of cycles to fracture, and α and C constants. Coffin [3] found the value of α to be 1/2.

After that, many numbers of experiments have been conducted and various kinds of formulas and methods of analysis have been proposed by many investigators. However, these have been done mainly for the uniaxial case and there are few studies for the multiaxial case. These low cycle fatigue studies have already been reviewed by some investigators, [4],[5],[6],[7],[8],[9],[10], so that in this chapter, mainly the studies on the multiaxial low cycle fatigue problems are explained briefly in the following few sections.

§2.2 Problems in the Field of Low Cycle Fatigue

The previous studies on low cycle fatigue are classified as follows:

(1) Damages by Sequential Loading

(2) Effect of Mean Stress and Strain

(3) Effect of Multiaxial Stress Condtions

(4) Effects of Temperature and Cyclic Loading Rate

(5) Change of Mechanical Properties during Cycling

(6) Effect of Stress Concentration

(7) Other Problems

1. Relationship between Themal Fatigue and Low Cycle Fatigue

2. Relationship between Creep and Low Cycle Fatigue at High Temperature

3. Effect of Circumstances of Test

4. Size Effect

5. Effect of the Pattern of Input Signal

In the following, the above effects are briefly explained in relation to the studies in this thesis.

(1) Sequential Loading and Damage Theory

This is the case where in the whole cycles the strain level is changed. In this case, regarding the problem whether the linear hypothesis is available when the ratio of maxiamum strain to minimum strain and the order of load application are changed, Gross and Stout [11], Low [12], Gucer [13], Kikukawa [14], Ohji,Miller,and Marin[15], Baldwin et.al. [16], Takenaka [17], D'Amato [18], Manson [8], etc. conducted the experiments and obtained

$$\frac{n_i}{N_i} = 0.6 \sim 1.99 \qquad (2.2)$$

where n_i is the number of cycles on a certain strain level and N_i the number of cycles to fracture on that strain level. Although there is no definite conclusion about the above problem, the linear damage hypothesis, i.e., $\frac{n_i}{N_i} = 1$, is considered reasonable. In this study, since the strain amplitude is constant during cycling, this effect is not relevant to this study.

As to the microscopic consideration of damage, Wood et al. [19], Forsythe [20], Laird and Smith [21,22], Avery and Backofen [23], Grosscreuz [24], Dolan and Sinclair [25], Yokobori [26], Thompson [27], Martin [28], Raymond and Coffin [29] published the papers. In this study, however, damage is considered from the macroscopic point of view.

There are some discussion whether energy or strain is chosen as the measure of damage. In the region where the stress-strain curve are steady, only strain can be a measure, because stress is determined by strain. Furthermore, since stress varies less than strain, it is enough to consider strain only.

Minor's hypotheses [30] and Martin's hypotheses [31] belong to the energy-type theory while Yao and Munse's [32], Ohji-Miller's [15], Halford-Morrow's [33], Weiss' [34], and Manson's [8] hypotheses belong to the strain-type theory. In this study, strain is chosen as a measure except in the nonsynchronous case, where the energy is also considered. Recently, Ohji discussed various damage theories in low cycle fatigue [35].

(2) Effect of Mean Stress and Strain

Although the case of zero mean strain is treated in this study, only the results of some studies on the effect of mean stress and strain [15],[18],[32],[36],[37],[38],[39],[40],[41],[42], are explained briefly. The effect of mean strain is large only in the range where the number of cycles to fracture is less than 10^2. This may depend on how many percent of total damage is suffered in the first 1/4 cycle. Damage after the hystereses loop begins is independent of the amount of the mean stress and strain. This fact can be mathematically explained by the damage theory described in the above references.

In high temperature, the effect of mean strain is magnified because the creep phenomenon increases.

Shiratori studied the low cycle fatigue with the mean stress. [43]

(3) Effect of Multiaxial Stress Condition.

This is explained in the next section.

(4) Effects of Temperature and Cyclic Loading Rate.

These two effects are related to each other. The temperature effect were studied by Gross and Stout [11], Baldwin et al. [16], Sachs et al. [38], Johanson [44], Swindemann and Douglas [45], Forrest and Armstrong [46], Tavernelli and Coffin [47]. As the results, so far as there is no structural change inside material, the temperature effect on the relationship between the plastic strain range and the number of cycles to fracture is very small in the case of strain cycling.

The effect of cycling rate were studied byForrest and Tapsell [48], Nishihara et al. [49], Taira and Koterazawa [50], Taira [51,52], Smith et al. [53], Gohn and Ellis [54], Echel [55], Crum and D'Appolonia [56], Gross and Stout [11], Illg [57], Swindemann and Douglas [45], Swindemann [58], and Forrest and Armstrong [46]. As the results, so far as there is no metallurgical change, the effect of cyclic rate on the relationship between the strain range and the number of cycles to fracture is not serious. However, when cyclic rate is extremely large, the number of cycles to fracture increases slightly. There are few information on these effects in low cycle fatigue.

(5) Change of Mechanical Properties during Cycling

This effect is for the purpose not only to know the meterial behavior but also to apply to the design by expecting the results of the stress controlled test from that of the strain controlled test.

The nature that the stress range increases (decreases) during cycling in the strain controlled test is called "Strain Hardening (Softening)". While in the stress controlled test, the strain range increases or decreases. Softening or hardening depends on kinds of material, treatments (cold work or anneal), test methods (mean strain), etc.. There are some materials whose stress-strain curves become stable during cycling after certain numbers of cycle. By noting this nature of material, the results of the stress controlled test can be expected from those of the strain controlled test. However, the theory is not completed yet on this problem. The following studies deal with this problem. The change of the mechanical properties has been studied by Pian and D'Amato [36], Benham and Ford [59], Benham [60], Kawamoto and Tanaka [61], Kawamoto et. al. [62],[63], etc.. The correlation between the stress controlled and the strain controlled tests have been studied by Marin, Ohji, Miller [15] and Yao and Munse [32].

(6) Effect of Stress Concentration

Geometrical discontinuities and notches often causes fracture even in low cycle fatigue. Some effort has been made in correlating low cycle fatigue data obtained from unnotched specimen with notched low cycle fatigue strength [36],[37],[57],[64],[65]. It is difficult to measure stresses and strains in the root of notches. Some engineering type information on this subject is available in the literature. [11],[66], [77].

(7) Other Important Areas

There are studies on the correlation between the thermal fatigue and the low cycle fatigue, on the correlation between the dynamic creep and the low cycle fatigue, on the difference between the low cycle fatigue in the air and that in the vacuum condition, and on the relationship between full size structures and experimental models.

The effect of the pattern of the input signal is not so much studied in low cycle range.

§2.3 Basic Consideration about Multiaxiality of Strains under Biaxial Stress Conditions

As stated in CHAPTER I, both "Multiaxial Strain Condition" and "Multiaxial Stress Condition" mean the same condition, that the multiaxial stresses are applied. According to Ohji [10], in the study on low cycle fatigue under biaxial stress conditions, it is not necessary to study for all the domain on ε_1-ε_2 plane, but to study for the limited domain, only, for the following reasons: In the case of complete reversal strain cycling of isotropic material, each component of the principal strains changes its sign after a half cycle. Therefore, the sign does not matter, but the ratios of $\varepsilon_1:\varepsilon_2:\varepsilon_3$ does. Hence, the strain conditions expressed in the first and third quardrants and those in the second and fourth quardrants are the same, respectively. Thus, it is possible to consider the strain condition problems in the first and fourth quadrants only.

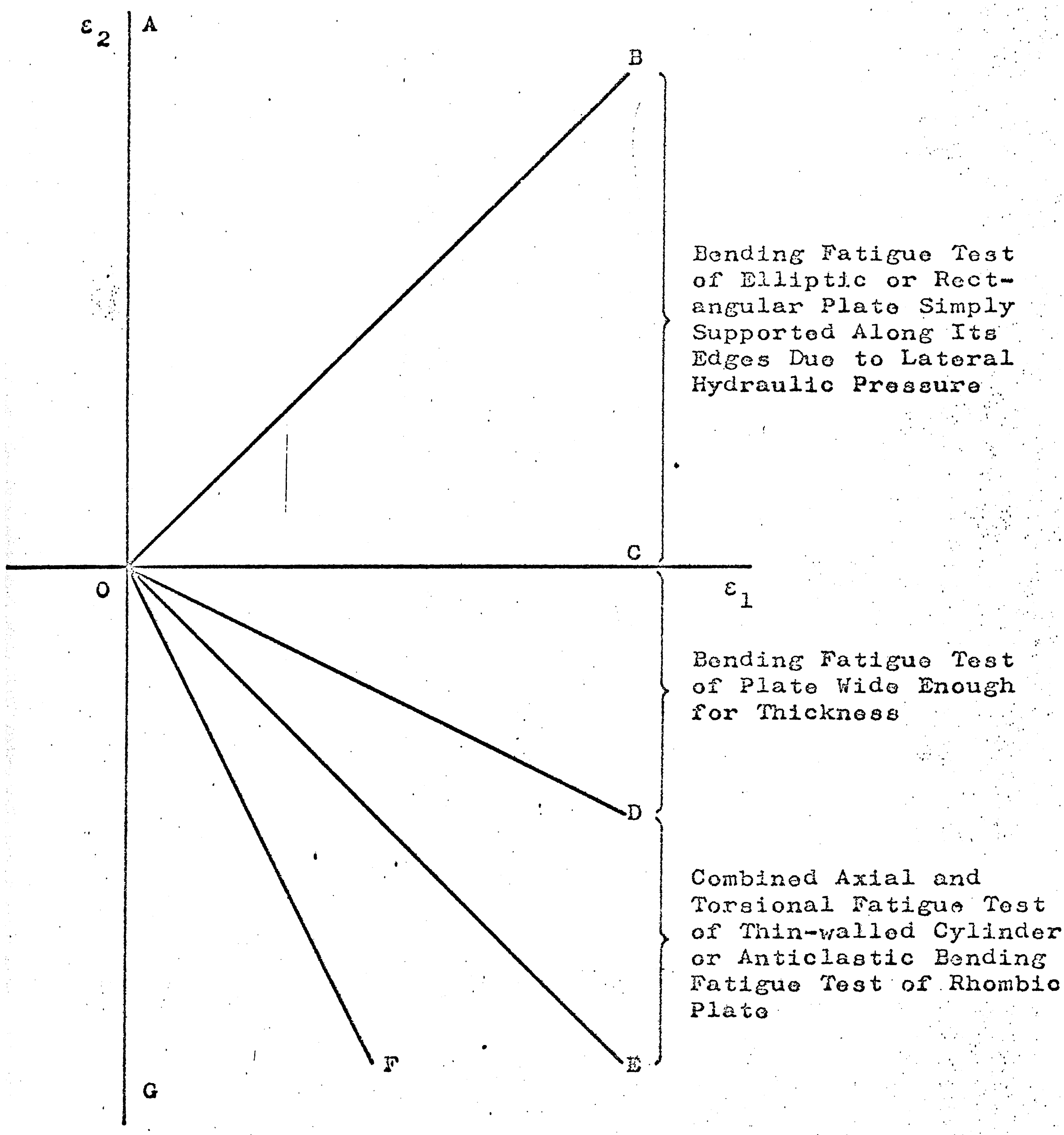

Fig. 2.1 Multiaxial Strain State under Biaxial Stress Condition.

Further, since, for the biaxial stress condition,

$$\varepsilon_1:\varepsilon_2:\varepsilon_3=1:\frac{\varepsilon_2}{\varepsilon_1}:-\frac{\nu}{1-\nu}\left(1+\frac{\varepsilon_2}{\varepsilon_1}\right) \tag{2.3}$$

ε_3 is not changed by exchanging ε_1 and ε_2. Thus, as shown in Fig. 2.1, denoting the lines deviding the first and fourth quardrants into two equal domains by OB and OE, respectively, one understands that domains AOB is equivalent to BOC and COE to EOG.

In addition, if incompressibility, that is, $\varepsilon_1+\varepsilon_2+\varepsilon_3= 0$ or $\varepsilon_3=-(\varepsilon_1+\varepsilon_2)$, is assumed, directions of principal stresses are irrelevant. That is, even if two arbitrary principal strains among ε_1, ε_2, and ε_3, are exchanged each other, strain conditions are unchanged. This means that a certain strain condition in the first quardrant corresponds to two strain conditions in the fourth quadrant.

Consequently, in the case that the condition of incompressibility (ν=0.5) is applied, one has only to test for the strain conditions in one arbitrary domain among those in six domains devided by the lines OB, OD, OE, and OF and the coordinate axes.

§2.4 Review of Previous Studies on Low Cycle Fatigue under Multiaxial Strain Conditions

Previous studies on low cycle fatigue under multiaxial strain conditions are classified as follows by the experimental method:

(1) Torsion fatigue test or combined axial and torsional fatigue test. [17],[62],[63],[78]~[83]

(2) Method to produce the biaxial stress condition near the center on the surface of a bending plate wide enough for thickness. [11],[38],[39],[41],[66],[68],[84]

(2) Method to produce the biaxial stress conditions near the center on the surface of a circular, oval or rectangular plate simply

supproted along its edge bent by lateral hydraulic pressure. [69]~[72],[85],[86]

(4) Method to produce the biaxial stress conditions on the whole suface of a rhombic plate bent anticlastically by two pairs of concentrated load at its opposite corners. [9],[87]

(5) Method to apply the axial load and the internal pressure on the thin-walled cylindrical specimen. [88],[89]

(6) Others. [90],[91]

Strain conditions for the above mentioned experiments are shown in Fig. 2.1. In the following, the previous studies by each experimental method are reviewed from the macroscopic or phenomenological point of view.

(1) Torsion Fatigue Test or Combined Axial and Torsional Fatigue Test.

Benham [78] conducted the torsion strain cycling test by using hollow specimens of both cold-worked and annealed copper and compared those results with his previous results [60] by the uniaxial test with the same material. He obtained the linear relationship between the plastic shear strain range vs. the number of cycles to failure on the log-log paper in the range of 10 to 1000000 cycles. In the uniaxial test, discrepancy between cold worked and annealed is small, while in the torsional test, the annealed specimen is five times as strong as the cold worked specimen regarding strain range. For the cold worked specimen, the results of the uniaxial and the torsional tests show good agreement if the equivalent plastic strain based on the octahedral shear strain theory was used. For the annealed specimen, torsion can take bigger strain range than tension-compression for the same life.

Takenaka [17] considered torsion strain cycling in a study of commulative damage of mild steel. However, only three tests were done with very high strain ranges, the total number of cycles being less than 47 cycles.

Halford and Morrow [33] made the torsion strain cycling test by using hollow specimens of SAE 4340 and Brass 60-40 and solid circular bars of Al 7075-T6 and Al 1100-0 and plotted the results on the log-log paper taking the plastic shear strain along the vertical axis and the number of cycles to failure along the horizontal axis. The data drop on straight lines with the solpes of -0.60, -0.52, -0.58 and -0.58. Later Ohji compared [9] some of these results with the results of the tension compression fatigue tests by Manson and Hirschberg [92] based on the octahedral shear theory and found that material for trosion is several times as weak as for tension-compression. Discrepancies may be because of difference in defining failure. Definite conclusions must be postponed until more test results are accummulated.

Kawamoto et al. [62],[63] also conducted the uniaxial strain cycling test and the torsion cycling test by using hollow specimens of Ni-Cr-Mo steel and obtained the results of good agreement for both test.

Kusumoto and Takeuchi [74] conducted the uniaxial and the torsion strain cycling tests and compared both the results by using the equivalent strain based on the octahedral shear strain theory and the maximum shear strain theory. As the results, agreement between the uniaxial and the torsion tests was found to be excellent for both theories. Also, they obtained the following relationships:

$$N^{\alpha}\Delta\varepsilon_{pe}\big|_{1/4\sim 3/4} = C, \qquad N^{\alpha'}\Delta\gamma_{max}\big|_{1/4\sim 3/4} = C'$$

where α=0.64, C=0.66, α'=0.60, C'=1.21 for SS41 and

α=0.63, C=0.65, α'=0.59, C'=1.21 for SUS27.

As shown in the above equations, the equivalent plastic strain range $\Delta\varepsilon_{pe}$ for the first cycle was used as a parameter, and failure was defined to be initiation of visible crack and reducing process of the load or torque on the recording paper.

The same researchers [80] compared the results of both uniaxial and torsional tests using Cr-Mo-V steel in high temperature(570°C) and found good agreement between the uniaxial and the torsional results.

Yokobori, Yamauchi, and Yamamoto [81] conducted the tension-compression and the torsion strain cycling test, by using thin-walled cyclindrical specimens of 0.1% carbon steel. During both tests, the amplitudes of deformation between the grips of the specimen were kept constant and then from this deformation strain was calculated with the calibration curve. Both results were compared by using the equivalent plastic strain range based on the octahedral shear theory and it was found that material for torsion is twice as strong as for tension-compression.

Ohji [82] has been being developing both the axial and the torsional strain cycling tests by using two kinds of carbon steel, aluminum, aluminum alloy, and copper specimens. Among them, the axial and the torsional results for 7075-T6 Al alloy show good agreement by using the equivalent strain range.

Taira [83] conducted the combined uniaxial and torsional strain cycling tests in high temperature of 450°C by using 0.16% carbon steel. In the tests, the total strain range was controlled and the results were analysed by means of the total equivalent strain range. The strain ratio A of the shear strain range $\Delta\gamma$ to the uniaxial strain range $\Delta\varepsilon$ was chosen to be 0, 1.46, 4.59, and infinity. Although scatter of data was not so small and there were few data for the same condition, an almost straight line was obtained by using the equivalent strain range based on the octahedral shear theory.

More lately, Taira et al. [115] carried out combined uniaxial and torsional low cycle fatigue tests with phase difference and compared those results with their own results in the same phase and the uniaxial tests.

They obtained the following conclusions: The strength of material subjected to multiaxial stress cycling with and without the rotation of principal axes can be predicted from the data of uniaxial low cycle fatigue if the equivalent strain range based on the octahedral shear theory is employed. When the equivalent strain varies in a complex manner during one cycle, it is better to use the effective mean strain range in which the damage in the material and the strain history are considered.

Consequently it is concluded that only one straight line to show relationship between the equivalent strain range based on the octahedral shear theory and the number of cycles to failure is obtained for both the uniaxial and the torsional fatigue tests.

(2) Bending Test of Wide Plate.

In the case of simply supported beams, as the width to thickness ratio increases, the stress conditions near the center on the surface varies from uniaxial to biaxial, that is the stress ratio approaches to 2:1 for ν=0.5. This ratio of 2:1 is equal to that of the membrane stresses in the circular and axial directions of thin-walled cylinder applied by internal pressure. Therefore, in order to obtain this stress condtion of pressure vessels, Gross and Stout [11],[66],[68] at Lehigh University proposed the bending test of wide plate. In

Japan, recently, Nakazawa and Kiso [84] used this test. However, because their interest was in the research on the pressure vessel, they did not study the effect of multiaxial stress conditions by changing the width-thickness ratio but studied the effects of loading rate, temperature, notch etc. by using one kind of specimens with sufficiently large width-thickness ratio. Stout et al. [11], [66],[67],[68], used the wide plate of A-201 steel and 90-B steel with the ratio of 1:5 and obtained the linear relationship $\Delta\varepsilon_p N^{\alpha}=C$ for the range of N=1000~100000.

Kiso also obtained the linear relatioship of α=0.70, C=1.56 by using the wide plate with the ratio of 30/4.

Sachs et al. [38],[39], and Weiss, Sessler, and Packman [41] at Syracuse University conducted the bending fatigue test of wide plate of A-302 B steel, 5454-0 Al, and 2024-T4 Al with various width-thickness ratios. The experimental data were plotted to show the relationship between the axial strain range and the number of cycles to failure, taking the width-thickness ratio as a parameter. This means that they took the maximum principal strain theory. As a result, strength decreased a little as the ratio increased. The ratio w/h was taken from 2 to 8.

Ohji [9] retreated the above results for 2024-T4 Al by using the equivalent strain range based on the octahedral shear theory and showed that all the data dropped along a straight line on log-log paper.

Miller [93] compared Sessler-Weiss' [40] uniaxial loading data for A-302 steel with Sachs et al.'s bending data [38] for the same A302 steel based on the octahedral shear theory and obtained good agreement although the overall range was small.

(3) Bending Test of Simply Supported Circular, Oval, or Rectangular Plate Subjected to Hydraulic Pressure.

Blaser et al.[69] developed a method of testing simulating the state of stress encountered in pressure vessels. In this testing machine a rectangular plate specimen of 10 in x 17 in x 3/4 in in size simply supported on the edges was uniformly loaded on one side by means of oil pressure in a periodic pulsating manner. Therefore, this cycling was rather loading cycling. An experimental stress analysis of the plate specimen and a preliminary test for detecting of fracture initiation were made and a relatively large area with a stress ratio of about two was found to exist in the center portion of the plate specimen.

Bowman and Dolan [70],[71],[72] used the same type of fixture as Blaser et at. in conducting the biaxial fatigue tests of pressure vessel steels at the stress ratio of 2:1. The plate specimens were subjected to pressure cycles of zero to maximum for about 100 cpm. In these experiments the magnitude of the maximum pressure was kept constant during each test. That is, the tests were conducted under load cycling condition at a stress ratio R_L=min. stress/max. stress of zero within a cycle range from 4000 to 100000 cycles. In these experiments, the failure was defined as cracks with length of 3/16 in. They plotted their experimental results in terms of the strain range for the steady state versus the number of cycles to failure on the log-log paper and obtained a linear relationship.

Ives [85] improved Bowman's method [70],[71],[72], and conducted complete reversal strain cycling tests with circular plate specimens under alternating oil pressure from both sides. The circular plate has the diameter of 16 in. and thickness of 11/16 in. and was simply supported along its edge. A circumferencial to radial strain ratio of unity is theoretically produced at the center of the plate specimen. Constant deflection tests were conducted on A-201, A-302 and T-1 pressure vessel steels in a failure cycle range from 100 to 100000. Fracture was defined to be the first crack detected by a break down of strain gages bonded on the specimen. The results of this investigation were compared with the data obtained at Lehigh University [73] on the basis of an equivalent strain determined by the octahedral shear strain theory with the assumption of volume constancy. Agreement between tests and theories was very good for A-201 and A-302 steels, but only fair for a T-1 steel.

Ohji and Shewchuck further improved [86] Ives' method [85] and used oval plate in addition to circular plates to generate various strain ratios. He conducted the deflection controlled test with circular, and oval plates of 7075-T6 Al alloy and compared those results with his results by cantilever plate bending of the same meterial in terms of the equivalent total strain range based on the octahedral shear strain theory assuming incompressibility. Agreement was excellent. The failure was defined by complete fracture near the center of the specimen. The range covered less than 2000 cycles. This results were also plotted in Fig. 4.11 for comparison with the results in this study and Goto's study. [87]

(4) Anticlastic Bending of Rhombic Plate

Ohji [10] invented a new method of the biaxial fatigue test by the use of rhombic plate specimens under two pairs of concentrated loads of opposite directions at two pairs of opposite corners. Goto [87] conducted the fatigue experiments based on the above-mentioned idea by changing the ratio of long and short diagonal lengths as 3" x3", 2"x2.5", 2"x3" with 7075-T6 Al alloy. In addition to anticlastic bending of rhombic specimens, he made bending tests of cantilever specimens and compared all the results based on the octahedral shear strain theory, maximum principal strain theory and the maximum shear strain theory, assuming incompressibility. As a conclusion, he obtained the best agreement by means of the octahedral shear strain theory. The cyclic range covered less than 2000 cycles. The definition of failure was initiation of visible hair crack. The results also plotted in Fig.4.11 for comparison with the results in this study and Shewchuk's study [86]. Agreement was fair.

(5) Combined Axial Load and Internal Pressure Cycling of Thin-walled Cylinder.

Kyriakakis [88] conducted biaxial fatigue tests on aluminum alloy 2024-T351 in a cyclic range between 10^4 and 10^5 cycles, using hollow cylindridal specimens subjected to combined internal pressure and axial compressive load. A linear relationship with a slope of about 0.5 between the octahedral plastic strain range versus the number of cycles to failure on the log-log coordinates was obtained.

Mullin [89] also conducted biaxial load tests using cylindrical hollow specimens of the same 2024-T351 alluminum alloy subjected to combined axial compressive load and internal pressure cycling. Again the tests were partly load cycling tests at a load ratio $R_L=0$, although the strain ranges in the axial and the tangential directions were controlled and kept constant during the tests. In the experiments the phase difference between the axial compression and internal pressure was changed as $\phi=0°$, 90°, and 180°. The range of cyclic life in these experiments was between 45 and 10^4 cycles, being mostly higher than 10^3 cycles. In this case, it appears that an appreciable magnitude of mean strain was produced at high strain ranges. This is one of the characteristic features in the low cycle fatigue under the one sided stress reversal, and it occurs when increase of mean stress associated with stress cycling is large. The results were later compared by Miller [93] with the axial strain cycling data with zero mean strain using the octadedral shear strain ranges as a basis of comparison. For cyclic lives less than 1000 cycles, poor agreement was obtained between theory and experiments. However, fair agreement was observed in low strain ranges.

(6) Others

The following other testing method of low cycle fatigue under the muliaxial stress conditions were proposed.

(a) To generate biaxial stress conditions by using perpendicularly crossing plate specimens. [90]

(b) To produce triaxial stress conditions by applying the tensile load on a special specimen. [91]

§2.5 Problems in Low Cycle Fatigue under Multiaxial Stress Conditions

So far, the previous studies on low cycle fatigue under multiaxial stress conditions were reviewed from the experimental method's point of view. In the following, studies on some problems in low cycle fatigue under multiaxial strain conditions are reviewed.

(1) Effect of Poisson's Ratio

In §2.3, biaxial strain states under cyclic load were considered on $\varepsilon_1 \sim \varepsilon_2$ plane. Further Ohji [10], Goto [87], and Shewchuk [86] took into account the effect of Poisson's ratio on the strain state. In the case of the intermediate cycle fatigue, the elastic strain is too large to neglect compared with the plastic strain. This means that the Poisson's ratio varies from the elastic value to 0.5 for the plastic range. In the intermediate range, the relationship between the total strain range vs. the number of cycles to failure becomes a little concave. Ohji [10] and Goto [87] drew the curve between $|\varepsilon_{eq}/\varepsilon_1|$ or $|\varepsilon_{eq}/\varepsilon_3|$ vs. $\psi=\varepsilon_2/\varepsilon_1$ taking ν as a parameter based on both the octahedral shear theory and the maximum shear strain theory.

(2) Effect of Phase Difference

The following series of studies on the effect of phase difference were done at the Pennsylvania State University.

Mullin [89] conducted the combined axial compression and internal pressure fatigue test on the thin-walled cylindrical specimen of 2024-T351 Al alloy. Although this test was a cycling loading test, amplitude of the load was controlled so as to maintain the strain ranges of axial and circular directions constant in recording them by means of strain gages. The phase difference between the axial compression and the internal pressure were changes as 0°, 90°, and 180°. The experimental results were plotted on the diagram between the equivalent total strain range for the varying component based on the octahedral shear strain theory vs. the number of cycles to failure ranging from 45 to 10^4 mostly higher than 10^3. The results for the combined tests were compared with his results for the uniaxial test. Agreement was good near the cycle range of 10^4, but discrepancy was very large for short cycles less than 1000. This is one of the characteristics of the low cycle fatigue under one sided reversal of stress, where the mean strain associated with the stress cycling increases.

In Mullin's test [92], the principal strain axes do not rotate. On the other hand, Miller [96] developed a modified octahedral shear strain theory in which restrictions for mean strain and rotation of the principal strain axes were eliminated. The main assumptions in Miller's theory are

1 The maximum low cycle fatigue damage leading to failure is on the

plane, for which the octahedral shear strain becomes maximum during the cycle.

2 The shear strain component in the direction of the maximum octahedral shear strain on the maximum octahedral shear plane in 1 determines the degree of damage. By considering the variation of the shear strain component during a cycle, the strain range and mean shear strain components can be determined for each cycle. These strain values were used in Miller's theory for predicting multiaxial low cycle fatigue life for the most general case.

Miller's theory reduces to the octahedral shear strain theory when the principal strain axes do not ratate and the principal strains are synchronous (in phase or 180° out of phase) at zero mean strains.

In Miller's theory, only shear strain component in the direction of the maximum octahedral shear strain was considered. However, there is likely some effect on failure produced by the shear strain component in the direction perpendicular to the maximum octahedral shear strain. This effect was taken into account in a modified octahedral shear strain theory developed by Pontzer [97]. He used Miller's first assumption but modified the second assumption as follows:

2' A variable which determines the magnitude of incremental damage on the above critical plane is the summed-up component of instaneous increment of shear strain on the maximum octahedral shear strain plane.

Both Miller's theory and Pontzer's theory have not been verified by experiments yet.

More recently, Taira et al. [115] conducted the combined uniaxial and torsional low cycle fatigue tests with phase difference in high temperature of 450°C by using 0.16 % carbon steel. The phase differences of 90° was selected. The results were compared with their results in the same phase and the uniaxial low cycle fatigue test. They obtained the following conclusions: The strength of meterial subjected to multiaxial strain cycling with and without the rotation of principal axes can be predicted practically from the data of uniaxial low cycle fatigue data by using the equivalent strain range based on the octahedral shear strain theory. When the equivalent strain varies in a complex manner during one cycle, it is better to use the effective mean strain range in which the damage in the material and the strain history are considered.

(3) Effect of Mean Strain

As mentioned in §2.2, there are many studies on the effect of mean strain under the uniaxial stress condition. In the case of the multiaxial stress conditions, Miller and Ohji [9] proposed that the theory of the effect of mean strain under the uniaxial stress condition can be applied to that under the multiaxial stress conditions, if the equivalent strain based on the octahedral shear strain theory is employed. The experimental varification has not been made yet.

(4) Comparison between the Load Controlled Test and the Deflection Controlled Test.

As mentioned in the preceding section, in the load controlled test like as the combined axial compression and internal pressure fatigue test, [89] accumulation of mean strain associated with load cycling is large. Then, Ohji [10] showed that life for load cycling with mean stress under the multiaxial stress condition can be estimated from the results of the complete reversal strain cycling. General comparison between the load controlled test and the deflection controlled test was already explained in §2.2.

(5) Thermal Fatigue

The thermal fatigue problem under the multiaxial strain conditions can not be explained unless correlation between thermal fatigue and low cycle fatigue under the uniaxial condition. Fortunately, this correlation was clearified already in Refs. [9],[95]. Based on this fact, Taira, Ohnami, and Inoue [96],[97] calculated numerically the thermal total strain caused by temperature change on the cyclindrical and spherical model of infinite length and, attempted to predict the results of thermal fatigue under the multiaxial stress conditions from the results of thermal fatigue and low cycle fatigue in high temperature under the uniaxial stress condition by means of the octahedral shear strain theory with 0.16 % carbon steel.

(6) Studies Related Directly to the Practical Problems

In the above, the studies on low cycle fatigue in the strength of materials scale were reviewed. While, fatigue of prototypes fabricated with those materials was studied in the fields of aeronautical engineering, ship building and structural engineering. One of the most typical studies was the group study on the pressure vessel by Pressure Vessel Research Committee. This study included the research on specimens [11],[66]~[68],[70]~[73], tests on small models [74],[75] and full size tests..[76],[77] Main interests were in estimation of the working stress of high strength steel for high pressure vessels, the method of forming including welding, the effect of stress concentration on the fined surface, welding bead, manholes and nozzles, etc.. According to the reports by Kooistra et al. [77], the results of model or full size fatigue test agree with those of the uniaxial test if the virtual stress of Langer [98] is used.

Low cycle fatigue studies in the field of structural engineering will be reviewod in CHAPTER V.

(7) Others

As other problems on low cycle fatigue under the multiaxial stress conditions, there are

1 Low cycle fatigue of notched specimens,

2 Low cycle fatigue of rotating discs caused by start and stop, and

3 Fatigue of deforming bellows.

1 The multiaxial stress condition appears at the root of notches even when the uniaxial load is applied. Its behavior during cycling in the plastic region is unknown yet. Manson and Hirschberg [65] conducted the fatigue tests on the round bar specimen which has notches on both sides by controlling the variation of the diameter of the critical cross section, that is, by controlling the mean value of the strain range. They compared its results with those of plain specimens.

2 Hagihara [99] studied experimentally fatigue of rotating discs caused by start and stop and attempted to correlate its results with those of the uniaxial test by using the results of stress analysis and the plastic strain analysis. According to the fact that in the rotating disc, the life varies largely by the small change of the strain range, this test shows the characteristics of load cycling with mean stress. Therefore, if modifying the uniaxial results on account of mean strain, the results of the uniaxial test agreed with those of rotating discs.

3 Hamada and Takezono [100] investigated the fatigue strength of bellows made of SUS 27 in both the elastic and the plastic ranges. They compared these results with those of the uniaxial test based on their own results of the stress analysis [101] and the limit analysis [102] of bellows. Agreement was good. All the results were treated from the stress'point of view. In the low cycle fatigue range, the virtual stress proposed by Langer [98] was used.

CHAPTER III EXPERIMENTAL STUDIES ON COMBINED AXIAL AND TORSIONAL LOW CYCLE FATIGUE

§3.1 Introduction

For the purpose to study experimentally biaxial low cycle fatigue, the following tests were conducted by using the thin-walled cylindrical specimen of aluminum alloy 7075-T6 with the internal diameter of linch, the wall thickness of 0.05 inch, and the gage length of linch.

(1) Tension-compression fatigue test

(2) Torsional fatigue test

(3) Combined axial and torsional fatigue test

  (a) Synchronous combined axial and torsional fatigue test with the strain ratio $A = \Delta\gamma_{xy}/\Delta\varepsilon_x$ of 2.

  (b) Synchronous combined axial and torsional fatigue test with the strain ratios of 3 and 1, and

  (c) Nonsynchronous combined axial and torsional fatigue test with the strain ratio of 2.

In order to perform the above tests, a testing machine utilizing the electrohydraulic servomechanism was constructed in the Fatigue Laboratory at the university.

All the tests were done for the completely reversal strain. In the nonsynchronous test, the phase difference is selected to be 45° and 90°.

The strain range covers from 0.015 in/in to 0.225 in/in for the axial test and from 0.03 in/in to 0.85 in/in for the torsion test. These strain ranges correspond to the number of cycles to fracture of 1/4 to about 2000, which was chosen for the purpose of comparison with the results of other biaxial low cycle fatigue tests with the same material.

Both strain and stress were recorded with time to obtain the hysteretically dissipated energy.

§3.2 Material and Specimen

(1) Description of Material

Aluminum alloy 7075-T6 was used as material in the experiment. This is a kind of semi-ductile material used in aircraft structures.

The chemical composition of this material is as below : [39]

Zn 5.6 %

Mg 2.5 %

Cu 1.6 %

Cr 0.3 %

Al Rest

This material is classified crystallographically into the face centred cubic crystal.

The mechanical properties of this material according to Ref. [103] and the tests in the laboratory [86],[87] are listed in Table 3.1.

The meterial used was supplied by the Alcoa Co. with the shape of seamless pipe with the outer diameter of 1 1/2", the internal diameter of 1", the wall thickness of 1/4", and the length of 3'.

(2) Description of the Specimen

The specimen used in the experiment is drawn in Fig.3.1. The specimen has the total length of 9 1/2", the internal diameter of 1", the gage length of 1", and the wall thickness of 0.05" in the gage length portion. The specimen has the thread and the key-way in both ends to fix specimen to the testing machine.

The shape of the specimen is determined by copying the plastic torsion specimen of Ref. [103] and the ASTM Standards [104], so that there occur neither stress gradient in the thickness direction nor

Table 3.1 Material Constants

	Ref. [103]	Shewchuk[86]	Goto[87]		Author
Elastic Constants, E 10^6psi	10.4	10.3			9
G 10^6psi	3.9				3.6 or 3.4
Poisson's Ratio, ν	0.33	0.32			
Yield Strength, σ_y, ksi	70	69	65.3	61.4	71
Tensile Strength, σ_u, ksi	80	79	85.3	82.9	81.5
Elongation in 2", %	10	8			
Hardness	150				
Melting Point, oF	1035±145				
Ductility, %			13.25	11	12
Strain-hardening Exponent, n					0.11
Strength Coefficient, k, psi					115700
			Parallel to the rolling-direction	Perpendicular to the rolling-direction	

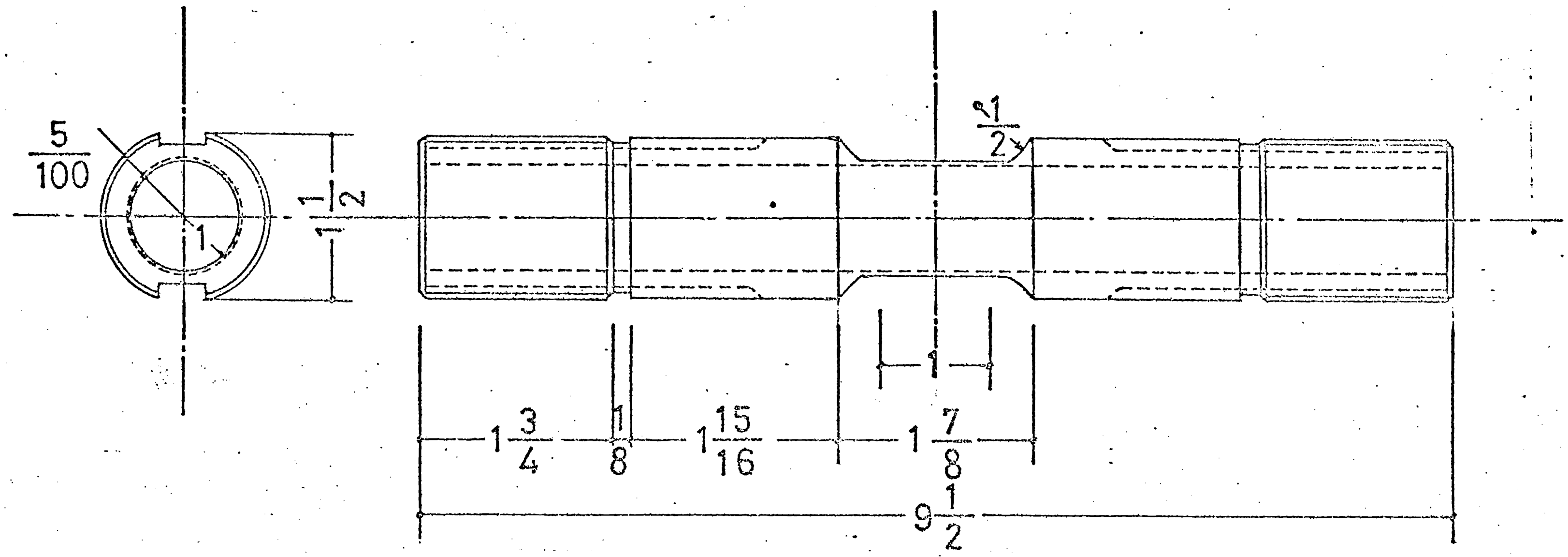

Fig. 3.1 Dimensions of Specimen

static local buckling.

The specimens were cut out of the original seamless pipe in the machine shop in the university.

§3.3 Testing Machine

(1) General Description

A new testing machine has been constructed so as to conduct the combined axial and torsional low cycle fatigue test. This testing machine can give the specimen the tension-compression and the cyclic torsion independently. The servomechanism is utilized in this machine and the hydraulic pressure is given according to the electric input signal. Capacity of this machine is determined by considering those of all machine parts as a whole. As the results, capability is limited by the hydraulic pump which has flow capacity of 15 gallon per minute under the hydraulic pressure of 2000 psi.

The cyclic loading rate depends directly on the input signal motor in which the gain is unity and the phase difference is zero as the results of the system analysis.

The machine consists of the following parts.

(A) Mechainal Part

(B) Electric Part

(C) Hydraulic Part

(D) Recording Part

The mechanical part is the part to set up the specimen at the specified position and to transmit the hydraulic force controlled electrically to the specimen.

The electric part includes two input signal generators, a power supply, and two servocontrollers, etc..

The hydraulic part generates hydraulic pressure and gives this to the mechanical part.

The recording part measures and records stresses and strains on the specimen.

Interrelation among these machine parts is shown in Fig.3.2. A picture of this machine is given in Photo.3.1. This machine consists of two independent channels like as an audiostereo set, so that each channel needs two identical parts besides the common part.

(2) Mechanical Part

The block diagram of the machaincal part is shown in Fig.3.3. This part is the part which gives the specimen independently the tension-compression force and the cyclic torque generated by the actuators and has the following mechanism.

The tension-compression force generated by the linear actuator (A) is isolated and at the same time, held alignment by the thrust bearing housing (D). The cyclic torque generated by the rotary actuator (B) is isolated and at the same time held alignment by the die-set (C). Thus, the actuators can give the specimen the tension-compression force and the cyclic torque independently. The specimen (E) is set up by fixing the nut to the thread of the specimen and putting this in the grip and then tightening the cap (F) against the axial force. Against the torque, the specimen is set up by fixing the nut to the specimen by putting the key to the key-way on both the specimen and the nut and by fitting the notch of the nut to the projection of the grip. Photo.3.2 shows a set of specimen, nut, and keys.

In other to measure the stress on the specimen the load-cell (G) made of leaded steel CL-III is set up between the linear actuator and the grip and the foil strain gages of rosette type with three elements is put on it.

All the mechanical part is designed to resist the maximum

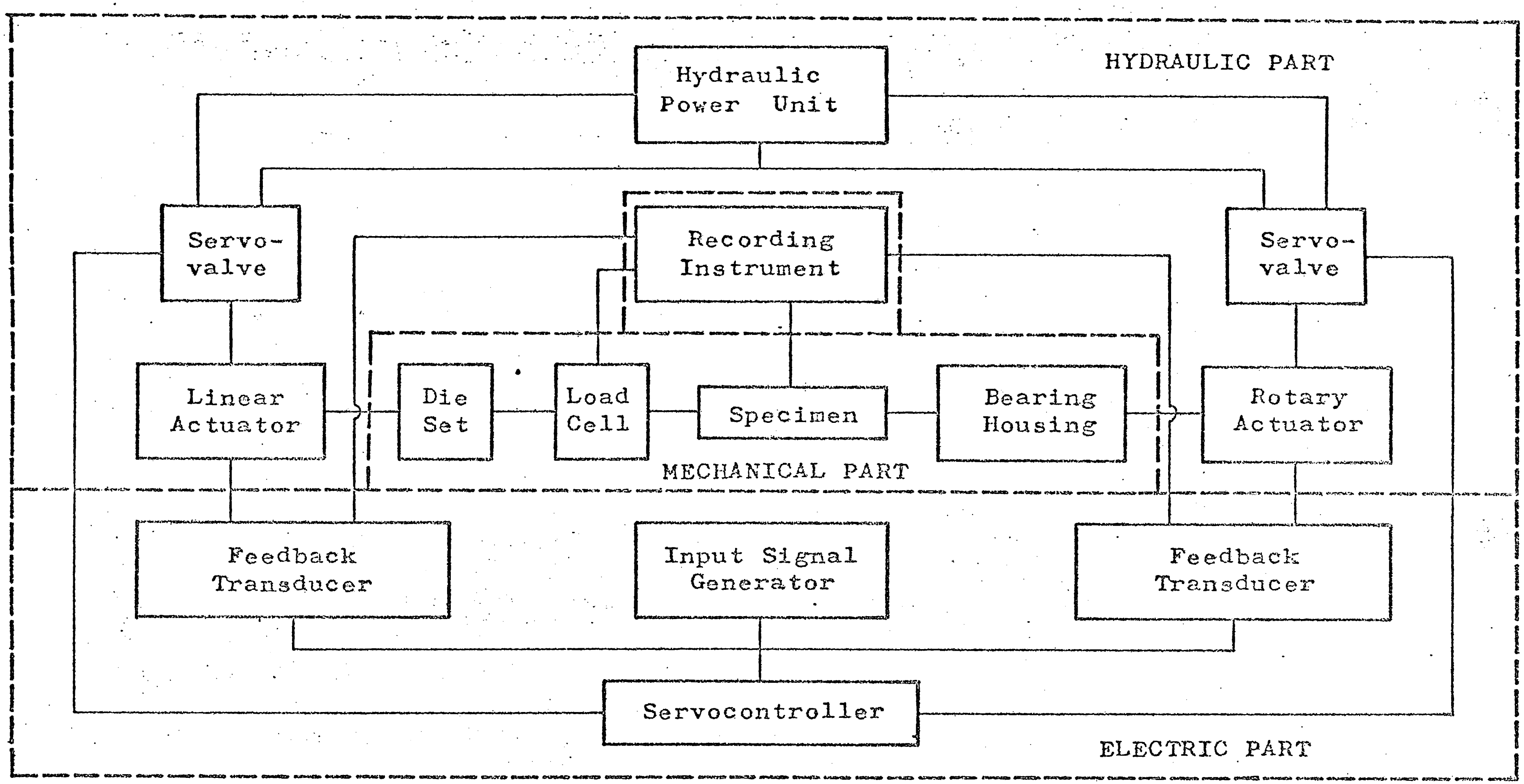

Fig. 3.2 Block Diagram of the Testing Machine.

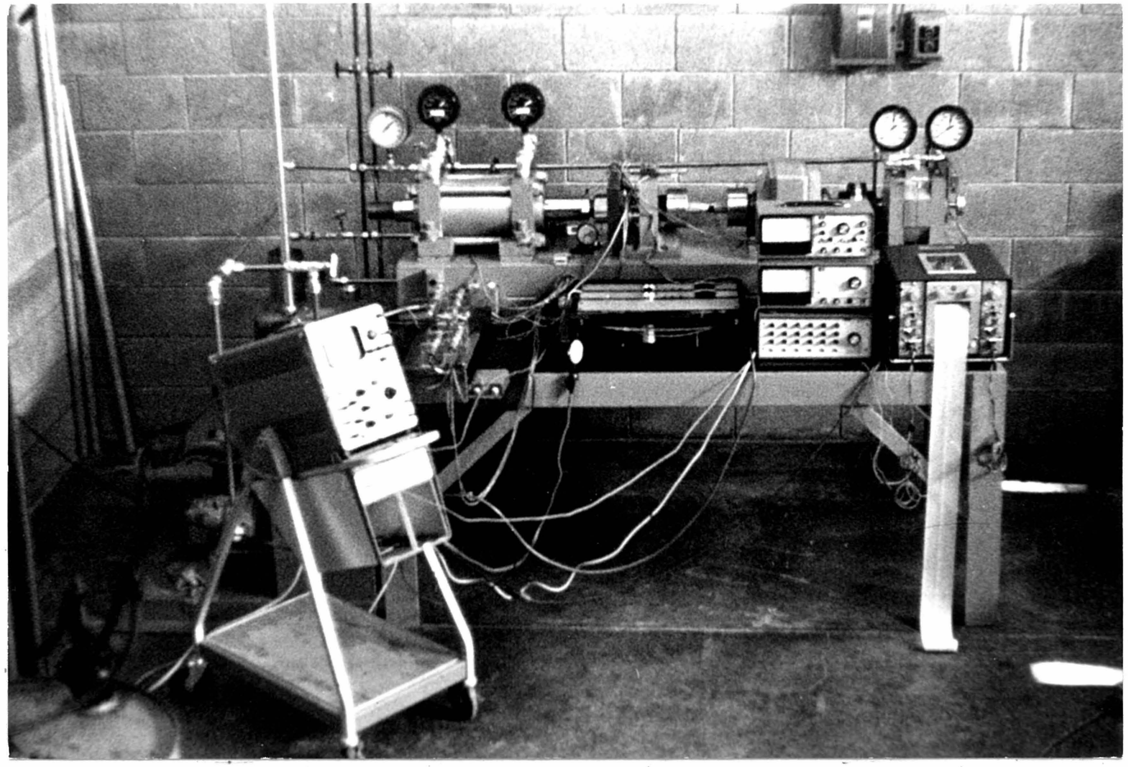

Photo. 3.1 Front View of the Testing Machine

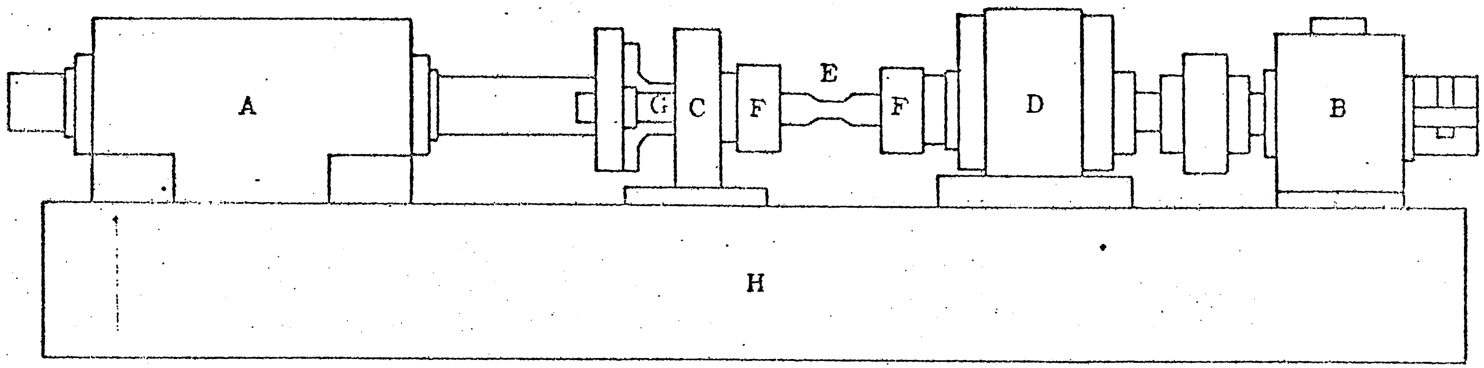

Fig. 3.3 Schematical View of the Mechanical Part.

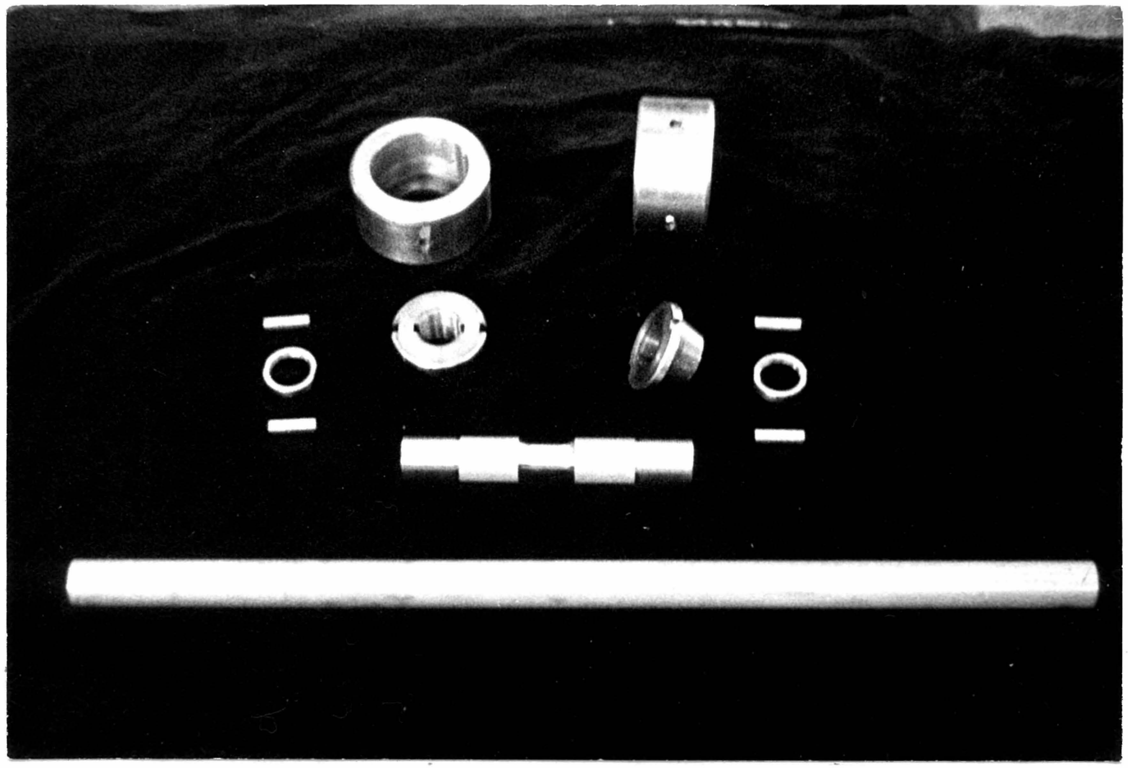

Photo. 3.2 Material, Specimen, and Fittings

strength of the specimen.

These machine parts are fixed on a box beam (H) of 7 ft. in length and 8 x 18 inch in section. Assembling was made in the machine shop at the University.

(3) Electric Part

The block diagram of the electric circuit is shown in Fig.3.4. The electric part consists of input signal transducers, and a feedback transducer (tracer), a servocontroller, and an electric power supply for each of the linear and the rotary channels. These parts make a closed-loop feed-back system. In the servocontroller the a.c. input signal generated by the input transducers is compared with the output of the feed-back transducer which picks up the motion of the actuator as the final response and the error is amplified by an a.c. amplifier and demodulated and again amplified by an d.c. amplifier and then sent to the servovalve as direct current. In the servovalve, the hydraulic pressure given to the actuator is controlled so as to cancel the error and, hence, the output response can follow the input signal accurately with certain frequency characteristics. Really, under the speed of 8 rpm., the output could follow the input signal without phase difference. In the a.c. amplifier the carrier of 400 cps. is used. The electric power pack is the power supply for the servo-controller. The servocontroller and the power pack used in this experiment are made by MOOG Servocontroller Inc..

The device which generates the input signal is shown in Photo.3.3. This device consists of two LVDT's (Linear Variable Differential Transformer) for a micrometer-stand and a common gear motor per channel. One of two LVDT's is for generating the mean strain and the other for the alternating strain. The input signal for mean strain can be

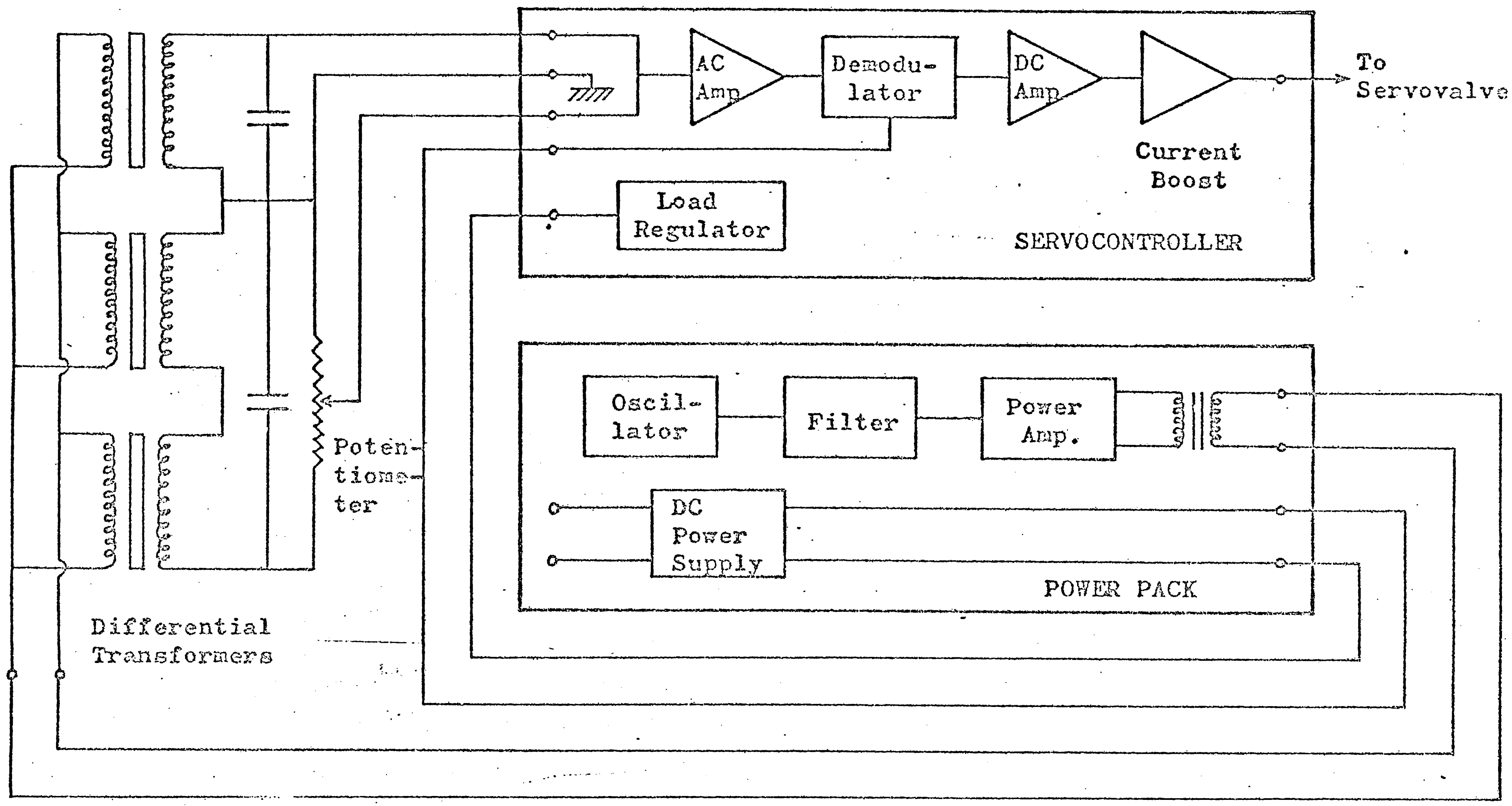

Fig. 3.4 Block Diagram of the Electric Part.

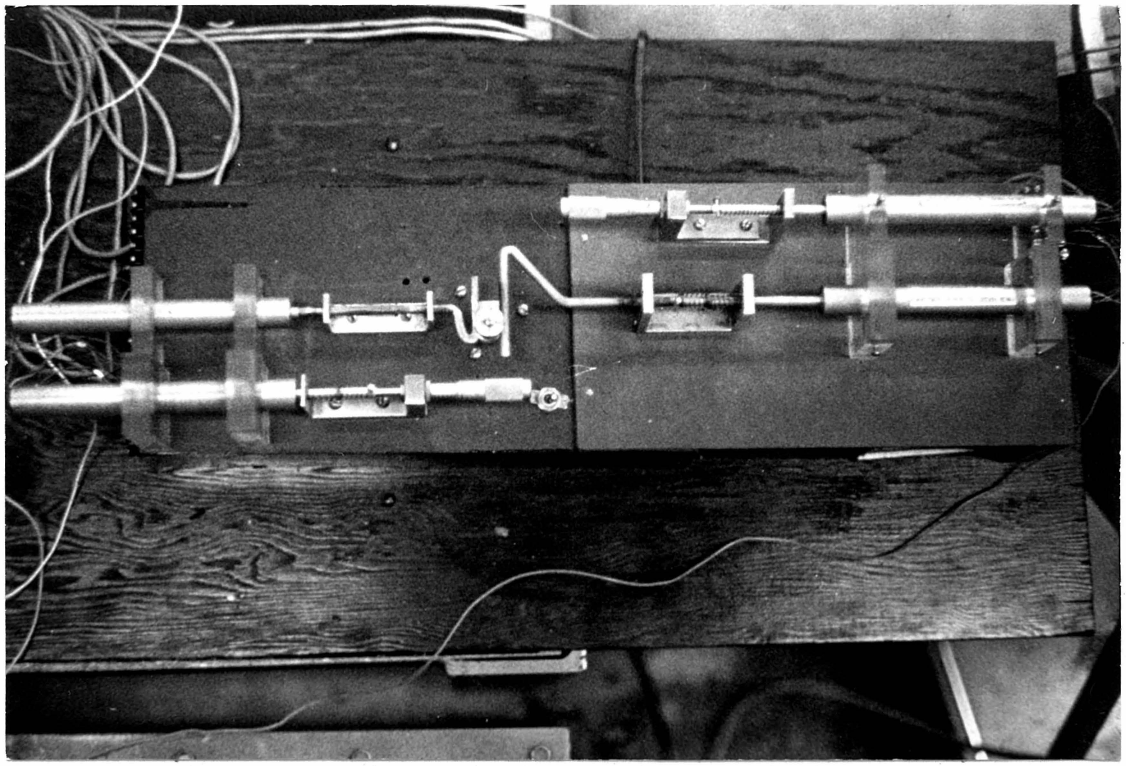

Photo. 3.3 Input Signal Generator for the Synchronous Case

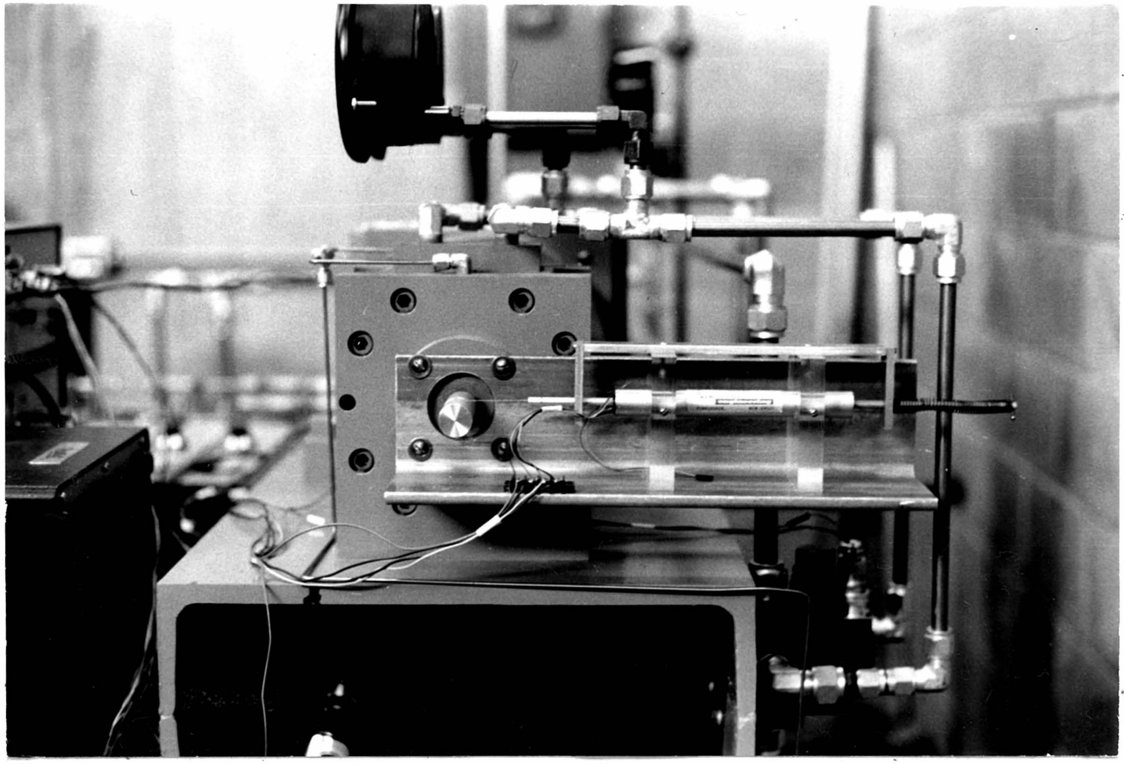

Photo. 3.4 Converter of Rotary Motion to Linear Motion

generated by changing the output voltage of the LVDT by turning the handle of the micrometer-stand. The input signal for the alternating amplitude can be generated by converting the projection of the motion of one end of the crank whose other end is fixed to the axis fo the gear motor of 8 rpm. into electric voltage by using the LVDT. Therefore, this signal is a sinusoidal curve whose frequency is 8/60 cps. The input signal for the mean strain plus the alternating strain can be reduced by turning the potentiometer of 100 turns which is set on the servocontroller. The phase difference between axial and torsional strains can be given by setting up two sets of such input device with various angles. The LVDT used in this machine is the LVDT-1000SSL of Schaevitz Inc., whose travel range is -1"-0-1" and sensitivity is 0.27 mv/0.001"/v.. The primary voltage is 9 v. and is supplied by the power pack. When the input signal is connected in parallel for each channel in order to get rid of higher harmonics of the carrier. The output or feed-back transducer which is the same kind of LVDT as in the input device picks up the motion of the piston whose end is fixed on the die-set for the linear motion, while for the rotary motion the output motion is fed back after converting rotation into linear motion by using the device as shown in Photo.3.4.

(4) Hydraulic Part

The flow diagram of the hydraulic part is shown in Fig.3.5. Since this machine utilizes an electrohydraulic system, the hydraulic part makes a closed loop together with the electric part. Although both parts can not be seperated, the sections are seperated for the convenience of explanation.

Texaco Moter Oil is used for the hydraulic fluid and is reserved in the reservoir of 6 ft^3. The hydraulic fluid should be incompressible. The fluid in the reservoir is circulated by the pump of 15 gallon

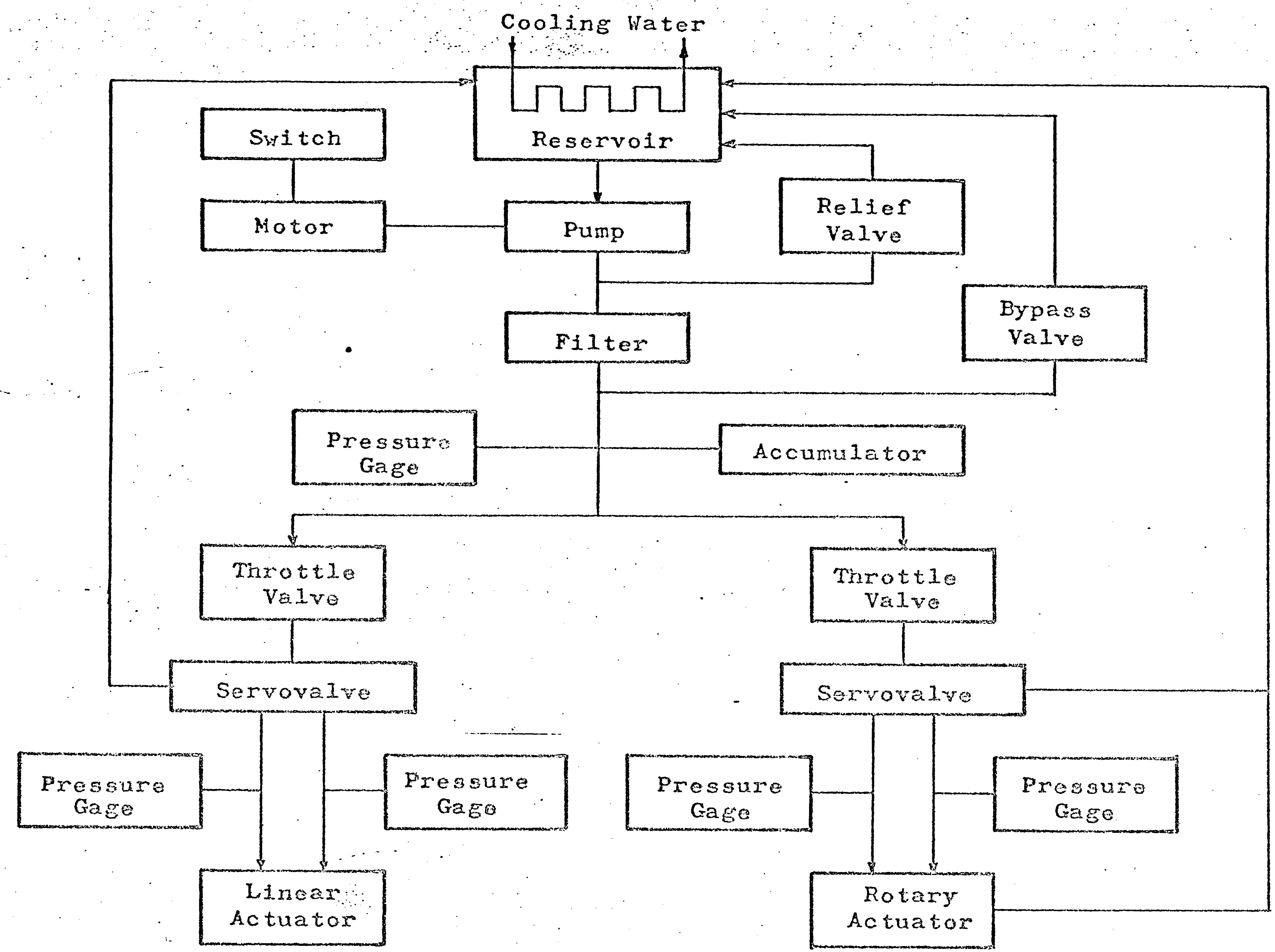

Fig. 3.5 Block Diagram of the Hydraulic Part.

per minute at 2000 psi. driven by an electric motor of three phase a.c. and gives pressure to two servovalves. Flow of the pump is controlled by the flow controller. The excess pressure returns to the reservoir. The fluid pressure controlled by the servocontroller is transmitted to the actuator from the servovalve. The hydraulic cylinder H-42 of Milwaukee Cylinder Co. is used as the linear actuator. The hydraulic cylinder should be of balanced type which has the same pressurized area for both directions since the four-way servovalve is used. The allowable pressure and the pressurized area of the cylinder are 3000 psi. and 31.416 in.^{2}, respectively, the maximum force being 94208lb.. The single vane rotary actuater RN-63-IV of Ex-Cell-O Co. is used for the rotary actuator. The allowable pressure is 1000 psi., the maximum torque being 8700lb. in.. As for the accessaries of the hydraulic system, there are a relief valve, an accumulator, and pressure gages.

The relief valve is a safety valve to keep the supplying pressure of the pump smaller than the allowable pressure of other hydraulic part.

The accumulator is a kind of buffer to reduce the shock of hydraulic pressure. The type NA4-4 of Milwaukee Cylinder Co. is used for an accumulator.

Totally five pressue gages are used in the system ; one of them is to show the supplying pressure and the other four are set up right before four ports of the actuators.

Steam seamless steel tubing of 3/4" and 1/2" in outer diameter of Williams and Company Inc. and steel fittings of F & L Fitting Co. and of Swagelock Co. are used for piping. Tubes and fittings can bear up to 3000 psi..

(5) System Stability

As mentioned before, the cyclic loading rate does not effect on low cycle fatigue in room temperature. However, the tests are preferably performed in the highest cyclic rate that the machine can run in order to save test time. For doing this, the response frequency characteristics of the testing machine is needed.

The testing machine has a natural frequency depending on the characteristics of the sevovalves, the actuators, and oil. The gain, i.e., the ratio of the input amplitude to the output amplitude as well as the phase difference between them are functions of the ratio of the frequency of the input signal to the natural frequency of the system.

The block diagram of the closed loop electrohydraulic servomechanism is shown in Fig.3.6.

The gain V_o/V_i as well as the phase difference φ are given as follows according to the calculations in Refs. [94],[105]
For the linear motion part,

$$\log \left|\frac{V_o}{V_i}\right| = -\frac{1}{2} \log\left[\left(\frac{\omega}{640} - \frac{\omega^3}{1.85 \times 10^8}\right)^2 + \left(1 + \frac{\omega^3}{2.8 \times 10^4}\right)^2\right] \qquad (3.1)$$

$$\varphi = -\tan^{-1} \frac{\frac{\omega}{640} - \frac{\omega^3}{1.85 \times 10^8}}{1 + \frac{\omega^3}{2.8 \times 10^4}} \qquad (3.2)$$

and for the rotary motion part,

$$\log \left|\frac{V_o}{V_i}\right| = -\frac{1}{2} \log\left[\left(1 + \frac{\omega^2}{590}\right)^2 + \left(\frac{\omega}{426}\right)^2\right] \qquad (3.3)$$

$$\varphi = -\tan^{-1} \frac{\left(\frac{\omega}{426}\right)^2}{\left(1 + \frac{\omega^2}{590}\right)^2} \qquad (3.4)$$

where

V_i : input voltage,

V_o : feed-back voltage,

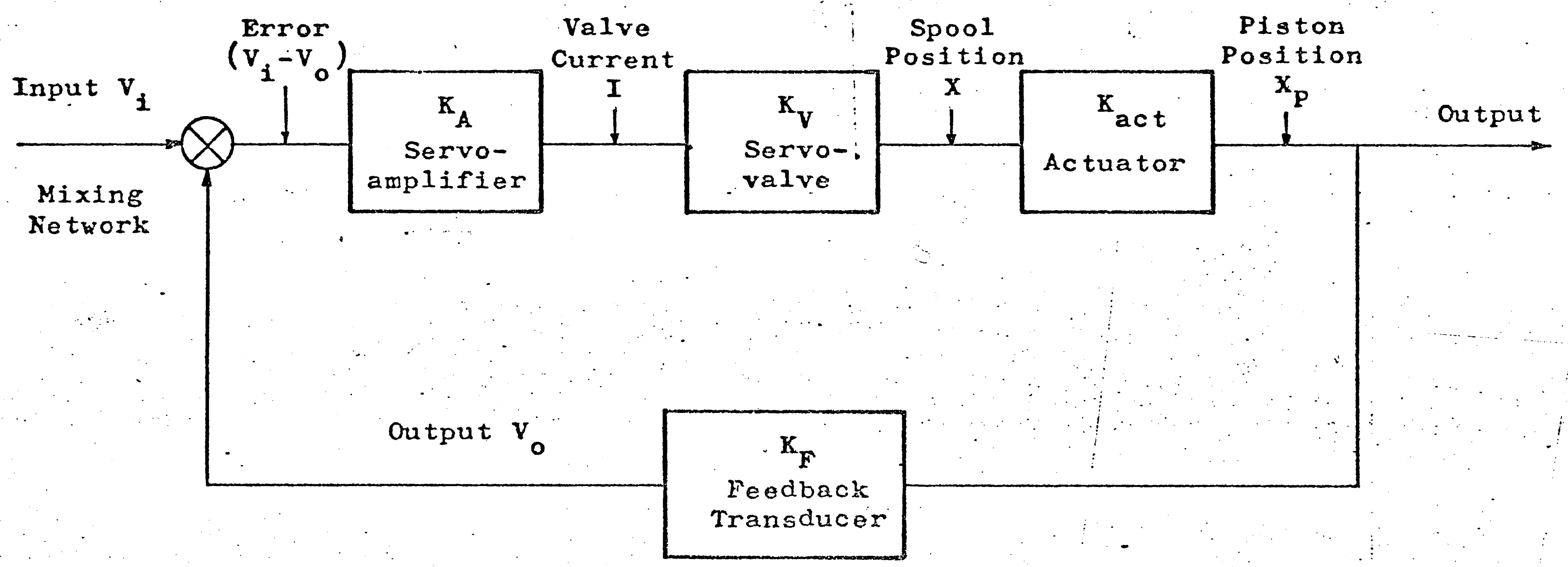

Fig. 3.6 Block Diagram of Electrohydraulic Servomechanism.

φ : phase angle between the input voltage V_i and the feedback voltage V_o, and

ω : circular frequency of the input signal of the testing machine.

For the circular frequency of the input signal $\omega=2\pi$ f=2 x 3.14 x 8/60=0.8 rad/sec, V_o/V_i is in the range of 1 and φ is 0°, hence, the system is stable for the input signal of 8 rpm.

The recording part is explained in the following section.

§3.4 Instrumentation (Recording Part)

In the experiment, the necessary and sufficient outputs for constructing a new theory should be measured. The following outputs may be considered: For axial motion: Pressure, Stress, Deformation, Strain, and for torsion: Pressure, Shearing Stress, Twisting Angle, Shear Strain.

For the purpose of energy consideration, these outputs must be read continuously with time. However, if appropriate calibration tests are done statically for each channel, all the above outputs need not be recorded in the case of cyclic combined test. If the relation between strain and elongation is plotted in the diagram preliminarily, either one of them has only to be recorded continuously with time. Similarly, either of pressure or stress has only to be recorded. In this experiment, as to the information of deformation type for axial motion, the reading of the extensometer equipped for the gage length or the reading of the strain gage put on the specimen was recorded continuously, while for torsion the strain gage reading was recorded. As to the information of force type, both axial and shear stresses were recorded continuously with time by the strain gages put on the load cell.

For the strain criterion, strain has only to be recorded, while for the energy consideration, both stress and strain should be recorded because the energy depends on the stress-strain curve.

In the analysis, the total strain ε_{tl}, was used. However, if the plastic strain ε_p is needed, it can be calculated by using

$$\varepsilon_p=\varepsilon_{tl}-\varepsilon_e=\frac{\Delta L}{L}-\frac{\sigma_e}{E} \qquad (3.5)$$

with the deformation ΔL and the elastic limit σ_e which are measured, where ε_e is the elastic limit strain, L the gage length, and E the Young's Modulus. In this experiment, the outputs were recorded as follows:

(1) Axial Motion

The pressure was recorded by reading the pressure gages equipped right before the ports of the actuator for both tension and compression. The stress was recorded by the pen-recorder as the output of the strain gages put on the load cell parallel to its axis. Since this shows the elastic deformation of the load cell, the stress on the specimen should be recalculated by using the Hooke's low and the condition of continuity between the specimen and the load cell. For the strain gage, the axial direction component of the steel compensated foil gage C6-121-R3A of Budd Company was used. For the strain indicator, 300CF of Daytronic Co. was used. For the pen writing recorder, 250A of Baldwin-Lima-Hamilton Co. was used. This recorder is an inkwriting recorder with two channels and can be used for recording the shear stress or the strain from the extensometer, also.

The deformation was measured by the dial gage fixed on the die set. The dial gage reading shows the deformation of the total length of the specimen plus the backlash of the thread. This quantity can be read out also as the electric voltage by means of the feedback LVDT fixed on the same die-set. The output of the LVDT can be recorded continuously by the cathode-ray oscilloscope with a memory.

The strain for the gage length was measured by both the extensometer attached to the specimen and the strain gage and, at the same time, directly by the telescopic gage and the micrometer. The output of the extensometer was recorded by the pen recorder following Daytromic 300CF Strain Indicater. The extensometer is shown in Fig.3.7.

In the uniaxial test, the relationship between the extensometer reading and the telescopic gage reading was first plotted for the static test and, then, for the cyclic tests the strains were obtained from the continuous reading of the extensometer by using this diagram.

In the combined test, the relationship between the strain range by the strain gage put on the specimen and that by the dial gage was first plotted for the typical test, and then, for other cyclic tests the strain range was obtained from the dial gage by using the diagram. The travel range of the dial gage is 0-1" and the minimum division is 0.001".

For the feed beck LVDT, as well as the input LVDT, Schaevitz LVDT 1000SS-L was used.

For the strain gage put on the specimen, the dynamic post yield strain gage SR-4, PFA-50 of the BLH Co. was used for the uniaxial test and the post yield rosette gage EP-08-250-RA-120 of William T. Bean Co. for the combined test.

For the cathode-ray oscilloscope, TEKTRONIX Type564 oscilloscope, Type3A3 Dual Trace Differential Amplifier, and Type 2B67 Time Base were used. This cathode-ray oscilloscope has the terminal for the external input in the Time Base and can be used as an X-Y recorder

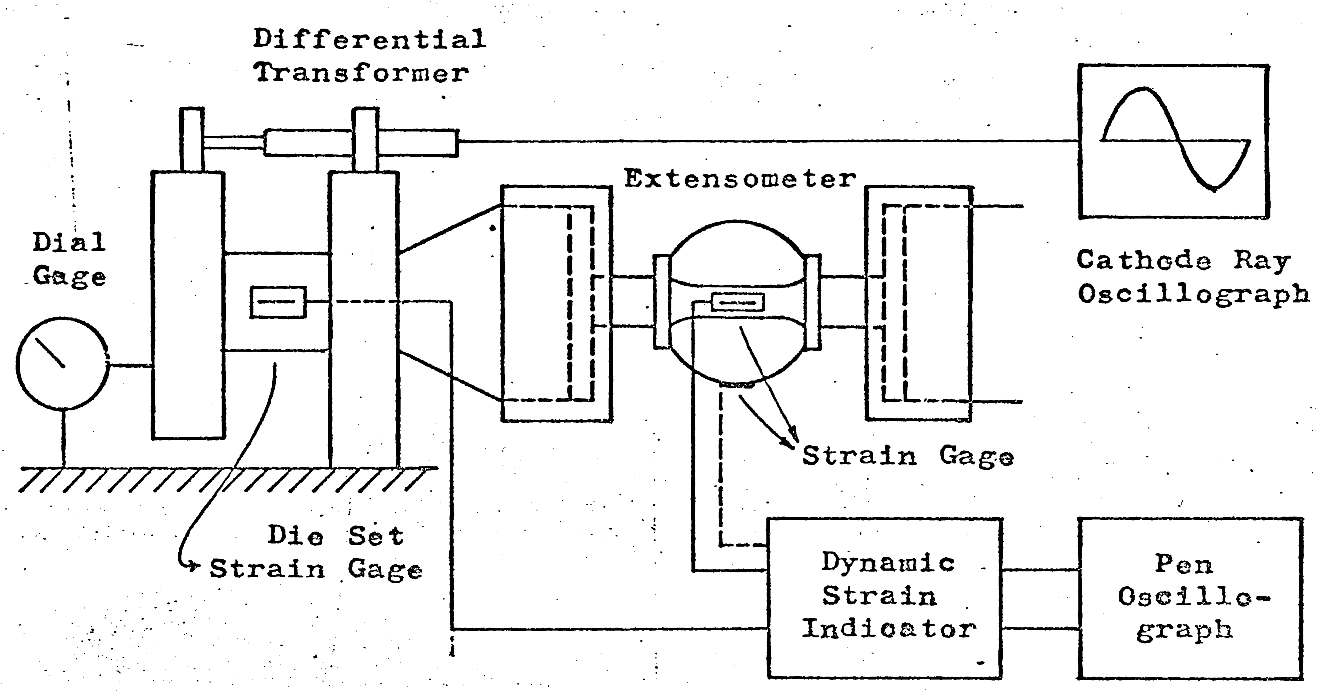

Fig. 3.7 Schematic Arrangement of Measuring System for Axial Motion.

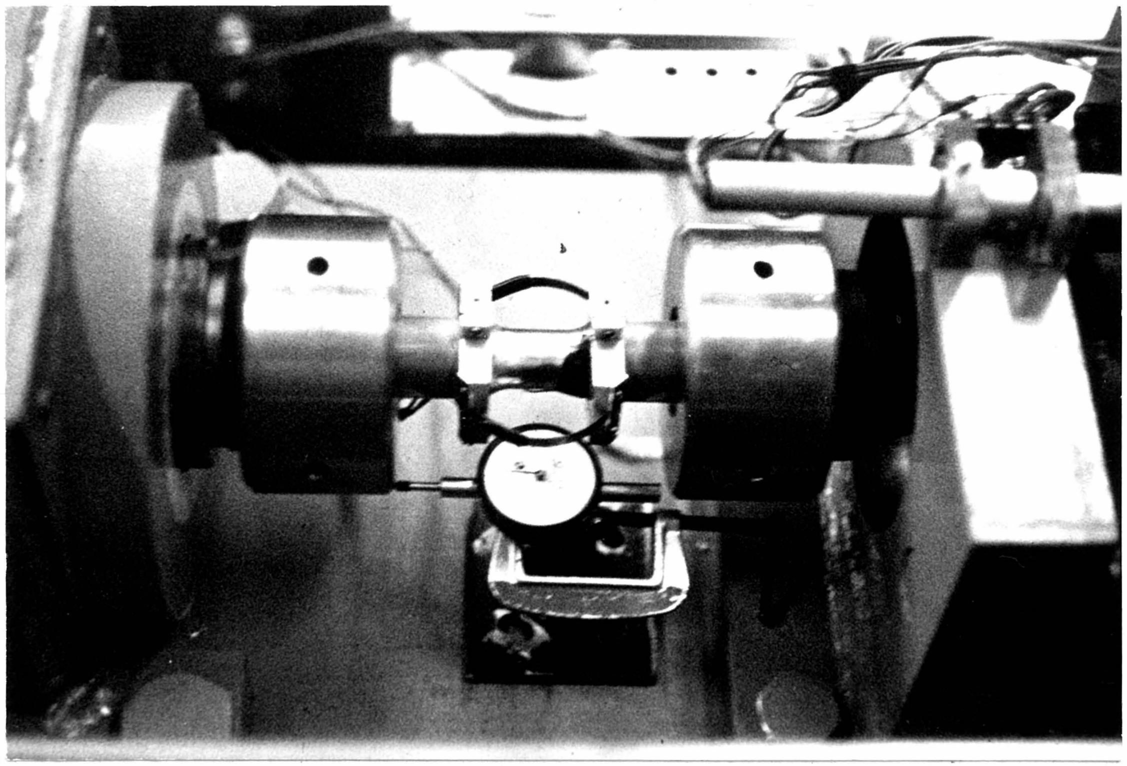

Photo. 3.5 Arrangement of Measuring Systems for a Uniaxial Test

together with the Type3A3. Also, it has the memory which can show the whole process of the test.

The strain indicator and the pen-recorder were used in common for both the stress and the strain recordings. The schematic diagram for recording the axial motion is shown in Fig.3.7.

The picture of the specimen set up with the extensometer is shown in Photo.3.5.

(2) Torsion

The pressure were read out by using the pressure gages right before the ports of the actuator for both the clockwise and the anticlockwise directions.

The shear stress due to torsion was measured by means of the four active gage method [106] by using four strain gages put on the load cell in the direction of 45° from the axis. The lead wires of the strain gages were connected to show the shear stress and led to the strain indicator, the output of which was recorded by the pen writing recorder in the same manner as in the axial case. The same indicator and the pen-recorder as in the axial case were used.

For the strain gage, the orthogonal components of the rosette foil strain gage C6-121-R3A were used. The stress by the strain gage can be compared with that by the pressure gage.

The twisting angles for the gage length and between the grips can be read out by using the protractor installed on the specimen and the angular scale drawn on the wall of the bearing housing, respectively. Also, the rotary motion can be obtained by converting it into linear motion by the device attached to the axis of the rotary actuator shown in Photo.3.4 and then by reading the linear motion through the LVDT. This LVDT is also the feed back transducer for

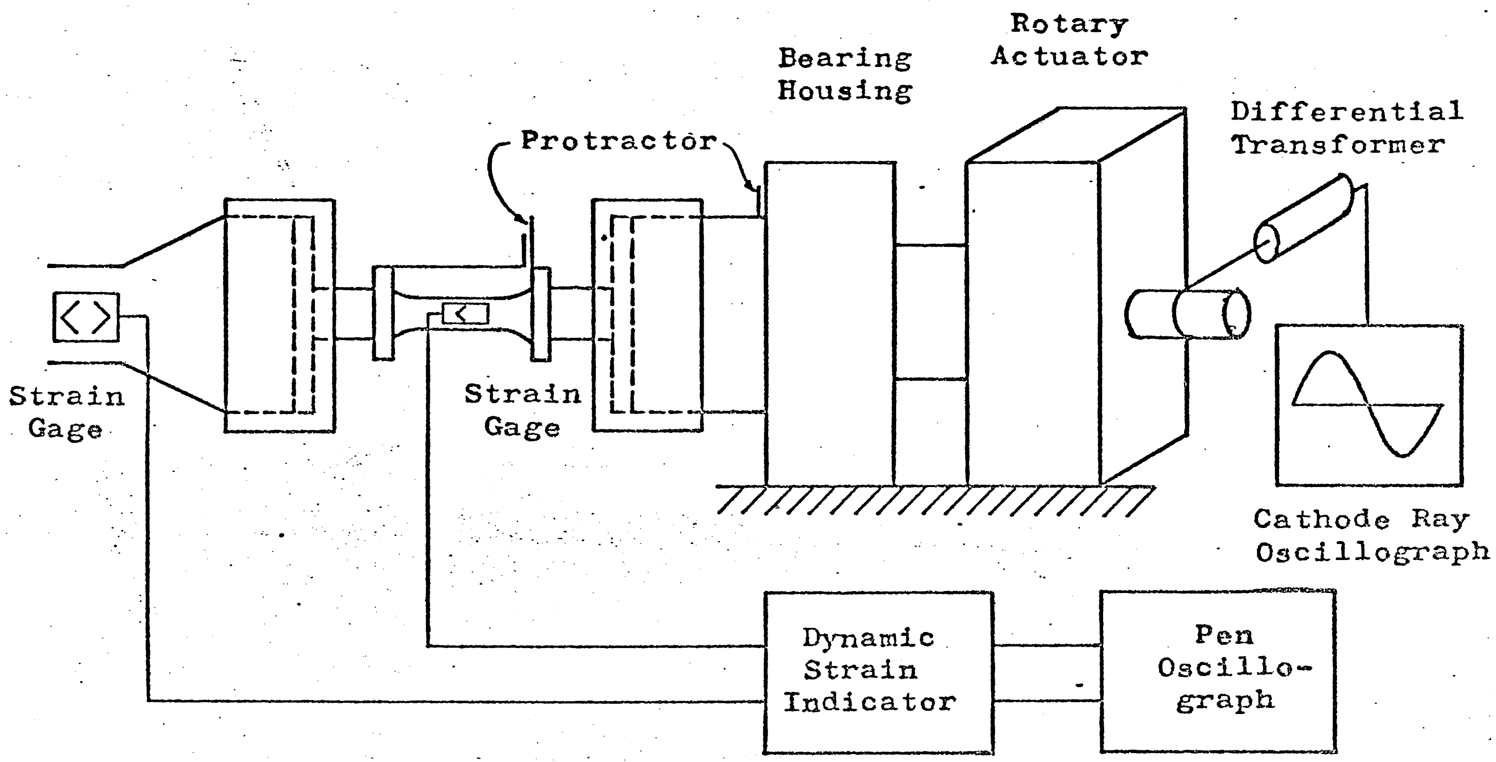

Fig. 3.8 Schematic Arrangement of Measuring System for Torsion.

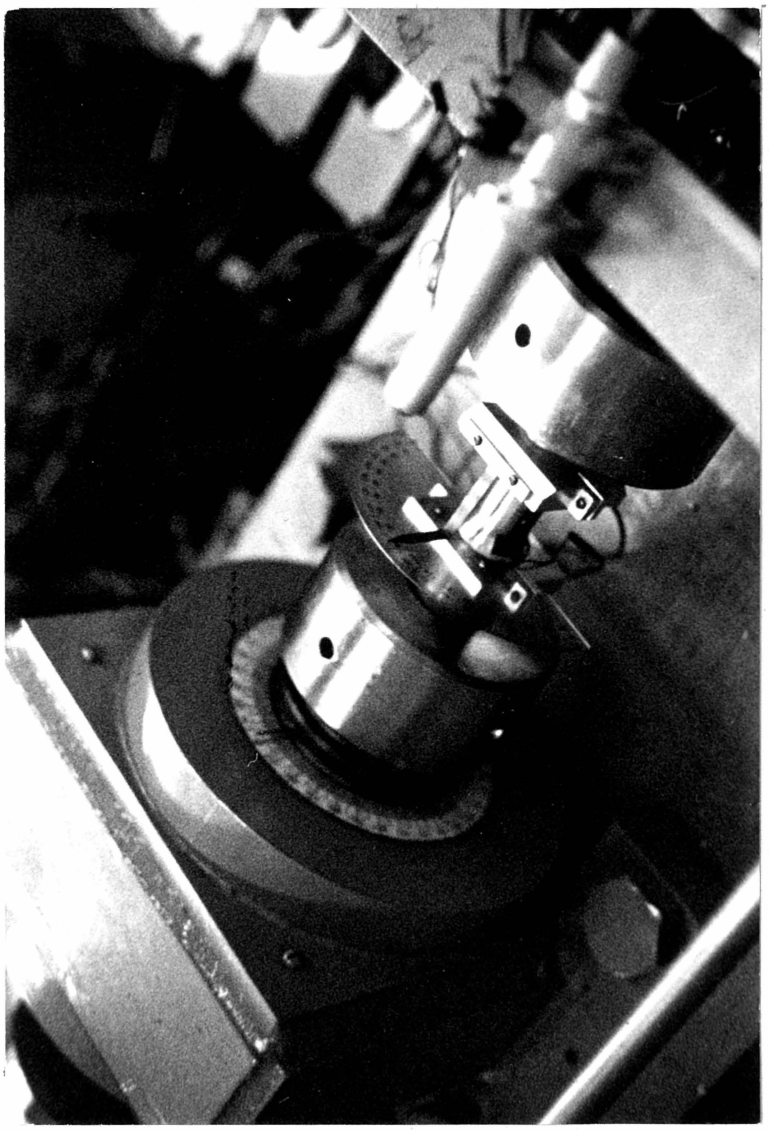

Photo. 3.6 Arrangement of Measuring Systems for a Torsion Test

torsion. For the feed back LVDT, the LVDT1000SS-L of Schaevitz Co. was used like as in the axial case. The output of the LVDT can be read on the cathode-ray oscilloscope.

The shear strain can be measured by two strain gages put on the specimen in the direction of 45° from the axis by means of the two gage method. For the strain gage, the post yield foil gage HE-141-R2VC-120 of Budd Co. was used for the torsion test and for the combined test the post yield foil gage HP-08-125-RA-120 of W. T. Bean Co. was used. Two kinds of gages can work up to 30 % shear strain. In the experiment, after it is made sure for the typical test that the strain by the strain gage agrees satisfactorily with that obtained theoretically by the protractor reading of the twisting angle, the strain was determined only by the protractor reading for the other tests.

The schematic diagram of the recording system in the torsion test is shown in Fig.3.8.

The picture of the specimen with the protractor is shown in Photo.3.6.

§3.5 Calibration Test

Before the experiments begin, some calibration tests of this testing machine are necessary. The calibration tests include the following items :

(1) Potentiometer setting vs. the output voltage of the feed-back LVDT which shows the output deformation of the machine,

(2) The voltage of the signal LVDT vs. the output voltage of the feed-back LVDT for both the linear and the rotary motion,

(3) The reading of the pressure gage vs. the strain indicator reading for the load cell with the fixed potentiometer setting,

(4) Die-set movement vs. the linear strain gage on the specimen,

(5) The angle of twist vs. the torsion strain gage on the specimen,

and

(6) The extensometer reading vs. the micrometer reading of the telescopic gage.

The results of (1) and (2) are shown in Fig.3.9(a) for the linear motion and in Fig.3.9(b) for the rotary motion.

The results of (3) are shown in Figs 3.10(a) and (b).

The results of (4) are shown in Figs. 3.11(a)~(g).

The results of (5) are shown in Figs. 3.12(a)~(c).

The results of (6) are shown in Fig. 3.13.

The first three items are for the machine itself, while the results for the last three items are used for obtaining the strains. All the results have been found good.

§3.6 Design of the Experiments

The experiments were done according to the following plan.

In order to compare the results in this study with Shewchuk's [86] and Goto's [87] results, the range of the number of cycles to fracture has been selected to be from 1/4 (static) to 2000. Since there are many outputs to read during the test, most of the tests covered from 10 to 2000 so as to comlete the readings. Except the uniaxial tests which include the preliminary tests for the purpose of watching how accurate the machine worked, four or five strain levels were chosen and on each strain level three tests were conducted.

For the combined tests, the ratio A of the torsional shear strain to the axial strain of 2:1 and the phase difference of zero were selected as the standard. The ratio of 2:1 gives the same damage to both the axial and the torsional shear strain gages if one uses the three element right angled rosette strain gage. The

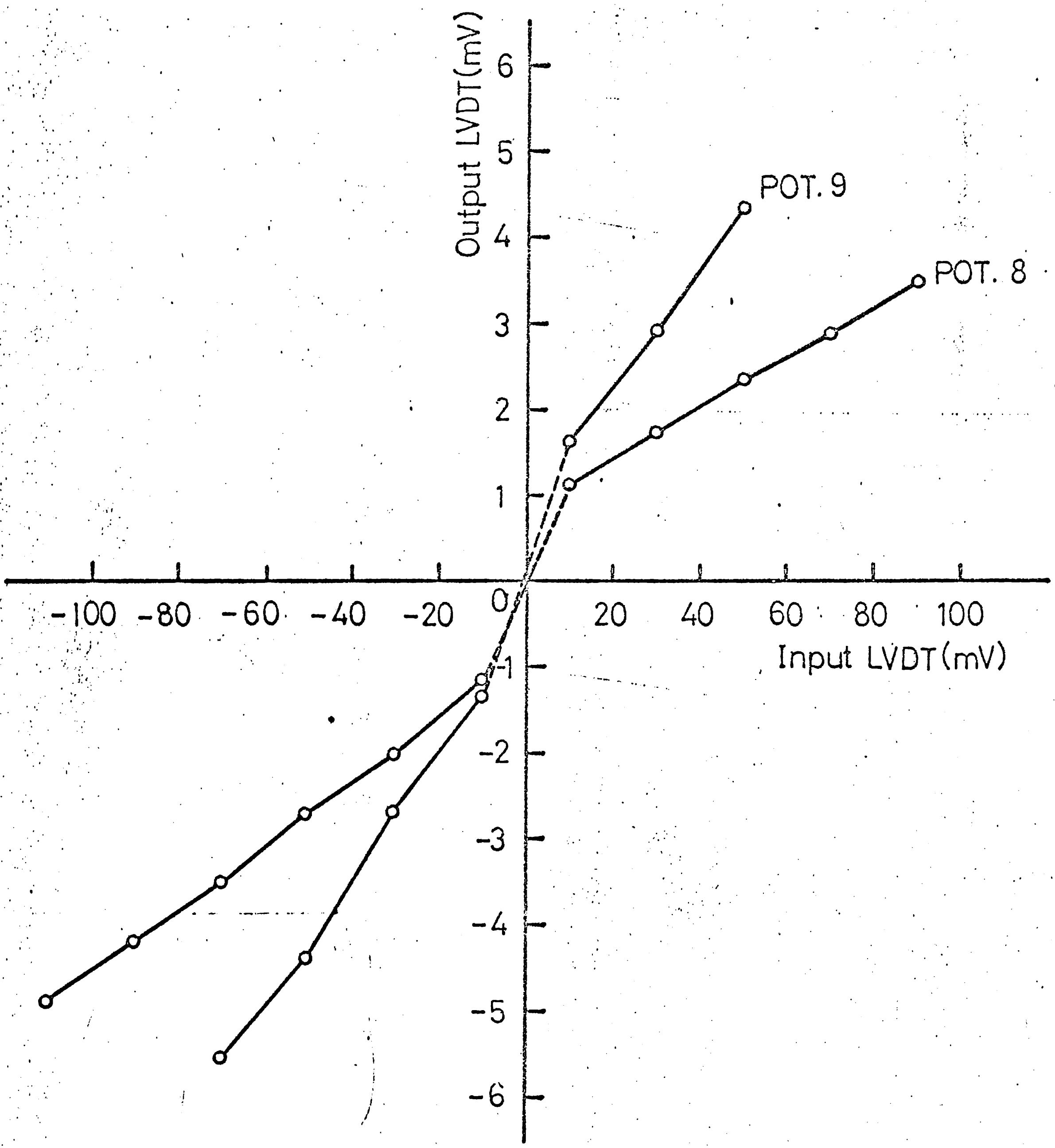

Fig. 3.9(a) Relationship between Input LVDT and Output LVDT for Axial Motion.

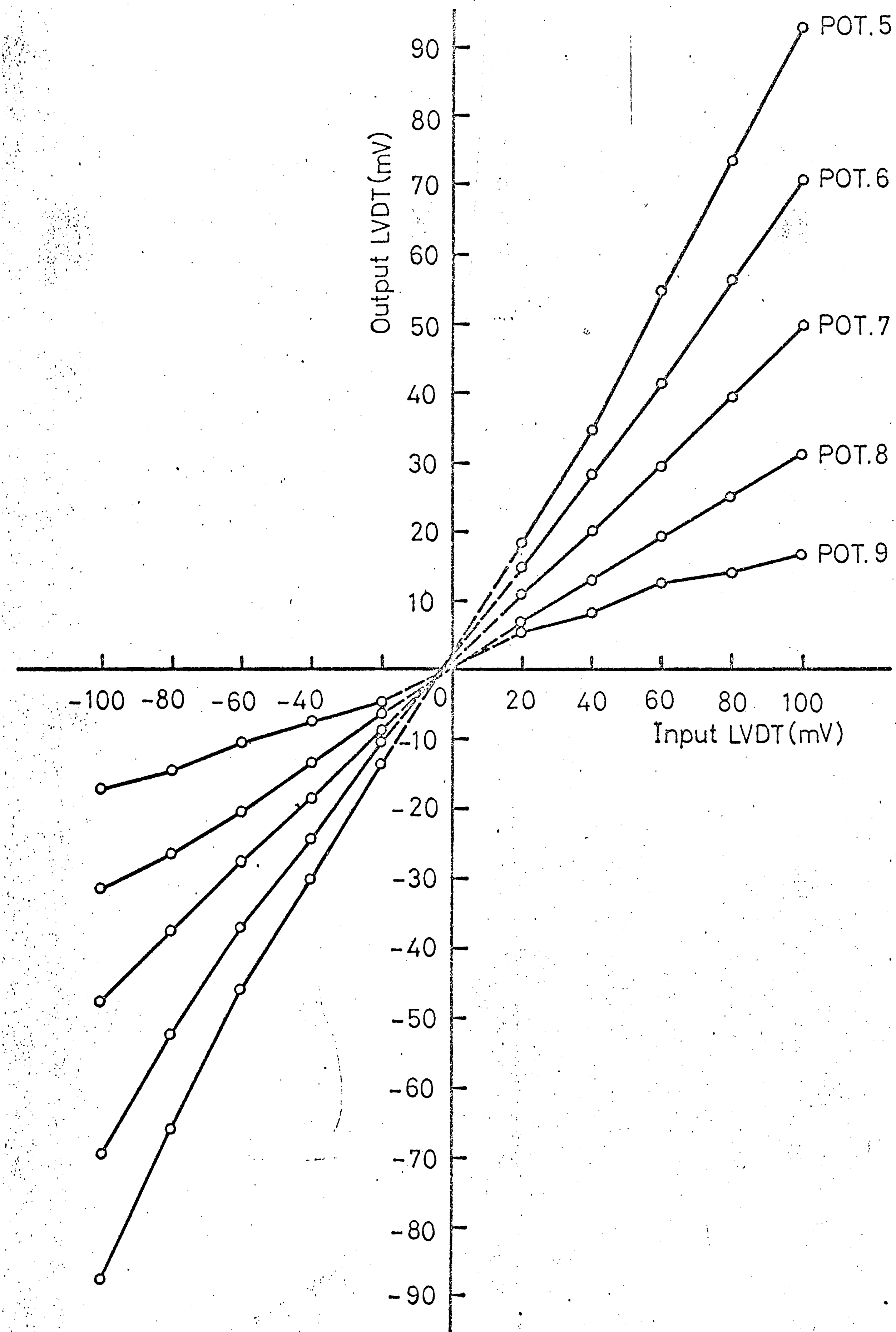

Fig. 3.9(b) Relationship between Input LVDT and Output LVDT for Rotary Motion.

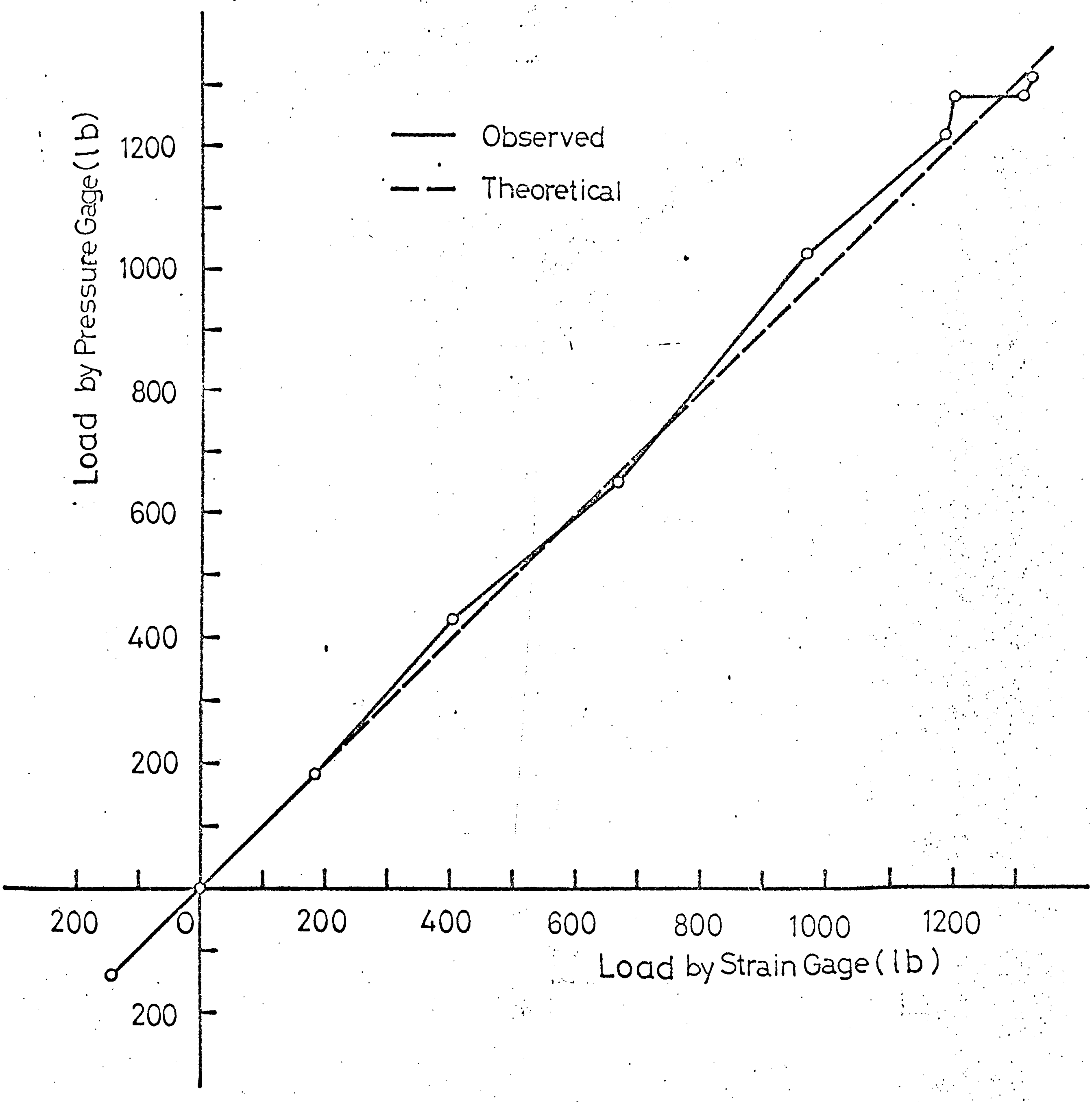

Fig.3.10(a) Relationship between Load by Pressure Gages and Load by Strain Gages for Axial Motion.

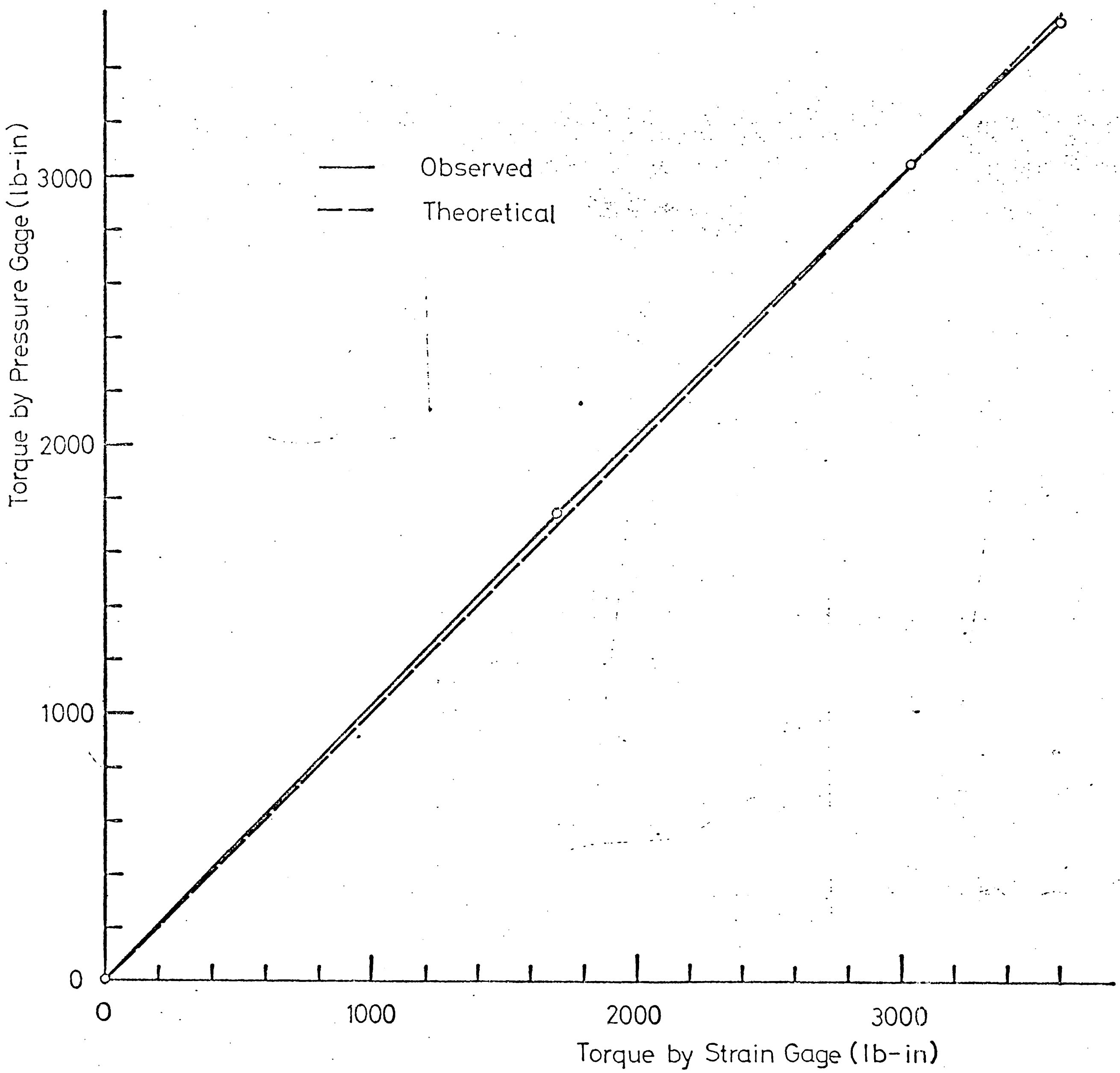

Fig. 3.10(b) Relationship between Torque by Pressure Gage and Torque by Strain Gage for Torsion.

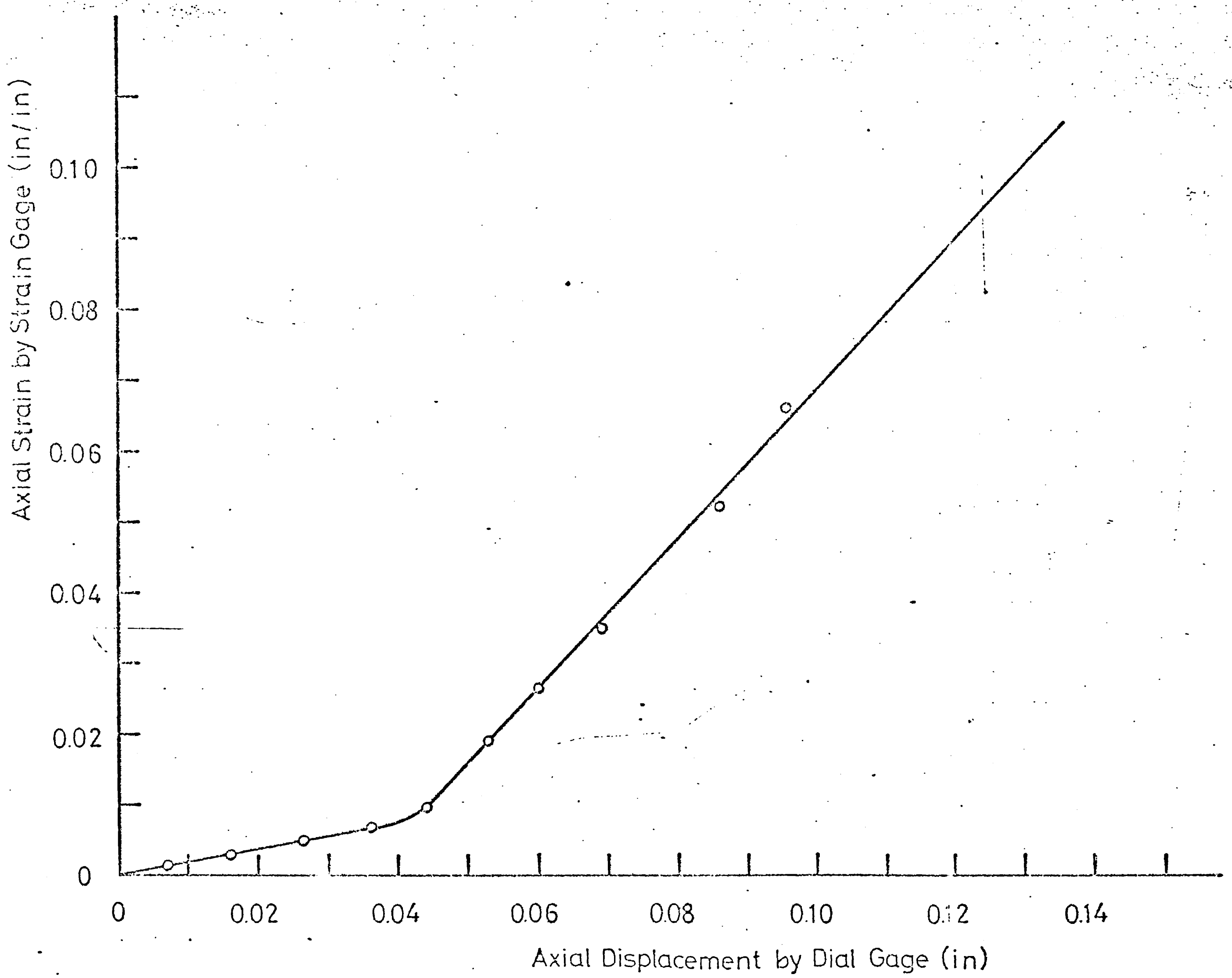

Fig. 3.11(a) Relationship between Axial Strain by Strain Gage and Axial Displacement by Dial Gage for the Uniaxial Static Test.

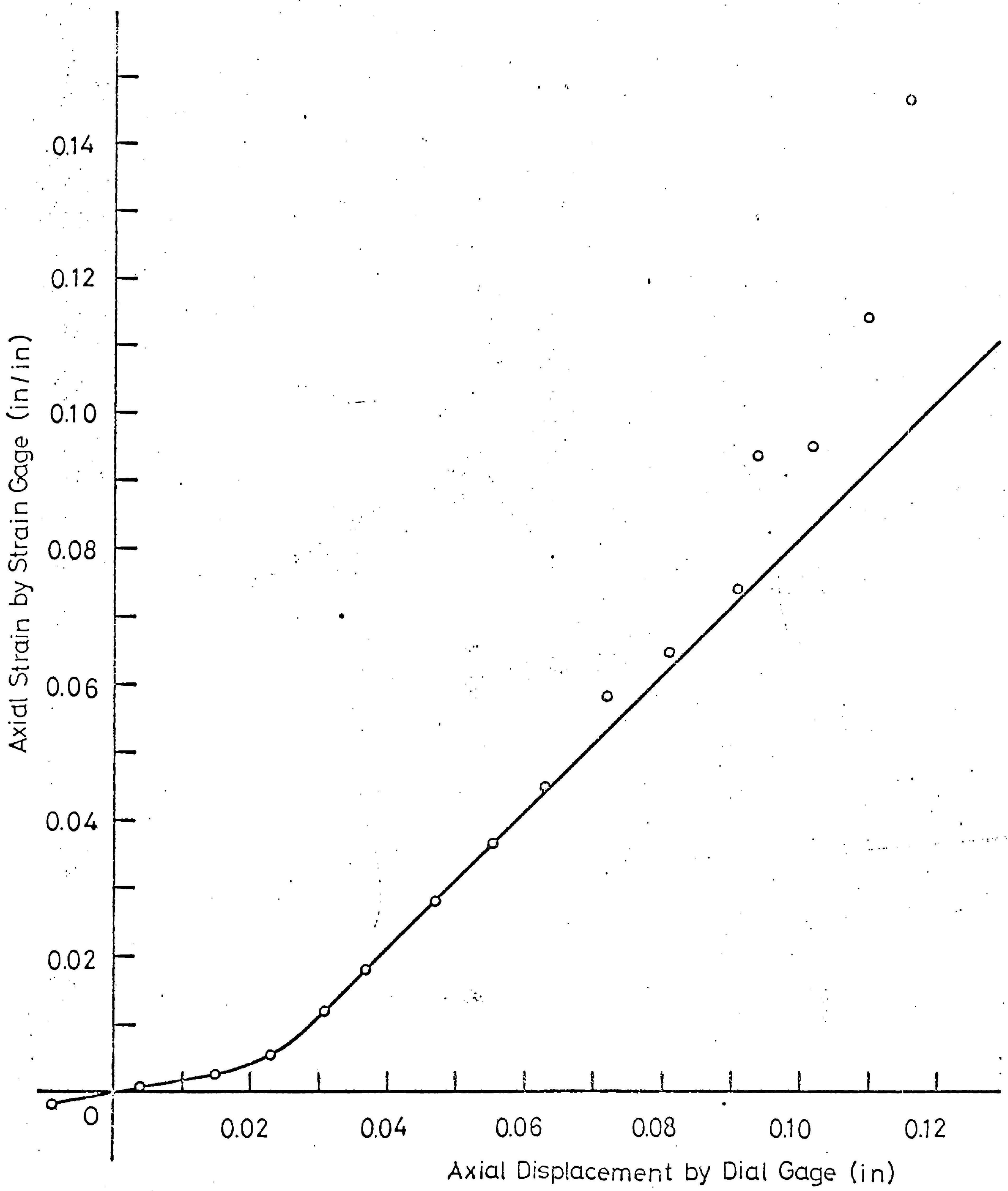

Fig. 3.11(b) Relationship between Axial Strain by Strain Gage and Axial Displacement by Dial Gage for the Combined Static Test.

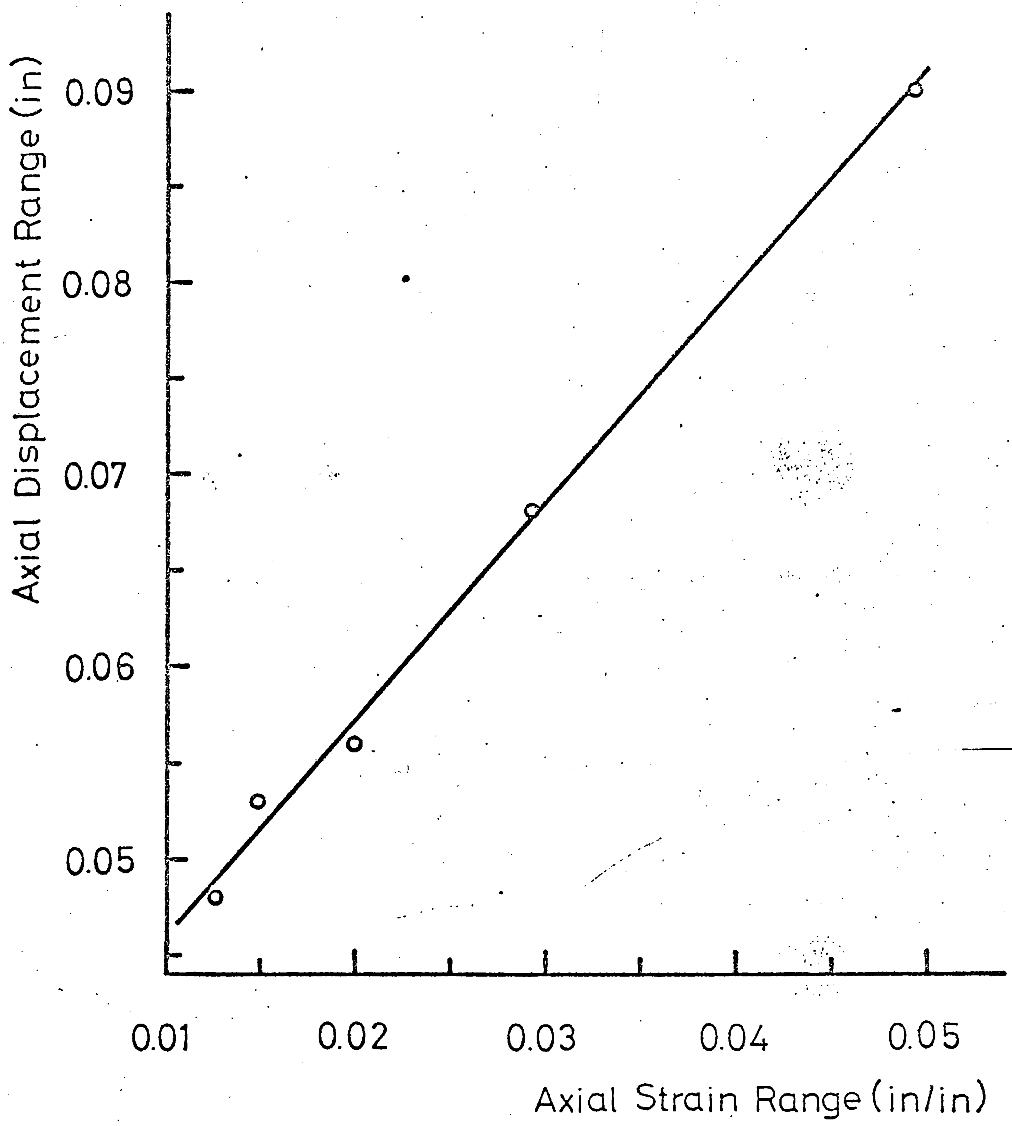

Fig. 3.11(c) Relationship between Axial Strain Range by Strain Gage and Axial Displacement Range by Dial Gage for Combined Synchronous Fatigue Tests of A=2.

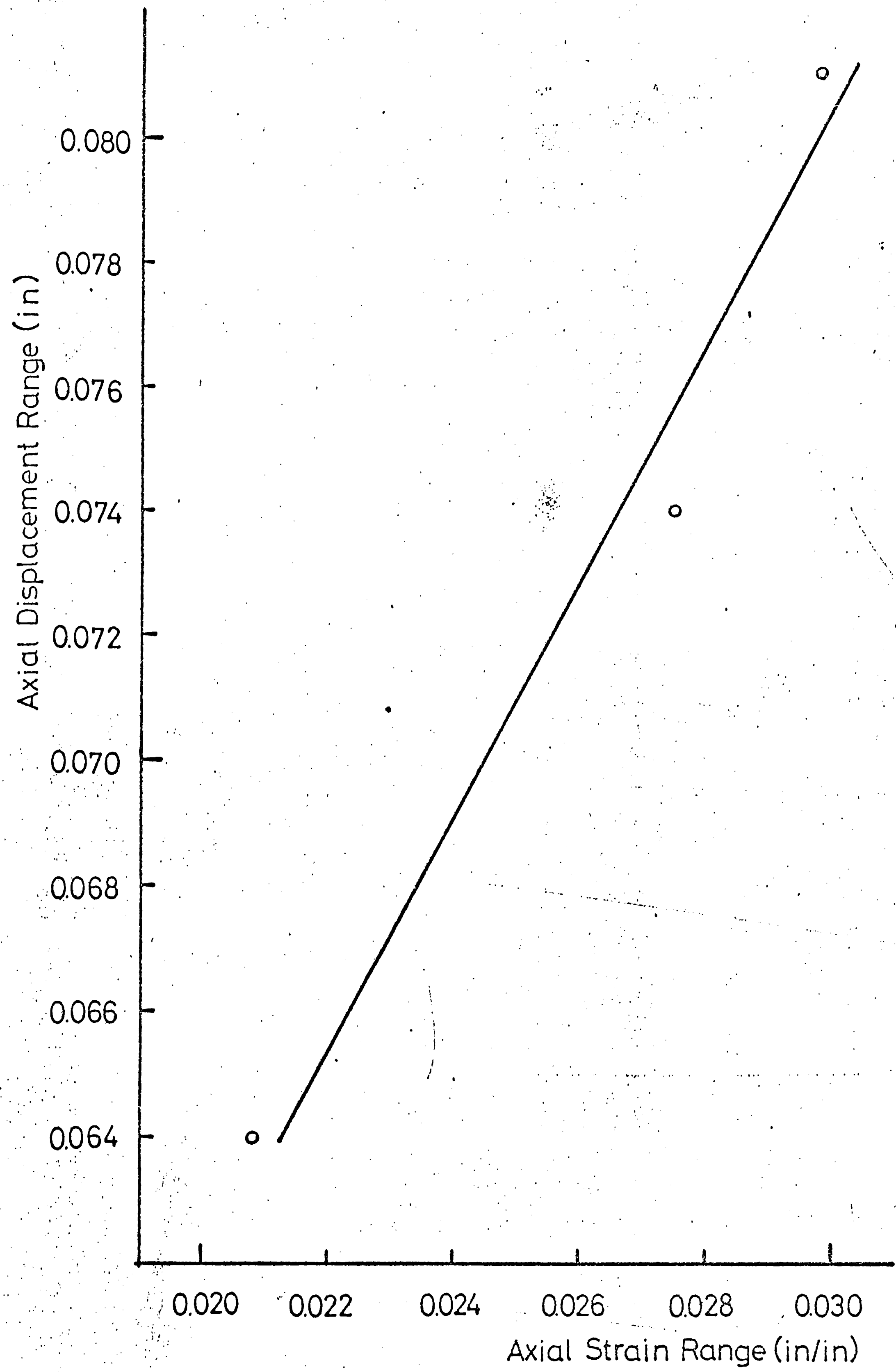

Fig. 3.11(d) Relationship between Axial Strain Range by Strain Gage and Axial Displacement Range by Dial Gage for Combined Synchronous Fatigue Tests of A=1.

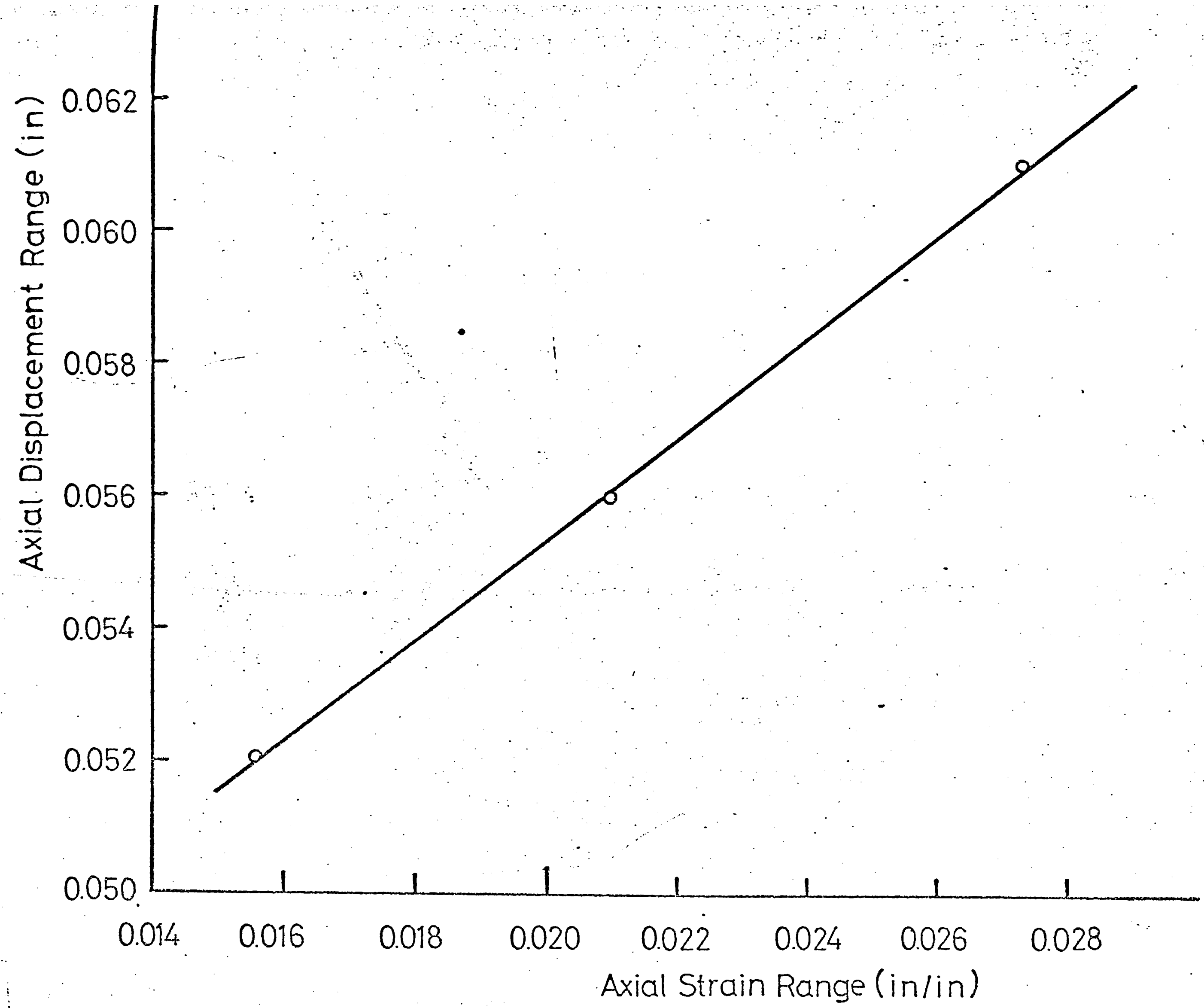

Fig. 3. 11(e) Relationship between Axial Strain Range by Strain Gage and Axial Displacement Range by Dial Gage for Combined Synchronous Fatigue Tests of A=3.

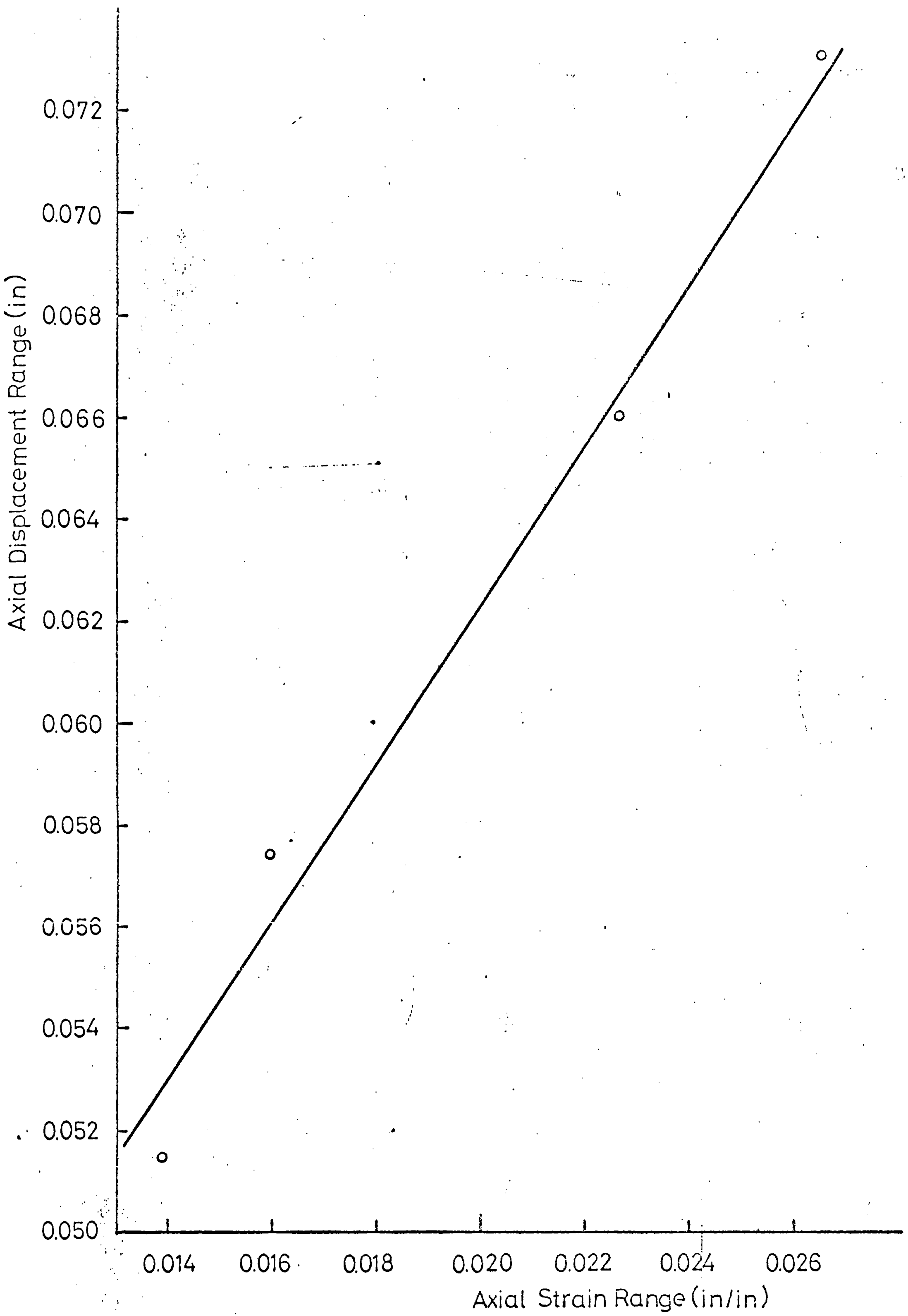

Fig. 3.11(f) Relationship between Axial Strain Range by Strain Gage and Axial Displacement Range by Dial Gage for Combined Nonsynchronous Fatigue Tests of A=2 and $\phi=45°$.

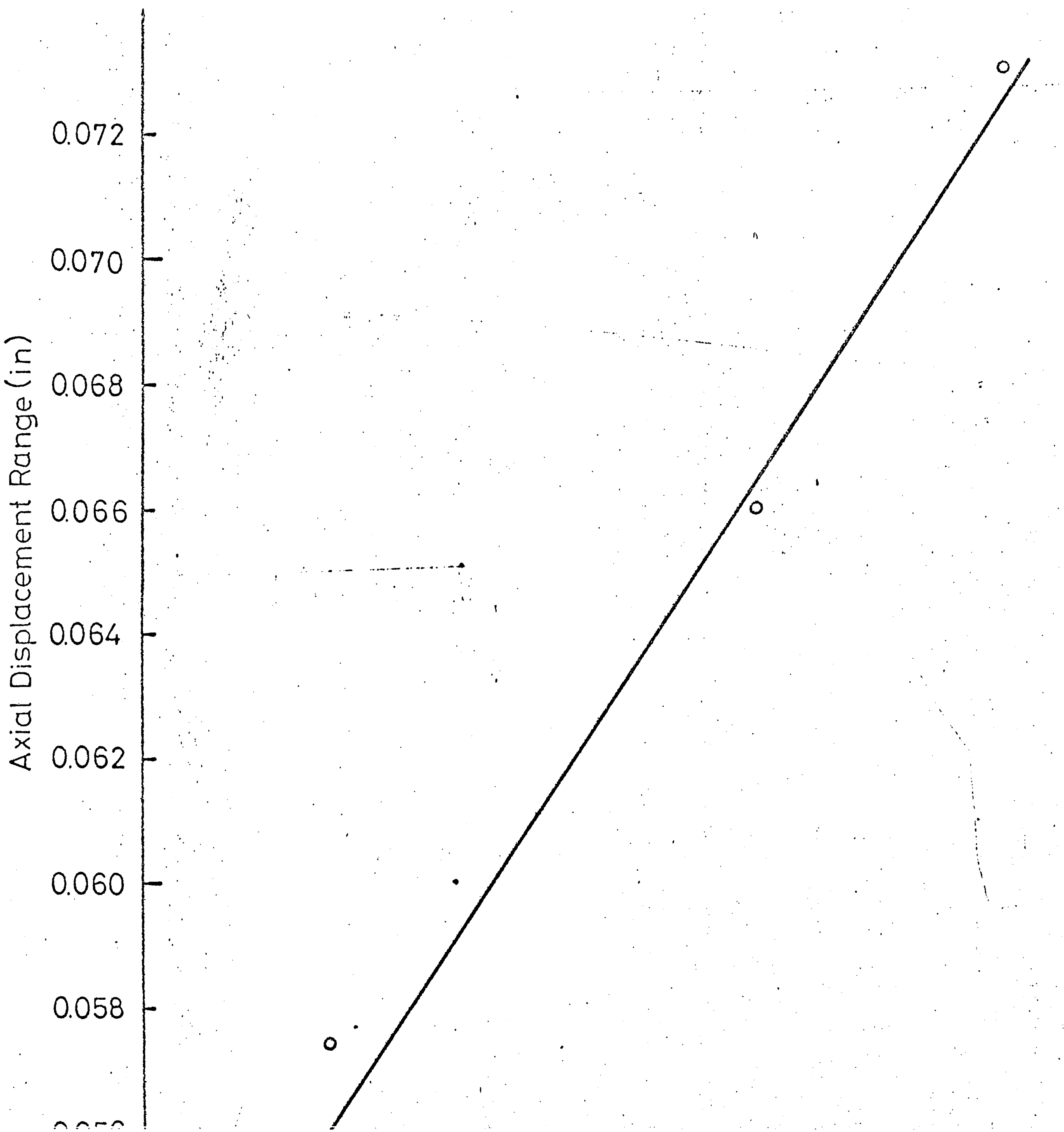
Axial Displacement Range (in)
0.072
0.070
0.068
0.066
0.064
0.062
0.060
0.058

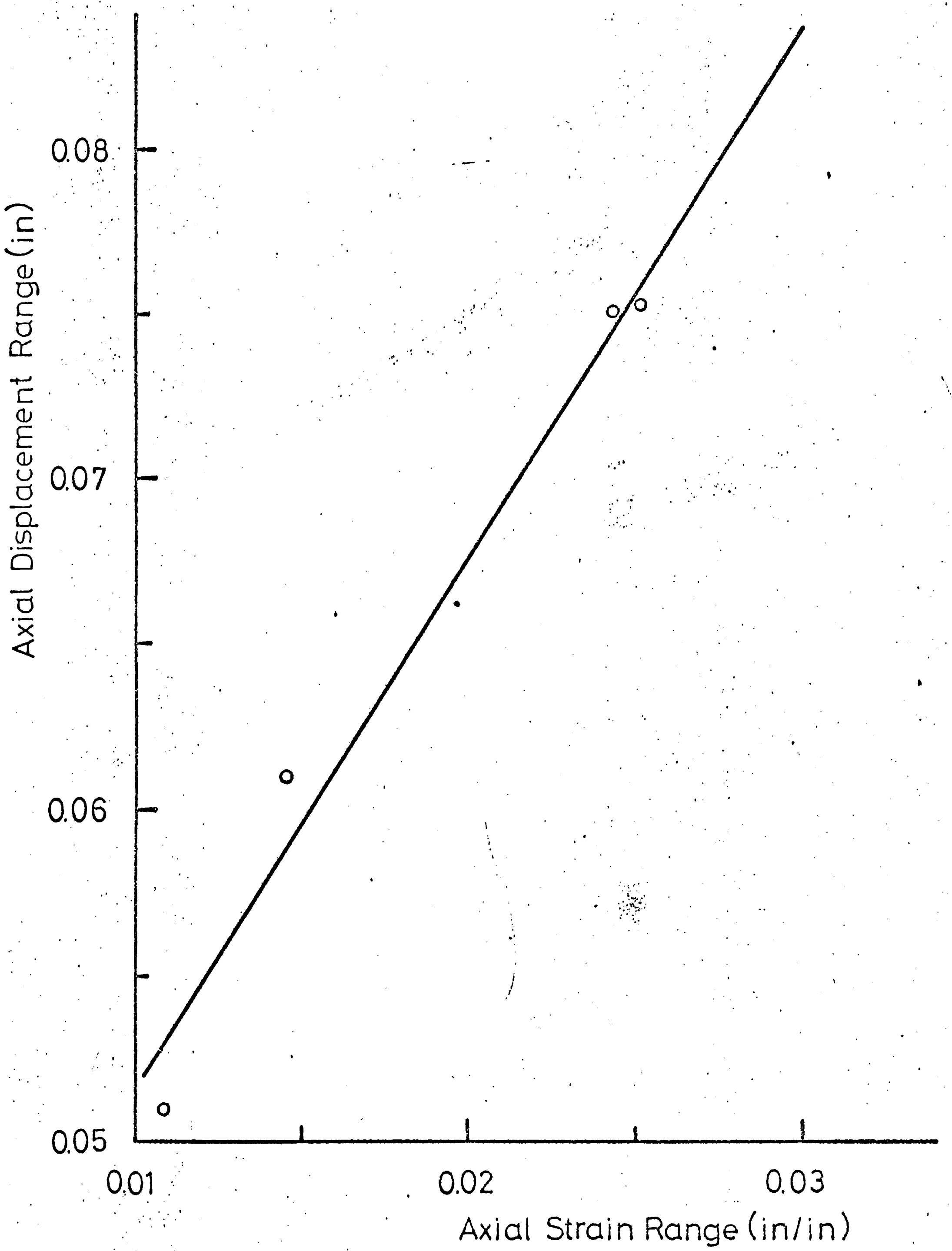

Fig. 3.11(g) Relationship between Axial Strain Range by Strain Gage and Axial Displacement Range by Dial Gage for Combined Nonsynchronous Fatigue Tests of A=2 and ϕ=90°.

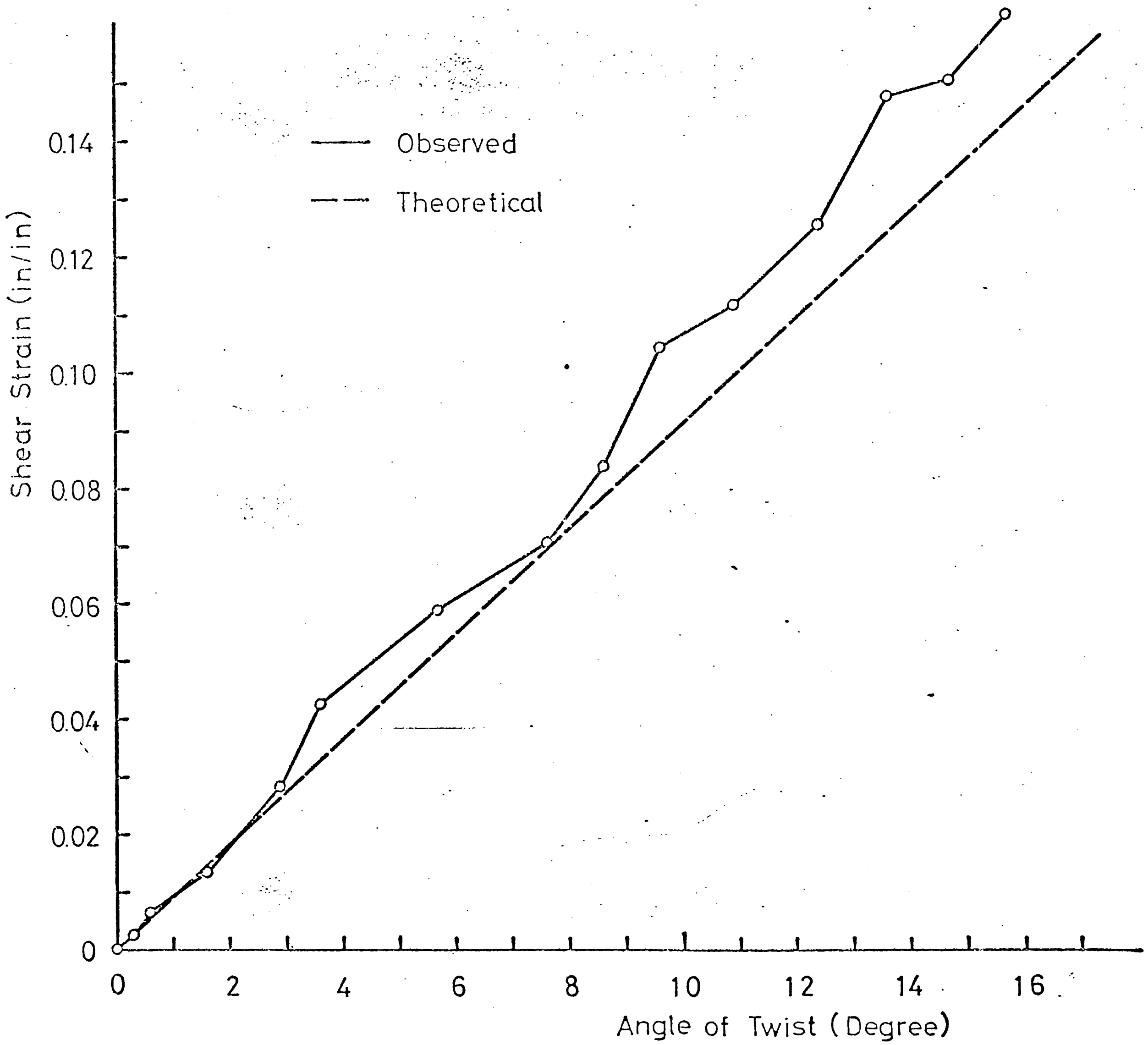

Fig. 3.12(a) Relationship between Shear Strain by Strain Gage and Angle of Twist by Protractor for the Combined Static Test of A=2.

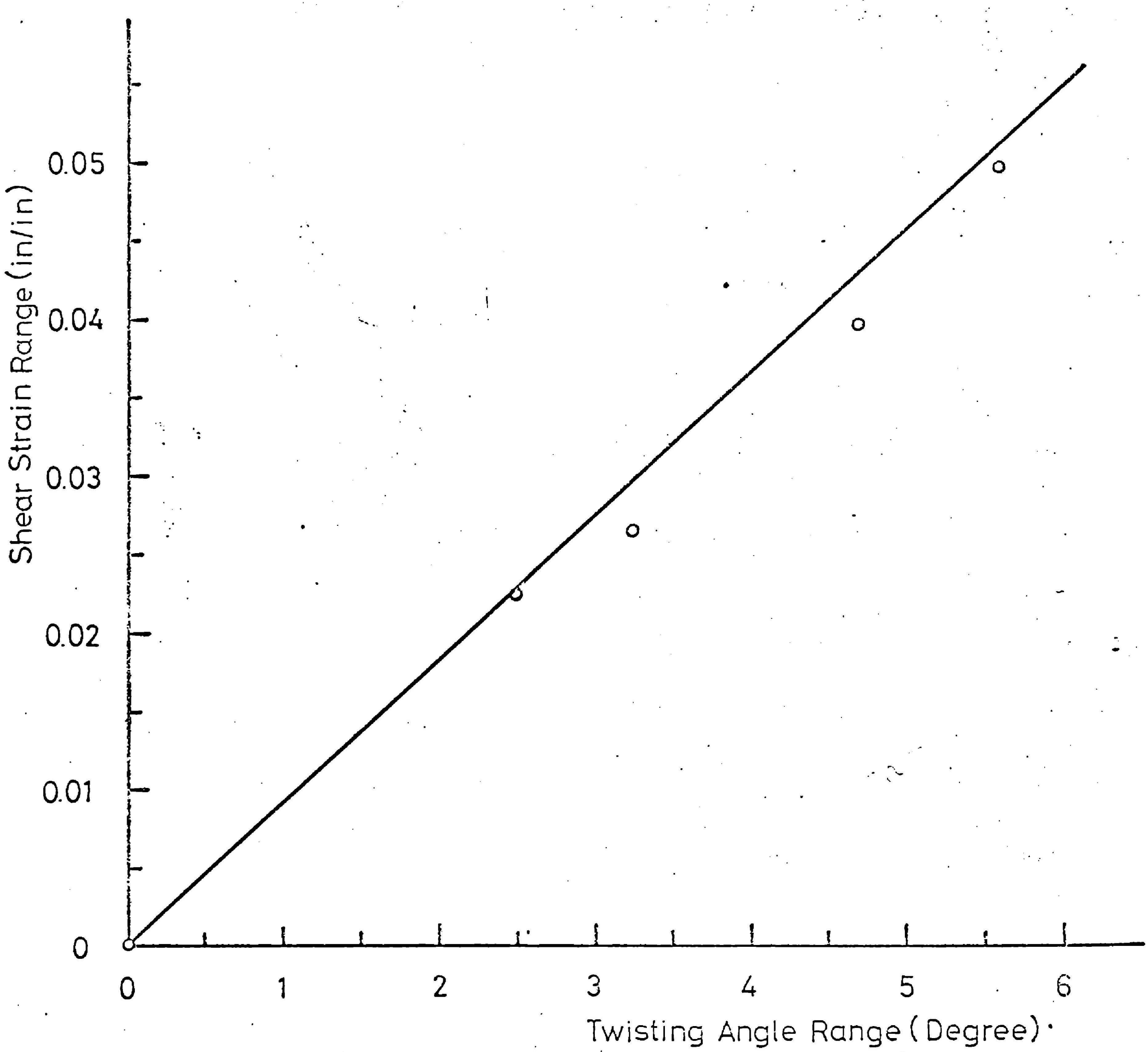

Fig. 3.12(b) Relationship between Shear Strain Range by Strain Gage and Twisting Angle Range by Protractor for Combined Synchronous Fatigue Tests of A=2.

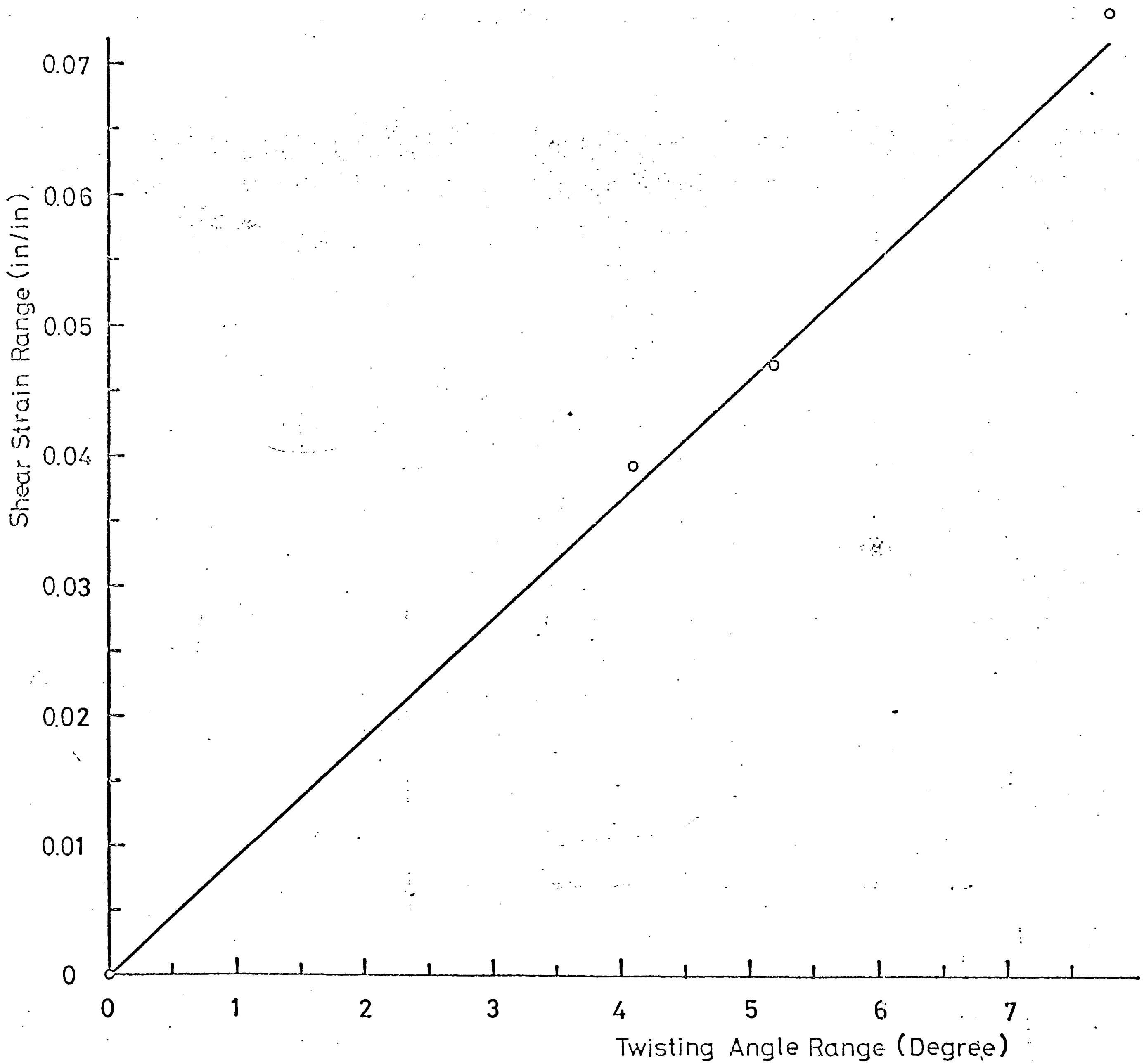

Fig. 3.12(c) Relationship between Shear Strain Range by Strain Gage and Twisting Angle Range by Protractor for Combined Synchronous Fatigue Tests of A=3.

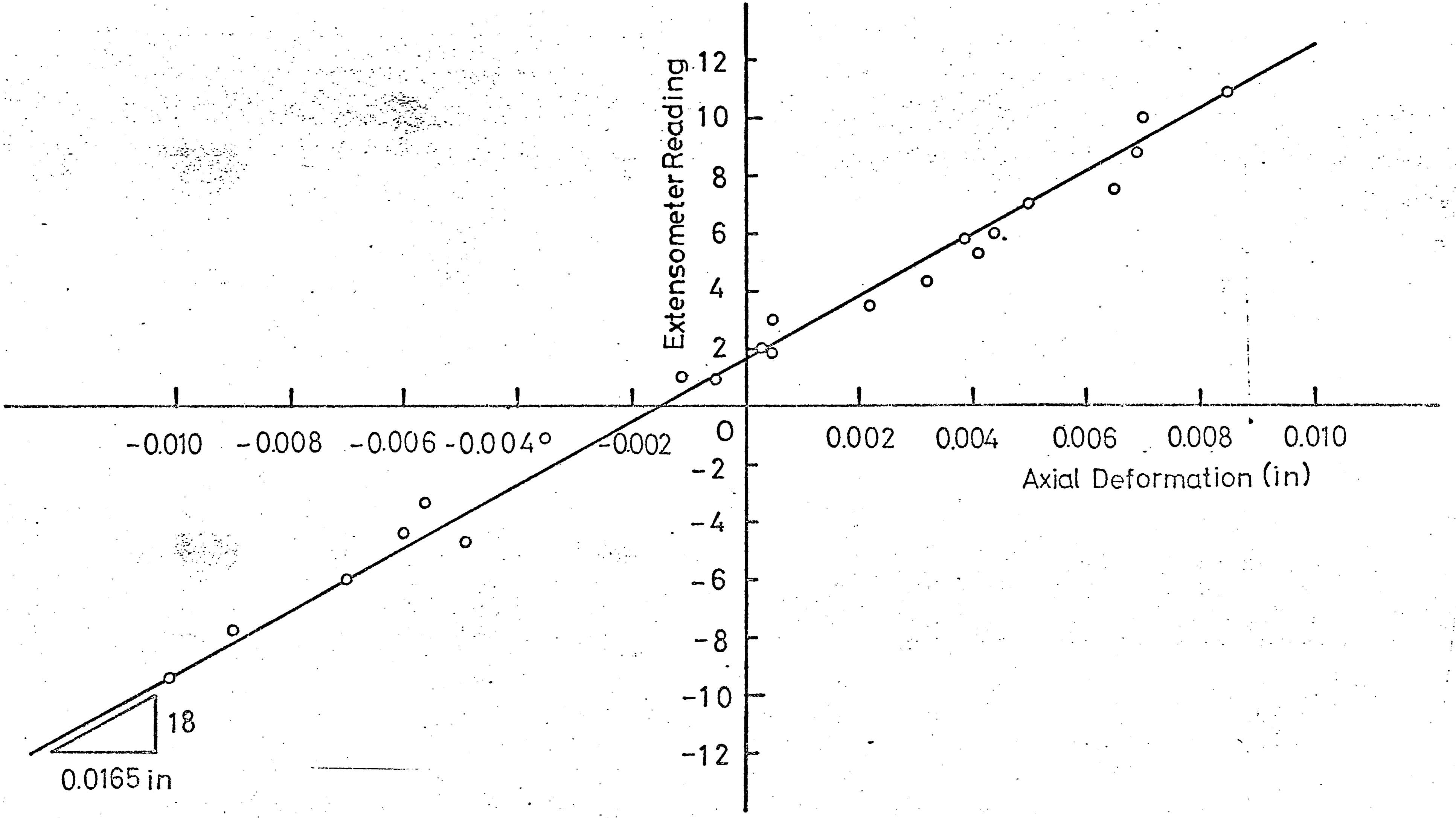

Fig. 3.13 Relationship between Axial Deformation by Telescopic Gage and Extensometer Reading for the Uniaxial Fatigue Test of No.16.

strain ratios were taken to be 1:1, 2:1, and 3:1, and the phase difference were 0°, 45°, and 90°. With the expectation that the test results for different strain ratios may appear on the straight line on the log-log plot of the octahedral shear strain vs. the number of cycles to fracture, only four tests on different levels including the static test were conducted for each ratio of strains.

For the phase differences other than 0°, that is, nonsynchronous case, the strain ratio was selected to be 2:1 only, to know only the effect of phase difference. For this series, two specimens, one of which has a strain gage, were tested for each strain level.

Besides the above-mentioned plan, a small number of arbitrary variations were added.

§3.7 Test Procedure.

The experiments were performed in the following three stages:

(1) To set up the strain range, the strain ratio, and the phase difference,

(2) To switch on the testing machine and to set up the specimen, and

(3) To observe and dispose of the test.

Each stage is explained as follows:

(1) To Set up the Strain Range, the Strain Ratio, and the Phase Difference.

The strain range is set up in the same manner for all the uniaxial, torsional, and combined tests, while the strain ratio and the phase difference are set up only for the combined test.

The strain range was set up by turning the potentiometer in the sevocontroller referring to the diagram in Figs. 3.9(a) and 3.9(b). The mean strain can be given by controlling the micrometer-stand of the input signal device. The machine is designed so that the sum of the alternating and the mean strains may be controlled by the potentiometer.

The strain ratio was given by setting up the strain ranges of the axial and the torsional channels, independently.

The phase difference was obtained by changing the angle between the input divices for both channels. Photos.3.3 and 3.7 shows the cases of 0° and 45° phase differences, respectively.

The handle for the flow control was held so that the main pressure gage may show 1500 psi. when the oil pressure was given in keeping both the by-pass and the throttle valves closed.

(2) To Switch on the Testing Machine and to Set up the Specimen

The procedure from switching on the testing machine to beginning to run the machine is explained for each of the axial, the torsional, and the combined cases in the following.

(A) Axial Test

1 Open two throttle valves and the by-pass valve.

2 Switch on the electric motor in the hydraulic power unit.

3 Push the main switch for the electric part and other instruments.

4 Switch on the cathode-ray oscilloscope.

5 Switch on the servocontroller in keeping the gain zero and then turn the gain control to the maximum.

6 Connect the terminal of the strain gage on the load cell with the strain amplifier and indicator and then switch on the amplifier.

7 Switch on the pen writing recorder.

8 Leave the machine for 30 minutes until it becomes the steady state. Mean-while, install the metal fittings with the specimen according to the following procedure.

9 Install the left nut with the specimen.

10 Insert the keys into the left key-ways of the specimen-nut system.

11 Install the left auxiliary nut with the specimen. This is done

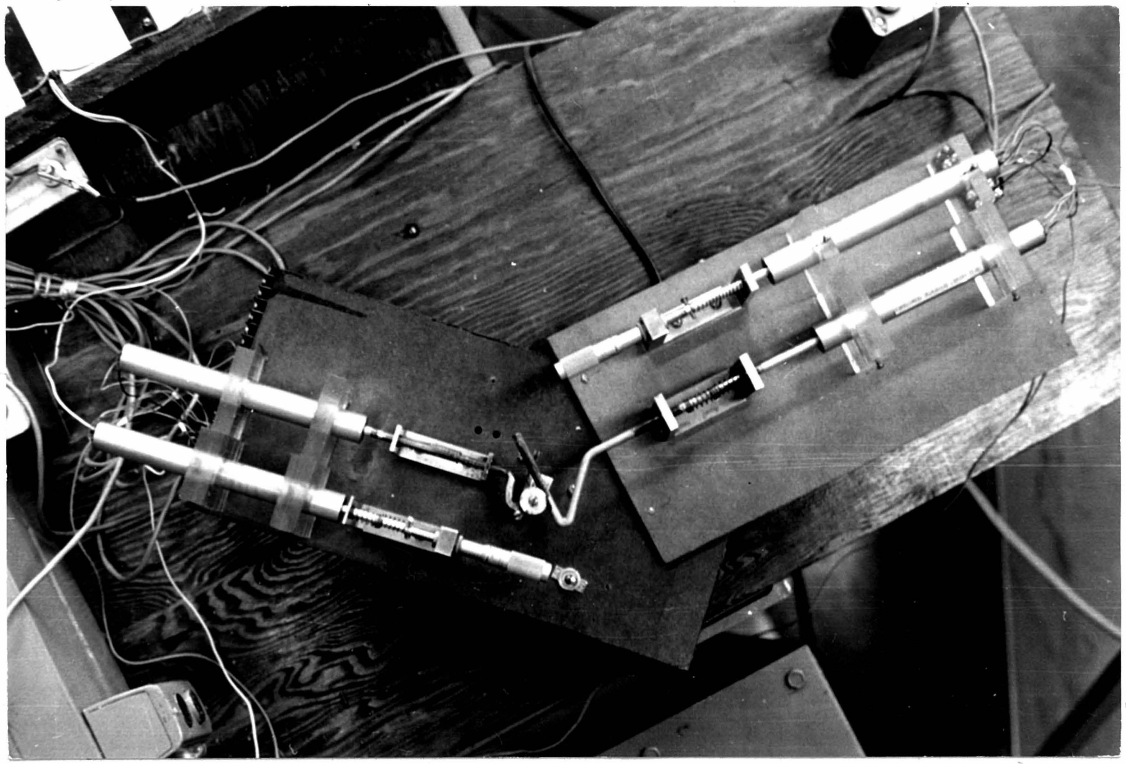

Photo. 3.7 Input Signal Generator for the Nonsynchronous Case ($\phi=45°$)

by tightening the nut by a wrench in catching the specimen by a vice.

12 Take the left and right caps on the specimen.

13 Install the right nut with the specimen.

14 Insert the keys into the right key-ways of the specimen-nut system.

15 Tighten the right auxiliary nut into the specimen by a wrench. Leave the specimen with the metal fittings on the table during the following procedure to prepare the machine.

16 Take null of the LVDT's. This is done by measuring the output of the LVDT by the cathode-ray oscilloscope with high impedance.

17 Set the potentiometer to get the objective strain range by Fig. 3.9(a).

18 Switch on the motor for the pressure and increase the pressure by shutting off the by-pass valve.

19 Driving the input device without load, check the amplitude of the output displacement.

20 Widen the distance of both the left and right grips by moving the axial output LVDT by hand.

21 Install the specimen-nut system prepared in the steps 9 to 15 with both grips of the machine. In this case, tighten first the right cap into the right gip and then move the left grip closer to the left nut of the specimen by moving the output LVDT by hand. (Do not tighten the left cap, yet.)

22 Attatch the extensometer to the specimen and connect its terminals to the strain amplifier and indicator.

23 Adjust the zero position of the strain indicator and the pen recorder and calibrate then with the strain gages.

24 Insert the left nut of the specimen closely into the left grip by moving the output LVDT by hand until the small elastic compression is applied to the specimen, watching the stress channel of the strain indicator. In case that the projection of the grip does not fit the notch of the nut, give a little bit of rotation to the rotary actuator by moving the torsional feed-back LVDT by hand.

25 Tighten both left and right caps to the grips firmly.

26 Release the elastic compression given in the step 24 by moving the output LVDT.

27 Close the torsionl throttle valve.

(B) Torsional Test.

1 Follow the procedure 1 through 21 in the axial test.

2 Connect the output of the strain gage on the specimen to the strain indicator.

3 Follow the procedure 20 through 23 in the axial test.

4 Install the protractor to the specimen.

5 Close the axial throttle valve keeping the torsional throttle valve open.

(C) Combined Test

1 Follow the procedure 1 through 4 in the torsional test.

2 Keep the both throttle valve open.

(3) Observation of the Experiment and Disposition.

1 Before the test begins, make the blanks to fill the results in. Some examples of the tables of the experimental results are shown in Tables 3.2 to 3.4.

2 Read and write the initial conditions of the items to be recorded.

3 Conduct one cycle of static test before the dynamic test. This is done as follows:

Table 3.2

Original Results of the Uniaxial Test, No. 13.

Potentiometer 9.55, Pressure 600 psi, N=759

Input LVDT (Core Position x 0.1 in)	Output LVDT (x 5 mV)	Pressure Left (psi)	Pressure Right (psi)	Dial Gage Reading for Axial Displacement (x 0.01 in)	Strain Gage on Specimen (x 10 Range)	Strain Gage on Load Cell (x 50 Range)	Extensometer Reading	Telescopic Gage Reading for Axial Deformation(in)
5	0.9	300	270	500	-0.1	-4.3	5.8	1.7462
6	1.1	310	250	494	3	-9	4	1.742
7	1.6	390	210	486	8	-21.5	1.8	1.740
7.5	1.75	420	200	483	10	-26	0.8	1.740
8	2.0	450	190	480	12	-31	0	1.7395
8.5	2.2	480	180	477	14.2	-35	-1.3	1.7385
9	2.4	500	160	473	17.2	-39.6	-2.5	1.7363
9.5	2.6	510	150	471	21	-41.3	-4.2	1.7334
7	1.65	370	230	485	11	-15.3	1	1.7395
5	0.9	270	270	499	4	-2	4	1.7445
4	0.85	250	300	506	0.3	3.5	5.5	1.7453
3	1	200	250	513.5	-3.1	11	7	1.7475
2.5	1.15	200	260	515.5	-4.3	12.3	7.5	1.7493
2	1.3	180	270	519	-6.2	16.5	8.2	1.7495
1.5	1.4	180	380	522	-8	19	9.1	1.7506
1	1.55	160	400	524	-9.4	22.3	9.8	1.7506
0.5	1.65	150	410	526	-11	24	10.5	1.7535
0	1.8	140	420	521	-13.5	27	11.3	1.7535
3	1	230	320	513	-5	6.5	7.1	1.7535
5	0.9	290	270	500	0.8	-4	4.5	1.747
4.5	0.8	260	270	502	0.5	-2	5.2	1.745
Dynamic	2.0 ~ 2.6	160 ~ 540	160 ~ 500	530 ~ 470	18.5 ~ -16.5	-41 ~ 31.5	-5 ~ 12.5	

Table 3.3

Original Results of the Torsional Test, No.7.

Potentiometer 8, Pressure 600 psi, N=27

Input LVDT (Core Position x 0.1 in)	Output LVDT (x 5 mV)	Pressure Left (psi)	Pressure Right (psi)	Angle of Twist by Protractor (Degree)	Strain Gage on Specimen (x 5 Range)	Strain Gage on Load Cell (x 50Range)
Initial					2.1	-5.8
5	0.63	50	250	0.1	-1.3	-14.3
6	0.8	90	200	0.6	1.6	-6
6.5	1.23	180	140	1.0	3.3	-2.4
7	1.7	130	130	1.35	5.3	4.7
7.5	2.1	200	100	1.8	7.4	11
8	2.55	280		2.3	9.5	16.5
8.5	3.0	300	80	3.2	12.7	18.8
9	3.4	350	60	3.9	17	20.2
9.5	3.8	380	50	4.6	21.5	21
10	4.2	350	50	5.3	26	21.7
8.5	3.05	110	160	4.1	19.6	-1
7	1.75	100	240	3.45	17	-8
6	0.9	0	310	2.25	11.1	-19
5	0.63	0	350	0.8	1.7	-26
4	1.5	0	440	-1.1	-10	-31.5
3.5	2	0	460	-2.1	-16.5	-33
3	2.5	0	450	-3.1	-23	-34
2.5	2.95	0	460	-3.9	-29.2	-35
2	3.4	0	470	-4.7	-35.7	-35
1.5	3.85	0	480	-5.6	-42	-36
1	4.3	0	490	-6.2	-47	-36
3	2.3	50	220	-4.4	-37.2	-8.2
4	1.6	110	200	-4.1	-36.1	-5.5
5	0.7	220	110	-3	-28.7	7
6	0.75	300	100	-1.5	-19.3	14.4
7	1.7	330	50	0.4	-7.1	17.3
8	2.6	350	50		-4.2	18.5
5.25	0.5	50	200	0	-6.6	-10.7

Table 3.4

Original Results of the Combined Test,No.12.

Pressure 1000 psi.,Potentiometer 9.6 for Axial, 9.35 for Torsion,N=330

				Axial Motion			
Input LVDT (Core Position x 0.1 in)	Output LVDT (x 5mV)	Pressure (psi) Left (psi)	Pressure (psi) Right	Dial Gage Reading for Axial Displ. (x 0.01 in)	Strain Gage on Specimen (x 10 Range)	Strain Gage on Load Cell (x 10 Range)	Telescopic Gage for Axial Deformation. (in)
Initial	0.83				4	-0.8	1.8315
5	0.9	700	400	500	3.4	-0.8	1.8315
4	1	680	430	507	8.6	2.7	1.8354
3	1.2	650	450	512.3	11.8	5.1	1.8365
2	1.4	620	460	517	14.4	7.1	1.8373
1	1.65	610	490	522	18	9.7	1.8399
0.5	1.75	600	490	523	20	10.3	1.8407
0	1.93	600	500	525	23.2	10.9	1.8424
2	1.4	650	450	516.5	17.8	5.6	1.8385
4	1	685	415	507	11.8	1.3	1.8372
5	0.85	700	400	500	7.5	-2.5	1.8350
6	0.83	730	420	493	2.5	-6.2	1.8317
7	1	760	390	488	-2.2	-9.7	1.8297
8	1.3	770	360	483	-8	-12.8	1.8266
9	1.6	800	350	479	-14.8	-14.8	1.8230
9.5	1.73	810	340	477	-19	-15	1.8204
10	2	810	320	474	-25.1	-16	1.8190
8	1.4	750	380	482.5	-18.4	-8.9	1.8230
6	0.85	690	450	493	-10.3	-2.3	1.8285
5	0.83	680	420	500	-5	1	1.8300
1	1.6			520	15.5	9.4	1.8382
5	0.83			500	2.7	-0.8	1.8325
Dynamic.							

Torsion
See next page.

Table 3.4-Continued

Torsion

Input LVDT (Core Posotion x 0.1 in)	Output LVDT (x 5 mV)	Pressure (psi) Left	Pressure (psi) Right	Angle of Twist by Protractor (Degree)	Strain Gage on Specimen (x 10 Range)	Strain Gage on Load Cell (x 10 Range)
Initial	0.55			0	-1.1	-2
5	0.55	350	320	0	-2	-2
6	0.55	350	330	0.1	2	0.3
7	0.8	390	260	0.5	5.3	2
8	1.1	410	240	1	8.9	4.5
9	1.4	450	220	1.3	12.7	6.5
9.5	1.6	450	210	1.5	15	7.7
10	1.73	480	200	1.85	19.3	8
8	1.1	370	270	1	11.3	3
6	0.53	350	320	0.3	4.2	-1.3
5	0.55	340	340	0.3	6.2	-0.1
4	0.8	250	410	0	2.8	-2.5
3	1.2	260	390	-0.1	-2.5	-4.5
2	1.55	210	430	-0.8	-8.8	-6.7
1	1.9	200	440	-1.2	-16.5	-8.5
0.5	2	180	450	-1.6	-21	-8.8
0	2.2	170	450	-1.9	-26.3	-7.3
2	1.6	260	390	-1.1	-19.7	-5
4	0.93	340	340	-0.9	-13	0
5	0.6	300	350	-0.8	-12.8	0
9	1.35			1	10	5
5	0.6			0	-2.5	0.7

(a) Apply the load to the specimen by moving the core of the LVDT with the micrometer of the two input LVDT's for each channel by 0.1" in one direction until the extreme position.

(b) Move the input LVDT in the other direction from the extreme position to the other extreme position.

(c) Move the input LVDT in the first direction, return the original position, and then, check the origin of the stress-strain curve of the specimen.

(d) If the stress-strain state is not on the origin, apply again certain plastic strain in the direction of (b) and return the LVDT to the zero position, so that the stress-strain state should be on the origin.

4 Speed up the pen-recorder, turn the cathode-ray oscilloscope to the memory position, and then, begin the test by switching on the motor of the input device.

5 Read and write the necessary quantities in order.

6 After the specimen breaks, switch off the motor of the input device and take the specimen off as follows:

(a) Take the extensometer (axial) or the protractor (rotation) off.

(b) Disconnect the strain gage from the specimen.

(c) Screw out the left cap.

(d) Widen the distance between both grips by moving the axial feed-back LVDT by hand.

(e) Screw out the right cap.

(f) Take the specimen-nut system with the caps out of the machine.

(g) Screw out both right and left nuts as well as keys from the specimen.

7 Mark the run number and the right and left on the specimen.

8 Return the input signal to zero.

9 Open the by-pass valve and switch off the motor in the hydraulic power unit.

10 Switch off the servo-controllers after making their gains zero.

11 Switch off the pen-recorder and, the cathode-ray oscilloscope.

12 Turn off the main switch of the electric circuit.

13 Turn off the original of the motor in the hydraulic power unit.

The test is over.

CHAPTER IV ANALYSIS OF EXPERIMANTAL RESULTS AND DISCUSSIONS

§4.1 Introduction

In this chapter, the experimental results are listed, analysed, plotted and then discussed. The experiment includes the following cases:

(1) Uniaxial Static Test (1)

(2) Uniaxial Fatigue Tests (21)

(3) Torsion Static Test (2)

(4) Torsion Fatigue Tests (19)

(5) Combined Uniaxial and Torsional Static Test with the Strain Ratio A of 2:1 (1)

(6) Combined Uniaxial and Torsional Synchronous Fatigue Tests with the Strain Ratio A of 2:1 (8)

(7) Combined Uniaxial and Torsional Static Test with the Strain Ratio A of 1:1 (1)

(8) Combined Uniaxial and Torsional Synchronous Fatigue tests with the Strain Ratio A of 1:1 (3)

(9) Combined Uniaxial and Torsional Static Test with the Strain Ratio A of 3:1 (1)

(10) Combined Uniaxial and Torsional Synchronous Fatigue Tests with the Strain Ratio A of 3:1 (3)

(11) Combined Uniaxial and Torsional Nonsynchronous Fatigue Tests with the Phase Angle ϕ of 90° and the Strain Ratio A of 2:1 (8)

(12) Combined Uniaxial and Torsional Nonsynchronous Fatigue Tests with the Phase Angle ϕ of 45° and the Strain Ratio A of 2:1 (8)

The numbers in the parentheses represent the numbers of tests.

Methods of analysis of experimental results were referred to Refs. [103],[107].

§4.2 Uniaxial Tests

Among all the tests the uniaxial test is fundamental. Especially, the uniaxial static test (tension test) gives the basic data of the material.

(1) Uniaxial Static Test (Tension Test)

Both the conventional and the true stress-strain curves were plotted in Fig.4.1 in the regular scale and in Fig.4.2 in the log-log scale. The numerical data were written in Table 4.1.

The stress was calculated from the reading of the strain indicator connected to the strain gages put on the load cell.

The strain was calculated from the reading of the strain indicator connected to the strain gages put on the specimen.

The origin of the stress-strain curve was adjusted.

The true stress was calculated by the formula

$$\sigma'=\sigma(1+\varepsilon) \qquad (4.1)$$

and the true strain was calculated by the formula

$$\delta=\log_e(1+\varepsilon) \qquad (4.2)$$

where σ and σ' represent the conventional and the true stresses, respectively, and ε and δ the conventional and the true strains, respectively.

From the conventional stress-strain curve in Fig.4.1, the following basic data of the material were obtained:

Young's Modulus: $E=9 \times 10^6$ psi.

Yield Strength : $\sigma_y=71000$ psi.

Tensile Strength: $\sigma_u=81500$ psi.

Ductility : $\varepsilon_f=12$ %, $\delta_f=11.13$ %

From the log-log true stress-strain line in Fig.4.2 the material constants were obtained as below:

Strain-hardening Exponent : $n_t=0.109$

Strength Coefficient : $k_t=115700$ psi.

Table 4.1

Results of the Tension Test, No.1.

Conventional Stress σ psi	True Stress σ' psi	Conventional Strain ε in/in	True Strain δ in/in
0	0	0	0
-8640	-8640	-0.000926	-0.000898
11390	11400	0.00123	0.00120
24750	24800	0.00277	0.002796
40500	40700	0.00455	0.00449
58900	59300	0.00647	0.00648
72300	73000	0.00918	0.00916
73100	74500	0.01844	0.01822
75800	77800	0.02602	0.02565
77000	79600	0.03432	0.0337
79750	83400	0.04612	0.0450
79750	83900	0.05172	0.0504
79750	84900	0.06532 *	0.0633
80600	86300	0.0707	0.0684
81000	87400	0.0790 **	0.0760
81000	88000	0.0867	0.0831
81000	88700	0.0952	0.0909
81000	89400	0.1037	0.0990
81700	90900	0.1121	0.1060
81700	91000	0.1142	0.1080
81700	91500	0.12	0.1131

*: From Strain Gage Reading
**: From Dial Gage Reading

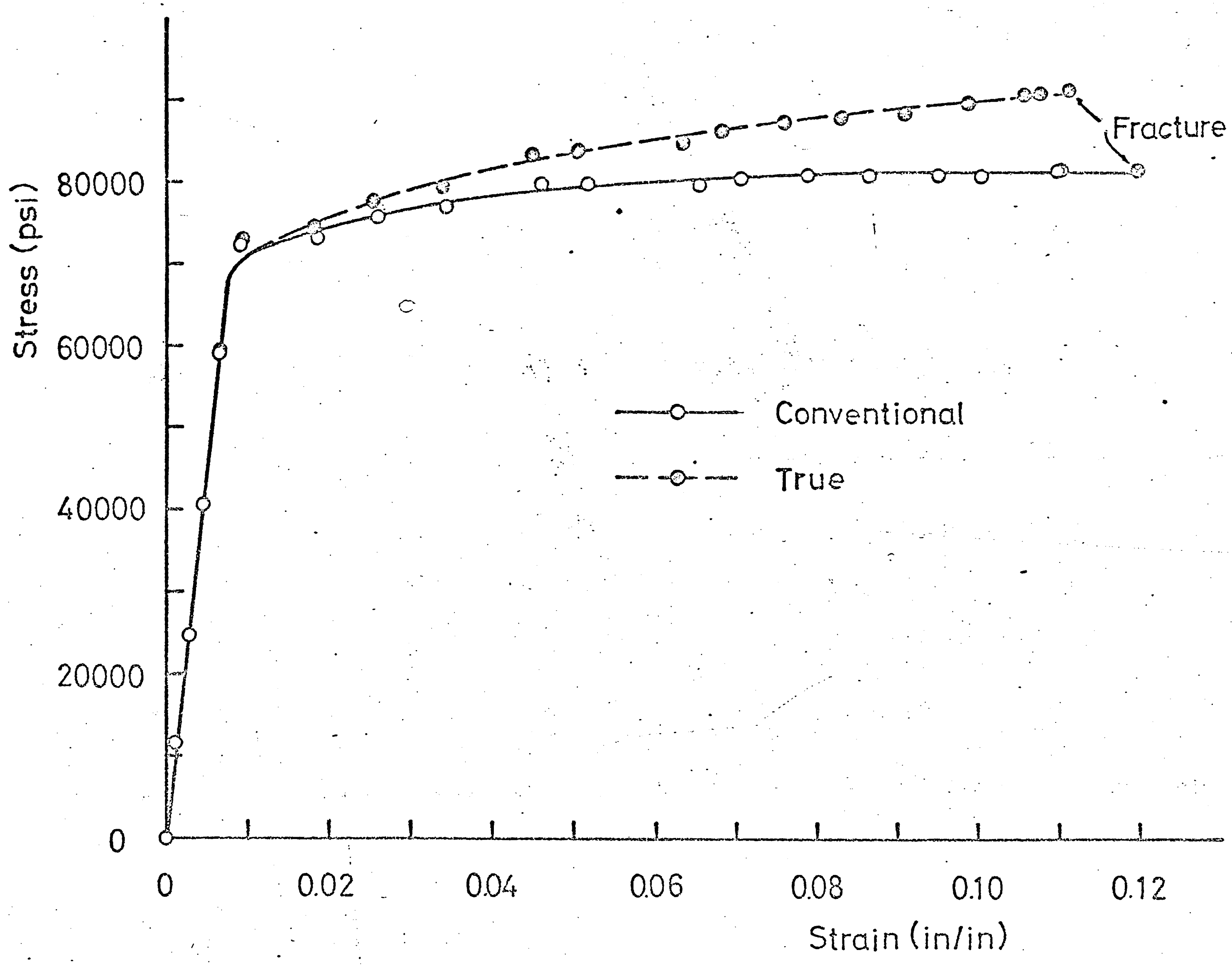

Fig. 4.1 Stress-Strain Curve for a Tension Test.

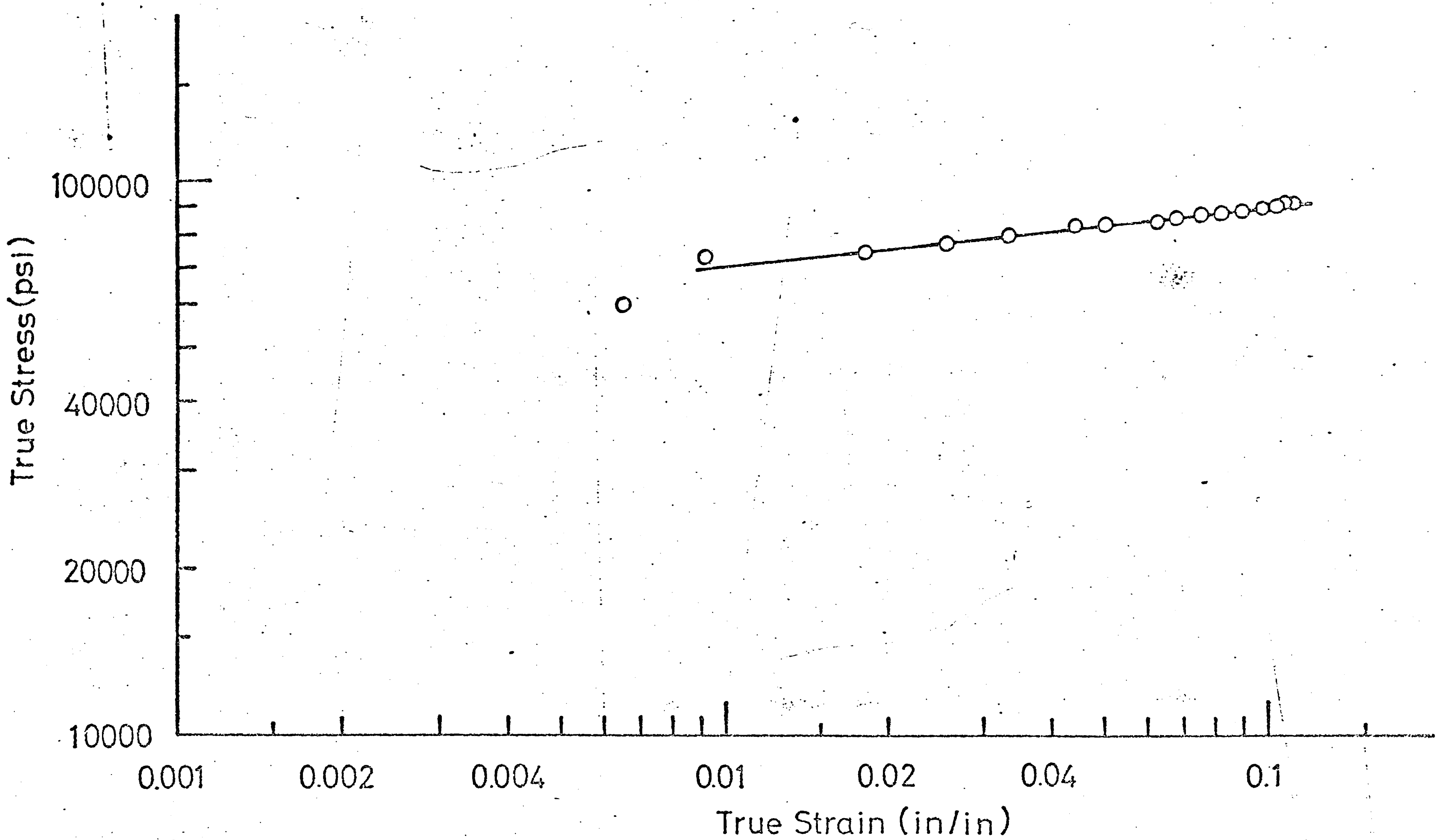

Fig. 4.2 Logarithmic True Stress-Strain Tensile Relation.

(2) Uniaxial Fatigue Tests

Twenty-one fatigue tests were conducted including the static test which corresponds to N =1/4, $\Delta\delta=2\delta_f$, [9] where N represents the number of cycles to fracture and $\Delta\delta$ the true strain range.

The number of cycles to fracture vs. the true strain range were plotted on the log-log graph paper as shown in Fig.4.3. The numerical data were written in Table 4.2 together with the corresponding octahedral shear strain ranges and the true stress ranges.

The strain range was obtained from the range of the extensometer reading by extraporating the static range in the diagram Fig.3.13 between the extensometer reading and the micrometer reading of the telescopic gage.

The octahedral shear strain range was calculated by

$$\Delta\gamma_{oct}=\sqrt{2}\ \Delta\delta \qquad (4.3)$$

These were plotted later in Fig.4.11 with the combined case.

Fracture was defined to be abrupt considerable reduction of stress on the pen-recorder when a pretty big sound was heard. Crack propagated from 70 %-90 % of the number of cycles to fracture. However, no considerable stress reduction could not be seen on the pen-recorder during the crack propagation. Position of the crack initiation was not definite for the cycles for lower cycles, while for higher cycles the crack initiated on the boundary between the straight portion and the curved portion. This may be because of the stress concentration.

In Fig.4.3, the experimental points were connected into one straight line given by

$$\Delta\delta N^{\alpha_t}=C_t \qquad (4.4)$$

where α_t=0.28 and C_t=0.13 including N=1/4, and α_t=0.24, and C_t=0.10

Table 4.2

Results of the Uniaxial Fatigue Tests

Run No.	No.of Cycles to Fracture N	True Strain Range, $\Delta\delta$ (=Max. Principal Strain Range,$\Delta\varepsilon max$) (in/in)	Octahedral Shear Strain Range,$\Delta\gamma_{oct}$ (in/in)
1'	1/4	0.2262	0.32
5	18	0.0601	0.0850
6	468	0.0247	0.0350
7	460	0.0247	0.0350
8	1913	0.0139	0.0197
9	10	0.0564	0.0797
10	39	0.0385	0.0545
11	316	0.0268	0.0380
12	212	0.0277	0.0392
13	759	0.0216	0.0306
14	679	0.0231	0.0327
15	727	0.0218	0.0309
16	487	0.0203	0.0287
17	739	0.0215	0.0304
18	298	0.0253	0.0357
19	142	0.0275	0.0389
20	218	0.0279	0.0395
21	45	0.0338	0.0478
22	1196	0.0171	0.0241
23	2169	0.0175	0.0248
24	14	0.0455	0.0643

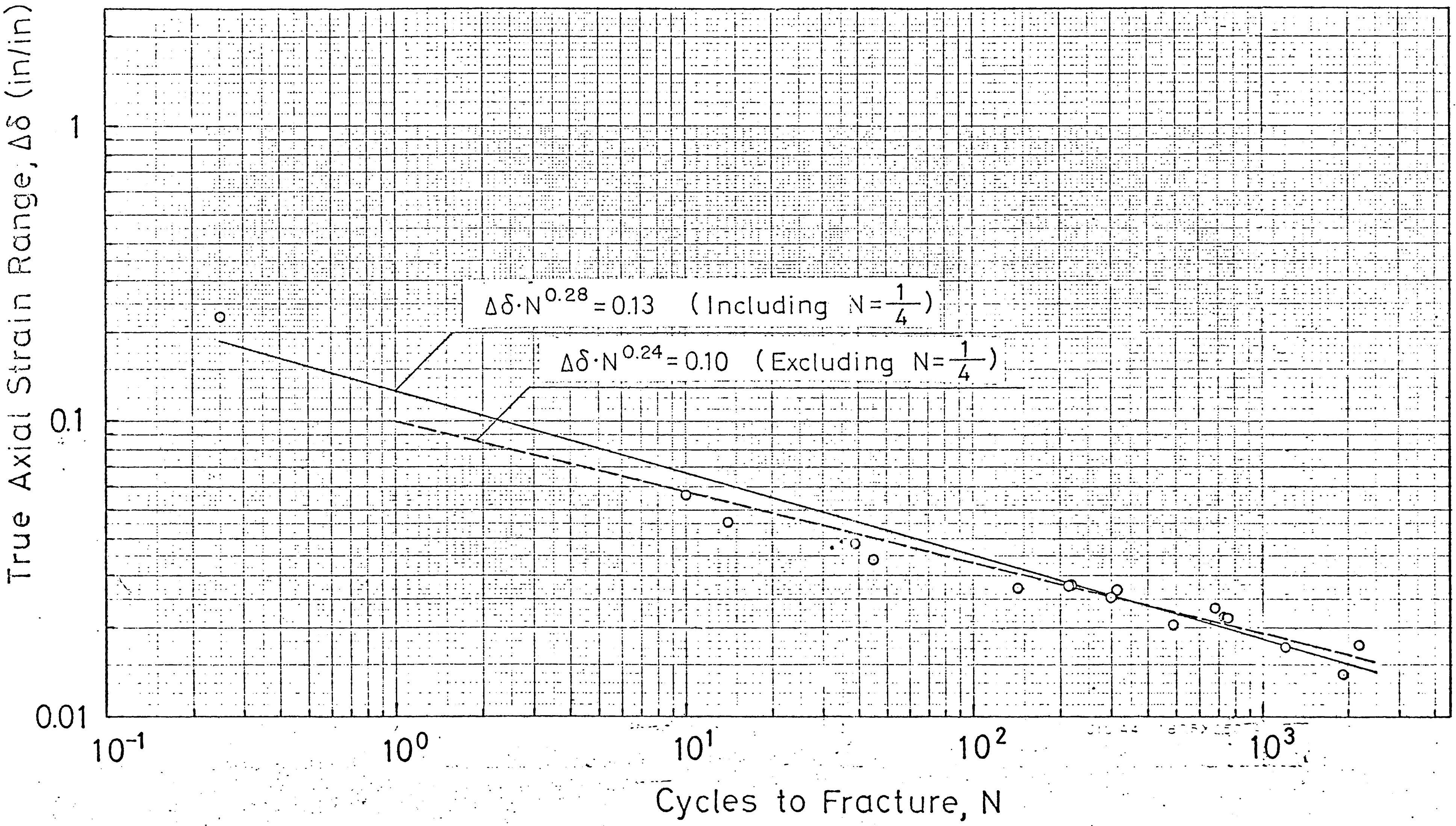

Fig. 4.3 Relationship between True Axial Strain Range and Number of Cycles to Fracture for Uniaxial Fatigue Tests.

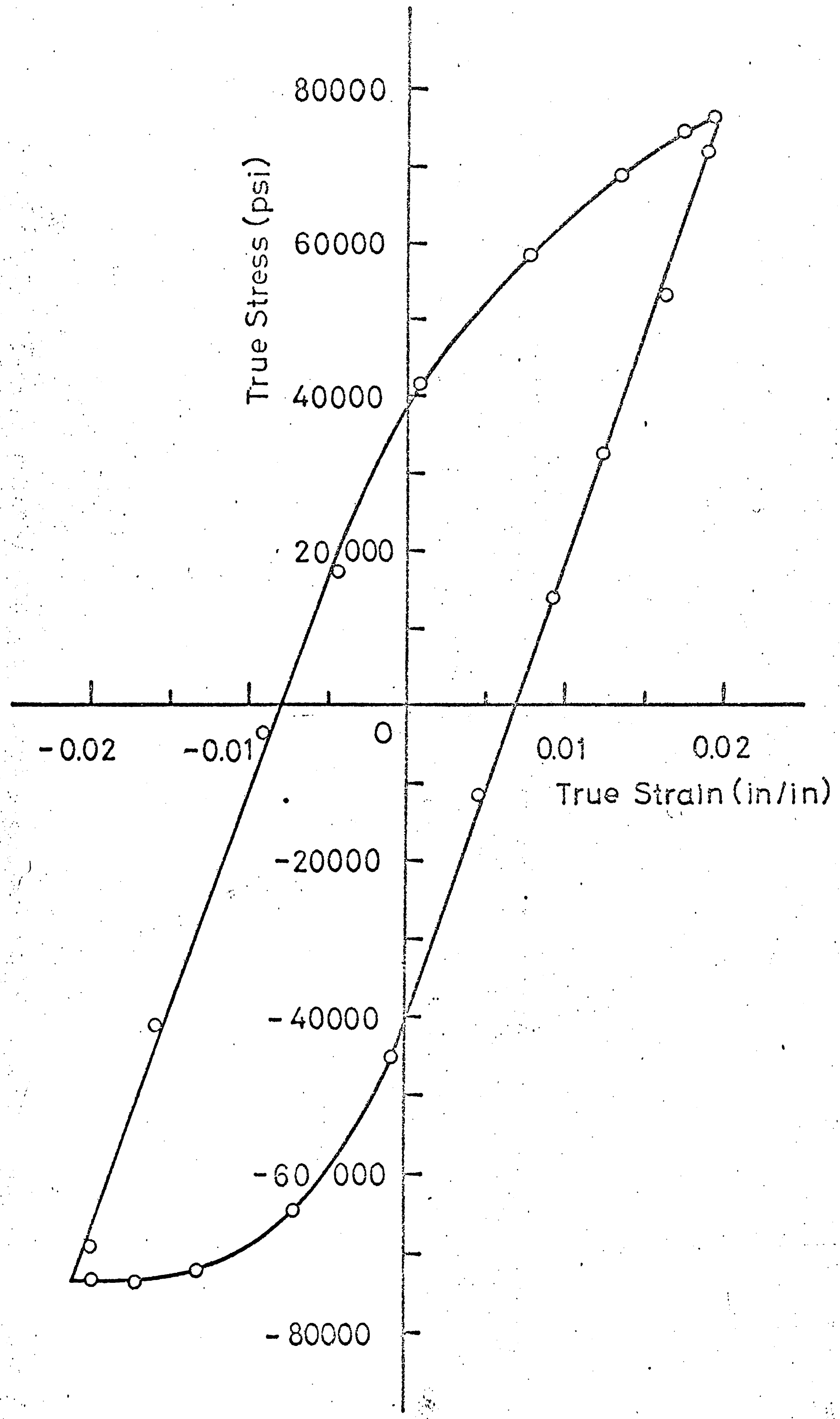

Fig. 4.4 True Stress-Strain Hysteresis Curve for the Uniaxial Fatigue Test of No.10.

Uniaxial Test No. 9, N=10

Uniaxial Test No.10, N=39

Uniaxial Test No.11, N=316

Uniaxial Test No.12, N=212

Photo. 4.1 Specimens after Uniaxial Tests excluding N=1/4. These values were obtained by the method of least square.

For the cycles less than about 100, the experimental points were found to drop below the line. This is because of the fact that the buckling mode appeared after some number of cycling and this mode became bigger and bigger, therefore, the real local strain became higher than calculated from the die set movement. This fact can be supported by observing the specimens after the test as shown in Photo.4.1.

On the other hand, Manson and Hirschberg [92] got α=0.5. The discrepancy may be caused by how to obtain the true strain. In the study in this thesis, the true strain was rather averaged along the gage length because the strain was calculated from the die set movement, while in Manson-Hirschberg's work, the local true strain was directly measured from the reduction of area.

The cyclic hysteresis loop of Run No. 10 is shown in Fig.4.4. The third cycle of N=39 has been chosen, because for earlier cycle the loop was not stable, while for later cycle the strain gage was deteriorated. According to Ref.[108] the stress-strain curve becomes stable in the cycles less than several percent of number of cycles to fracture.

In Fig.4.4, cyclic strain-hardening exponents were calculated to be 0.35 for tension and 0.21 for compression.

§4.3 Torsion Test

Totally nineteen torsion tests were conducted, but two of them ran out.

(1) Static Torsion Test.

Two static torsion tests were done. The torsion stress-strain curve was drawn for one of the two tests in which the better strain gage was used. This curve is shown in Fig.4.5 in the regular scale and in Fig.4.6 in the log-log scale. The nemerical data was listed in Table 4.3. By this test, the following results were obtained:

Shear Modulus: $G=3.36 \times 10^6$ psi. (Obserbed)

3.38×10^6 psi. (Calculated from the Young's Modulus)

Yield Stress: $\gamma_y=34800$ psi.

Ultimate Stress: $\gamma_u=43700$ psi.

Fracture Strain: $\gamma_f=0.38$

Yield Twisting Moment: $M_y=3012$lb-in

Ultimate Twisting Moment: $M_u=3784$lb-in.

Fracture Angle of Twist: $\theta_f=0.806$ rad. (41°)

Strain-hardening Expenent: $n_s=0.124$

Strength Coefficient: $k_s=566000$ psi.

The shear stress was obtained from the strain gages put on the load cell and the smaller shear strains from the strain gage put on the specimen. The fracture angle of twist was read on the protractor set up between the gage length, and then, from this value, the fracture strain was calculated. For large angle of twist, the shear strain obtained from the rosette strain gage did not show the real value, therefore, the strain was calculated from the angle of twist obserbed by the formula

$$\gamma_{xy}=\frac{r\theta}{L} \tag{4.5}$$

where γ_{xy} denotes the shear strain, r the ratius of the specimen, θ the angle of twist, and L the gage length.

The twisting moment was calculated, from the shear stress obtained, from the shear stress obtained, by the formula

$$M_t=2\pi r^2 h \tag{4.6}$$

This was checked by the moment obtained from the pressure gages set up at the pressure ports of the rotary actuator.

The shear modulus obtained from the experimental stress-strain

Table 4.3

Results of the Torsion Test, No.1'.

Shearing Stress τ psi	Shear Strain γ in/in	Twisting Moment Mt lbin	Angle of Twist θ degree
0	0	0	0
688	0.000817	59.6	0
6196	0.00297	536	0.3
19620	0.00631	1698	1
21320	0.00706	1847	1
35100	0.0144	3040	2.1
36120	0.0297	3130	4
38200	0.0443	3310	5.8
38540	0.0587	3338	7.3
42320	0.0832	3604	10.3
43000	0.108	3724	12.1
43000	0.1129 *	3724	14
43700	0.1277	3784	16
43360	0.1558 **	3753	17
42320	0.1823	3660	19.9
42000	0.19975	3635	21.8
41260	0.2181	3576	23.8
40600	0.2566	3516	28
40260	0.2932	3488	30.2
37840	0.30145	3280	32.9
35800	0.3848	3100	42
35100	0.4004	3040	43.7
	0.4233		

* : From Strain Gage Reading
**: From Twisting Angle Reading

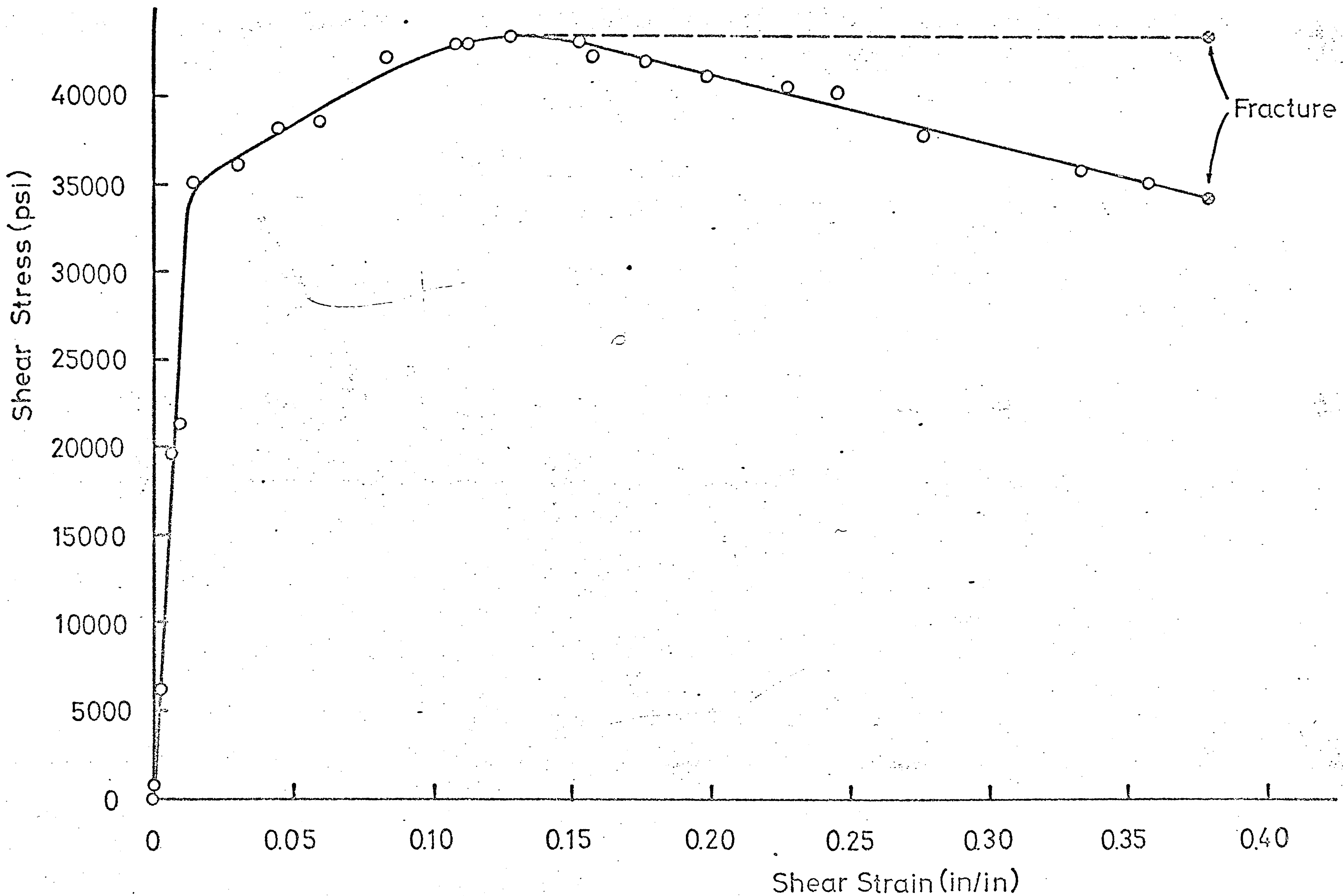

Fig. 4.5 Shear Stress-Strain Curve for a Torsion Test.

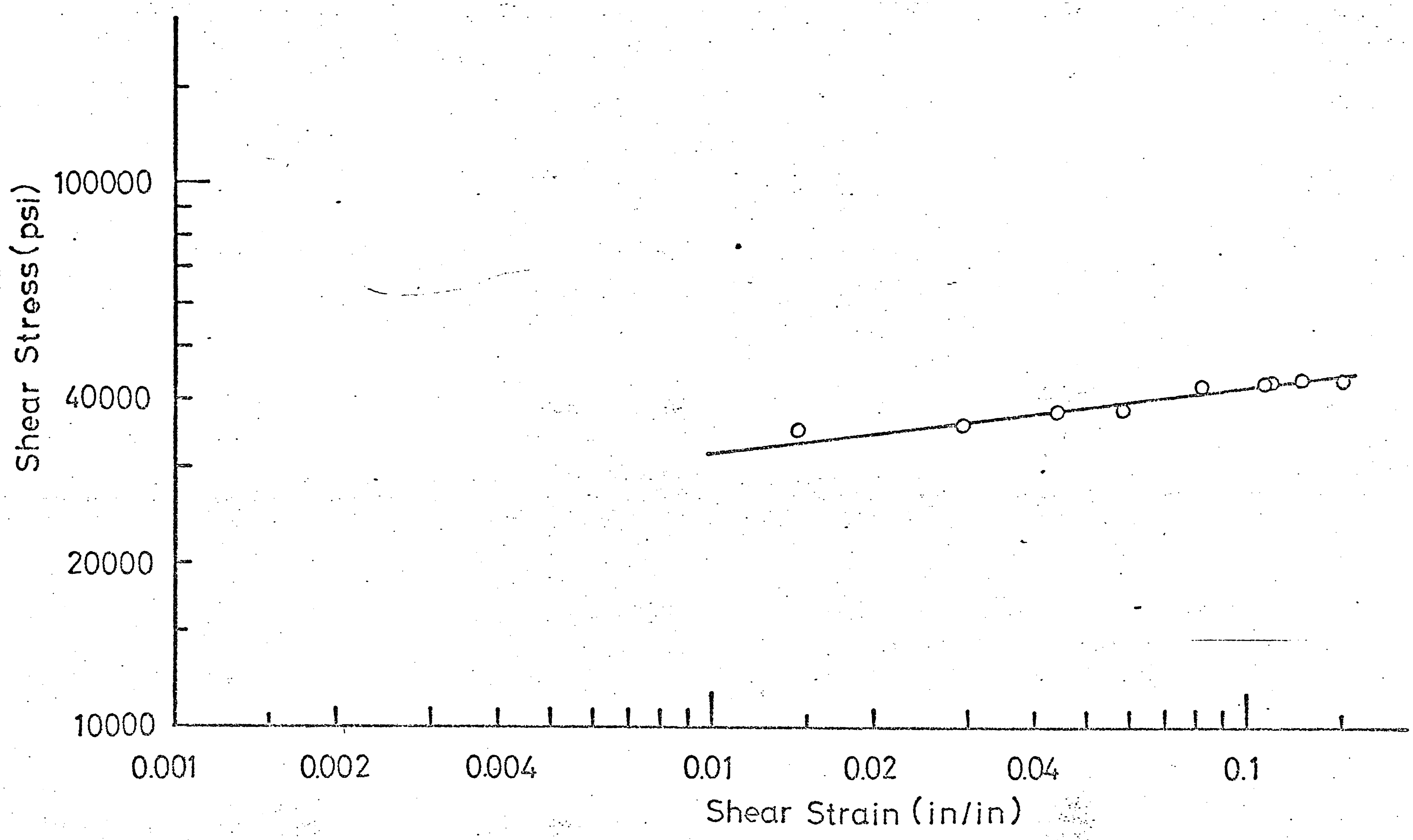

Fig. 4.6 Logarithmic Shear Stress-Strain Relation in Torsion.

curve was compared with the calculated value from the Young's Modulus obtained from the tension test by the formula

$$G=\frac{E}{2(1+\nu)} \tag{4.7}$$

The negative slope of the stress-strain curve after the maximum stress is reached seems to be because of twisting buckling caused by the principal compressive strain.

The octahedral shear strain at fracture, also was calculated for the purpose of comparing with other states of strains and was listed in Table 4.4 and was plotted on Fig.4.7 as fatigue data.

(2) Torsion Fatigue Test

Nineteen torsion tests including two static torsion tests were conducted. Two of them resulted to run out. The shear strain ranges vs. the number of cycles to fracture were plotted in Fig.4.7 in the log-log scale. The numerical data were listed in Table 4.4, in which the octahedral shear strain range, the principal strain range, and the shear stress range were also written. The octahedral and proncipal strains were calculated by

$$\Delta\gamma_{oct}=\frac{\sqrt{6}}{3}\Delta\gamma_{xy} \tag{4.8}$$

$$\Delta\varepsilon_{max}=\frac{\Delta\gamma_{xy}}{2} \tag{4.9}$$

respectively.

The shear strain ranges were calculated from the angle of twist read on the protractor between the gage length. Relationship between the shear strain and the angle of twist was also calibrated in the static test.

In Fig.4.7 the linear relationship between the shear strain range and the number of cycles to fracture in the log-log scale was obtained as

Table 4.4

Results of the Torsion Fatigue Tests

Run No.	No. of Cycles to Fracture, N	Shear Strain Range $\Delta\gamma$ in/in	Octahedral Shear Strain Range, $\Delta\gamma_{oct}$ in/in	Max. Principal Strain Range $\Delta\varepsilon$ max. in/in
1	1/4	0.67806	0.554	0.33903
1'	1/4	0.84666	0.691	0.42333
2	96	0.05772	0.0471	0.02886
3	45	0.0944	0.0771	0.0472
4	68	0.0714	0.0583	0.0357
5	99	0.0714	0.0583	0.0357
6	84	0.0697	0.0570	0.03485
7	27	0.1081	0.0883	0.05405
8	21	0.1081	0.0883	0.05405
9	29	0.11	0.0898	0.055
10	375	0.042	0.0343	0.021
11	357	0.042	0.0343	0.021
12	198	0.0476	0.0389	0.0238
13	143	0.0476	0.0389	0.0238
14	Run Out	0.0229	0.0187	0.01145
15	Run Out	0.0229	0.0187	0.01145
16	2000	0.0306	0.02507	0.01535
17	517	0.0375	0.0306	0.01875
18	610	0.0375	0.0306	0.01875

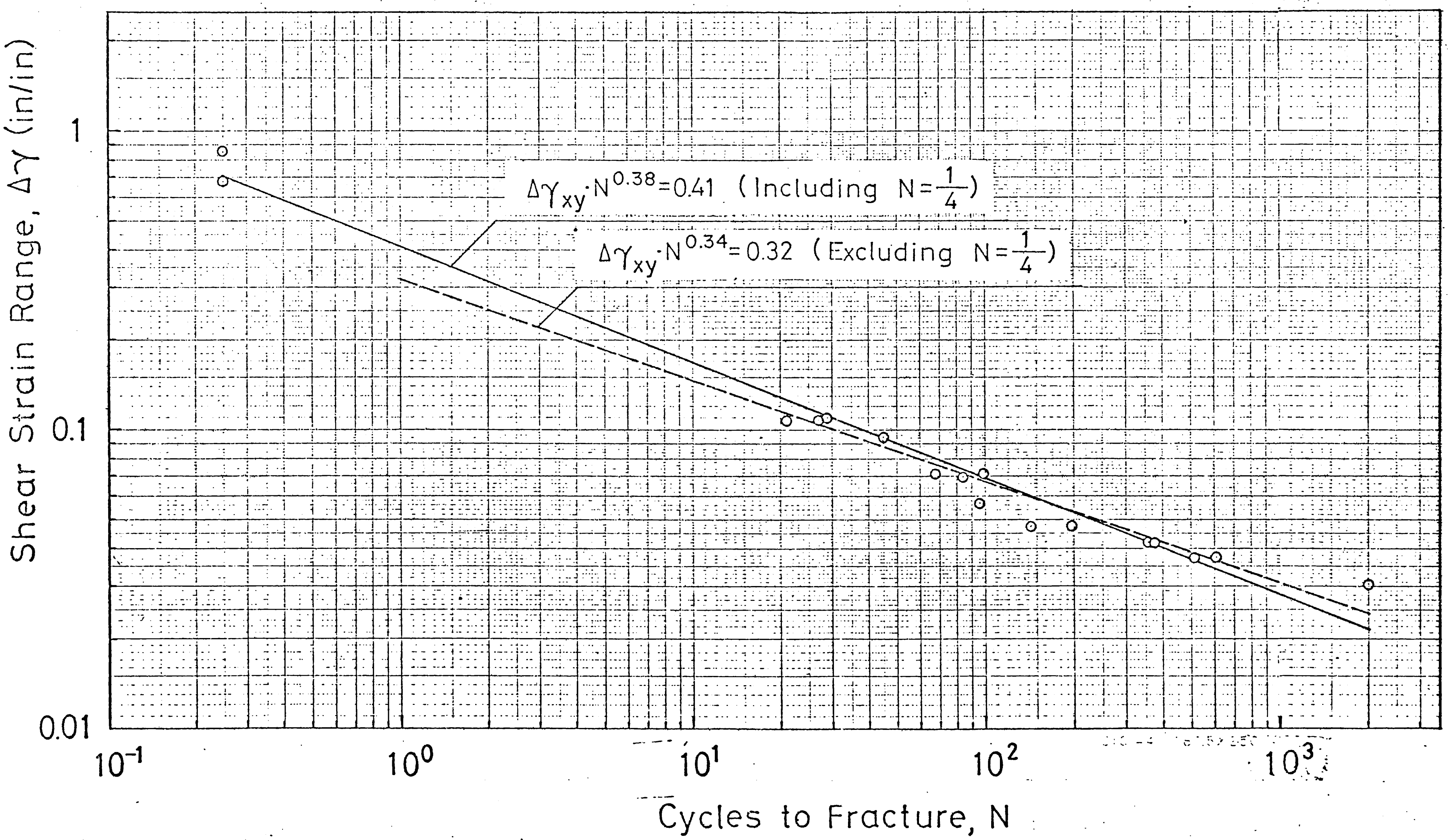

Fig. 4.7 Relationship between Shear Strain Range and Number of Cycles to Fracture for Torsion Fatigue Tests.

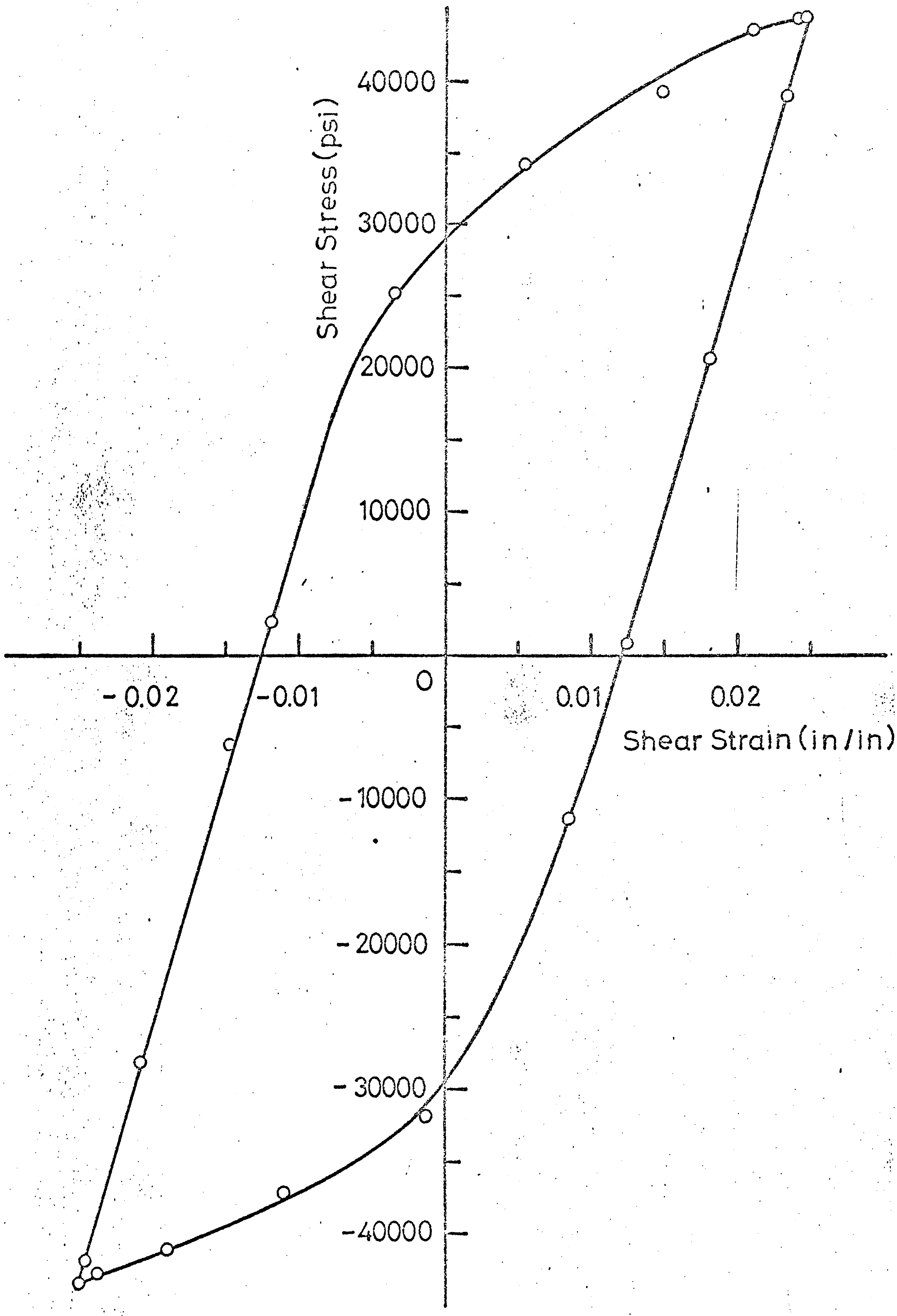

Fig. 4.8 Shear Stress-Strain Hysteresis Curve for the Torsion Fatigue Test of No.4.

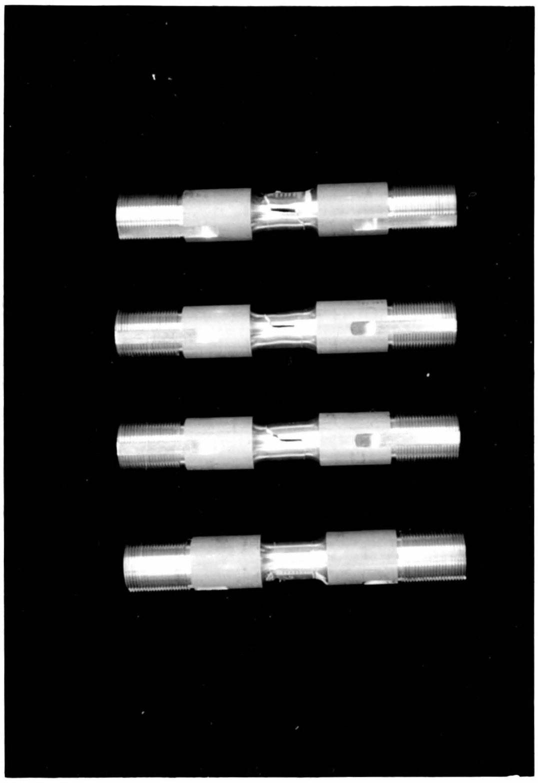

Torsion Test No. 7, N=27

Torsion Test No. 8, N=21

Torsion Test No. 9, N=29

Torsion Test No.10, N=375

Photo. 4.2 Specimens after Torsion Tests

$$\Delta\gamma_{xy} N^{\alpha_s} = C_s \qquad (4.10)$$

where the slope of the straight line α_s is 0.38 and the intercept C_s is 0.41 when N=1/4 is included, and α_s is 0.34 and C_s is 0.32 when N=1/4 is excluded.

Fracture was determined by considerable reduction of stress.

Previously, Halford and Morrow [33] obtained the expression as

$$\Delta\gamma_p N^{\frac{1}{2}} = C \qquad (4.11)$$

for the solid specimen of 75S alluminum alloy, where $\Delta\gamma_p$ denotes the plastic shear strain range. For low cycle range, difference between the total and the plastic strains is negligible. The discrepancy of these slopes may be caused by the bucking mode of tubler specimen.

Crack initiated at the crossing point of two hills caused by the compressive principal stress for large strain and crack propagated along the direction of axis for all torsional tests.

The octahedral shear strain ranges vs. the numbers of cycles to fracture were plotted in the log-log scale later in Fig.4.11 to compare other strain conditions.

A typical cycling shear stress-strain curve was plotted in Fig. 4.8. From Fig.4.8, the cyclic strain-hardening exponents were obtained to be n_s=0.212 and 0.270. Stress and strain were obtained from the strain gages.

§4.4 Derivation of the Principal Stress and Strain and the Octahedral Shear Stress and Strain for the Combined Axial and Torsional Case

Before analysing the experimental data, one needs to have the expression of the principal stress and strain and the octahedral shear stress and strain by means of the axial stress and strain and the torional shear stress and strain, respectively, as follows:

For the combined axial and torsional case,

$$\begin{aligned} \varepsilon_x &= \varepsilon_x , \quad \gamma_{xy}=\gamma_{xy} \\ \varepsilon_y &= -\frac{1}{2} , \quad \gamma_{yz}=0 \\ \varepsilon_z &= -\frac{1}{2} , \quad \gamma_{xz}=0 \end{aligned} \tag{4.12}$$

By solving

$$\begin{vmatrix} \varepsilon_x - S & \gamma_{xy}/2 & \gamma_{xz}/2 \\ \gamma_{xy}/2 & \varepsilon_y - S & \gamma_{yz}/2 \\ \gamma_{xz}/2 & \gamma_{yz}/2 & \varepsilon_z - S \end{vmatrix} = 0 \tag{4.13}$$

or

$$S^3-(\varepsilon_x+\varepsilon_y+\varepsilon_z)S^2+(\varepsilon_x\varepsilon_y+\varepsilon_y\varepsilon_z+\varepsilon_x\varepsilon_z-\frac{\gamma^2{}_{yz}}{4}-\frac{\gamma^2{}_{xz}}{4}-\frac{\gamma^2{}_{xy}}{4})S$$

$$-(\varepsilon_x\varepsilon_y\varepsilon_z+\frac{\gamma_{yz}\gamma_{xz}\gamma_{xy}}{4}-\frac{\varepsilon_x\gamma^2{}_{yz}}{4}-\frac{\varepsilon_y\gamma^2{}_{xz}}{4}-\frac{\varepsilon_z\gamma^2{}_{xy}}{4})=0 , \tag{4.14}$$

the principal strains become

$$\begin{aligned} \varepsilon_1 &= \frac{1}{4}\varepsilon_x+\frac{1}{4}\sqrt{9\varepsilon_x^2+4\gamma^2{}_{xy}} \\ \varepsilon_2 &= \frac{1}{4}\varepsilon_x-\frac{1}{4}\sqrt{9\varepsilon_x^2-4\gamma^2{}_{xy}} \\ \varepsilon_3 &= -\frac{1}{2}\varepsilon_x \end{aligned} \tag{4.15}$$

The octahedral shear strain for general case [107] is

$$\gamma_{oct}=\frac{2}{3}[(\varepsilon_1-\varepsilon_2)+(\varepsilon_2-\varepsilon_3)^2+(\varepsilon_3-\varepsilon_1)^2]^{1/2} \tag{4.16}$$

For biaxial case, Eq. (4.16) turns out under consideration of incompressibility, i.e.

$$\varepsilon_1+\varepsilon_2+\varepsilon_3=0 \tag{4.17}$$

as

$$\gamma_{oct}=\frac{2\sqrt{6}}{3}[\varepsilon_1{}^2+\varepsilon_1\varepsilon_2+\varepsilon_2{}^2]^{1/2} \tag{4.18}$$

Substituting Eq. (4.15) into Eq. (4.18), one gets

$$\gamma_{oct}=\frac{\sqrt{6}}{3}[3\varepsilon_x{}^2+\gamma_{xy}{}^2]^{1/2} \tag{4.19}$$

In cycling, the strains are expressed by

$$\begin{aligned} \varepsilon_x &= \Delta\varepsilon_x \sin \omega t \\ \gamma_{xy} &= \Delta\gamma_{xy} \sin (\omega t+\phi) \end{aligned} \tag{4.20}$$

Substituting Eq. (4.20) into Eq. (4.19), one obtains

$$\gamma_{oct}=\frac{\sqrt{6}}{3}[3\Delta\varepsilon_x^{\ 2}\ \sin^2\omega t+\Delta\gamma_{xy}^{\ 2}\ \sin^2(\omega t+\phi)]^{1/2} \tag{4.21}$$

To get the time when the octahedral shear strain becomes maximum one lets

$$\frac{d\gamma_{oct}}{dt}=0 \tag{4.22}$$

then

$$\tan 2\omega t'=-\frac{\Delta\gamma^2_{xy}\ \sin 2\phi}{3\Delta\varepsilon^2_x+\Delta\gamma^2_{xy}\ \cos 2\phi} \tag{4.23}$$

For synchronous case, $\phi=0$, the octadedral shear strain is maximum, when sin ωt is maximum.

For $\phi=\frac{\pi}{2}$, Eq. (4.23) turns out as

$$\tan 2\omega t'=0 \tag{4.24}$$

then

$$t'=0,\ \frac{\pi}{2},\ \ \pi,\ \frac{3}{2}\pi\ ,\ \cdots \tag{4.25}$$

For $\sqrt{3}\Delta\varepsilon_x>\Delta\gamma_{xy}$, the maximum occurs when $\omega t=\frac{\pi}{2},\ \frac{3}{2}\pi$,$\cdots$ and the maximum value is

$$\gamma_{oct,max}=\sqrt{2}\Delta\varepsilon_x=1.1414\varepsilon_x \tag{4.26}$$

and at this time

$$\varepsilon_{1,2}=\Delta\varepsilon_x,-\Delta\varepsilon_x/2 \tag{4.27}$$

and for $\sqrt{3}\Delta\varepsilon_x<\Delta\gamma_{xy}$, the maximum occurs when $\omega t=0,\ \pi,\cdots$ and the maximum value is

$$\gamma_{oct,max}=\frac{\sqrt{6}}{3}\Delta\gamma_{xy}=0.8165\Delta\gamma_{xy} \tag{4.28}$$

and at this time

$$\varepsilon_{1,2}=\pm\frac{\Delta\gamma}{2}xy \tag{4.29}$$

For $\phi=\frac{\pi}{4}$, Eq. (4.23) turns out as

$$\tan 2\ \omega t'=-\frac{\Delta\gamma^2_{xy}}{3\Delta\varepsilon^2_x} \tag{4.30}$$

and at this time,

$$\gamma_{oct,max}=\frac{1}{\sqrt{3}}[3\Delta\varepsilon_x^{\ 2}(1-\cos 2\omega t')+\Delta\gamma^2_{xy}(1+\sin 2\omega t')]^{1/2} \tag{4.31}$$

$$\varepsilon_{1,2}=\frac{\sqrt{2}}{8}[\Delta\varepsilon_x\sqrt{1-\cos 2\omega t'}\pm\sqrt{9\Delta\varepsilon_x^2(1-\cos 2\omega t')+4\Delta\gamma_{xy}^2(1+\sin 2\omega t')}] \qquad (4.32)$$

$\omega t'$ should be carefully chosen so as γ_{oct} is maximum.

For true strain expressions, one has only to change ε into δ, where

$$\delta=\log_e(1+\varepsilon) \qquad (4.2)$$

For the combined axial and torsional case,

$$\sigma_y=\sigma_z=\tau_{xy}=\tau_{yz}=0 \qquad (4.33)$$

Then, the principal stresses are

$$\sigma_1=\frac{\sigma_x}{2}+\sqrt{\frac{\sigma_x^2}{4}+\tau^2_{xy}}$$

$$\sigma_2=\frac{\sigma_x}{2}-\sqrt{\frac{\sigma_x^2}{4}+\tau^2_{xy}} \qquad (4.34)$$

$$\sigma_3=0$$

The octahedral shear stresses for general case [107] is

$$\tau_{oct}=\frac{1}{3}[(\sigma_1-\sigma_2)^2+(\sigma_2-\sigma_3)^2+(\sigma_3-\sigma_1)^2]^{1/2} \qquad (4.35)$$

For biaxial case, Eq. (4.35) turns out as

$$\tau_{oct}=\frac{\sqrt{2}}{3}[\sigma_1^2+\sigma_2^2+\sigma_1\sigma_2]^{1/2} \qquad (4.36)$$

Substituting Eq. (4.34) into Eq. (4.36), one obtains

$$\tau_{oct}=\frac{\sqrt{2}}{3}[\sigma_1^2+3\tau^2_{xy}]^{1/2} \qquad (4.37)$$

In cycling, the stresses are expressed by

$$\sigma_x=\Delta\sigma_x \sin\omega t$$

$$\tau_{xy}=\Delta\tau_{xy} \sin(\omega t+\phi) \qquad (4.38)$$

Substituting Eq. (4.38) into Eq. (4.37), one obtains

$$\tau_{oct}=\frac{\sqrt{2}}{3}[\Delta\sigma_x^2 \sin^2\omega t+3\Delta\tau_{xy}^2 \sin^2(\omega t+\phi)]^{1/2} \qquad (4.39)$$

To get the time when the octahedral shear stress becomes maximum, one gets

$$\frac{d\tau_{oct}}{dt}=0 \qquad (4.40)$$

then

$$\tan 2\omega t'=-\frac{3\Delta\tau^2_{xy} \sin 2\phi}{\Delta\sigma^2_x+3\Delta\tau^2_{xy} \cos 2\phi} \qquad (4.41)$$

For the synchronous case, $\phi=0$, the octahedral shear stress is maximum, when $\sin\omega t$ is maximum.

For $\phi=\frac{\pi}{2}$, Eq. (4.41) turns out as

$$\tan 2\omega t'=0 \tag{4.42}$$

For $\Delta\sigma_x>\sqrt{3}\Delta\tau_{xy}$, the maximum occurs when $\omega t'=\frac{\pi}{2}, \frac{3}{2}\pi, \cdots$ and the maximum value is

$$\tau_{oct,max}=\frac{\sqrt{2}}{3}\Delta\sigma_x \tag{4.43}$$

For $\Delta\sigma_x<\sqrt{3}\Delta\tau_{xy}$, the maximum occurs when $\omega t'=0, \pi, \cdots$ and the maximum value is

$$\tau_{oct,max}=\frac{\sqrt{6}}{3}\Delta\tau_{xy} \tag{4.44}$$

For $\phi=\frac{\pi}{4}$ Eq. (4.41) turns out as

$$\tan 2\omega t'=-\frac{3\Delta\tau^2_{xy}}{\Delta\sigma^2_x} \tag{4.45}$$

In general, the times for the maximum octahedral strain and stress do not coincide.

§4.5 Combined Axial and Torsional Synchronous Test

The combined axial and torsional tests conducted are devided into following three cases:

(1) Synchronous tests with the torsional to axial strain ratio A of 2:1 as the standard combined test,

(2) Synchronous tests with the torsional to axial strain ratio A of 1:1 and 3:1 to know the effect of strain ratio, and

(3) Nonsynchronous tests with the torsional to axial strain ratio A of 2:1 and with the phase angle ϕ of 45° and 90° to know the effect of phase difference.

In this section, the static and fatigue tests of cases (1) and (2) are analyzed and discussed. Case (3) will be analyzed and discussed in §4.6.

(1) Static Combined Test

Three static combined tests were done. One of them has the shear to axial strain ratio A of 2:1; one does that of 3:1; the other does that of 1:1.

The important data in these tests as the basis of the fatigue test are the fracture stress and strain, which are expressed by means of the octahedral stress and strain or the principal stress and strain and their strain data were obtained as bellow:

Octahedral fracture shear strains:

$\gamma_{oct,f}=0.55$ for the strain ratio A of 2:1,

$\gamma_{oct,f}=0.34$ for the strain ratio A of 1:1, and

$\gamma_{oct,f}=0.56$ for the strain ratio A of 3:1,

Princial fracture strains:

$\varepsilon_{1f}=0.191$, $\varepsilon_{2f}=0.129$, $\varepsilon_{3f}=-0.062$ for the strain ratio of 2:1,

$\varepsilon_{1f}=0.121$, $\varepsilon_{2f}=0.067$, $\varepsilon_{3f}=-0.054$ for the strain ratio of 1:1,

$\varepsilon_{1f}=0.195$, $\varepsilon_{2f}=0.131$, $\varepsilon_{3f}=-0.064$ for the strain ratio of 3:1.

These data were plotted with the fatigue data in Figs.4.11, 4.12, and 4.13.

The octahedral shear stress-strain curve for the strain ratio A of 2:1 were plotted in Fig.4.9 in the regular scale and in Fig.4.10 in the log-log scale as a reference. The numerical data for this curve were listed in Table 4.5. The strain-hardening exponent and the strength coefficient were obtained from Fig.4.10 as $n_{oct}=0.117$ and $k_{oct}=50357$ psi. These values were compared with the values calculated from the static tension test as follows: $n_{oct}=0.109$, $k_{oct}=52600$ psi.

The principal and octahedral stress and strain were calculated by using Eqs. (4.15), (4.19), (4.34), and (4.37) from the axial true stress and strain and the torsional shear stress and strain obtained from the strain gages put on the load cell and the specimen, respectively.

The diagram showing the relationship between the die-set movement and the axial strain gage reading was plotted and used for

Table 4.5

Results of the Combind Static Test, No. 1.

Die-Set Mcvement D in	Conventional Axial Strain ε in/in	True Axial Strain δ in/in	Conventional Axial Stress σ psi	True Axial Stress σ' psi	Shear Strain γ_{xy} in/in	Shearing Stress τ psi	Angle of Twist θ degree	Twisting Memont M_t lbin	Octahedral Shear Strain γ oct in/in	Octahedral Shearing Stress τ oct psi
0	0	0	0	0	0	0	0	0	0	0
-0.009	-0.002017	-0.00378	-9030	-9010	-0.001169	-1720	-0.2	-149		
0.004	0.000789	0.00082	9430	9430	0.00251	10360	0.3	922	0.002358	19550
0.015	0.00263	0.00260	29050	29150	0.00566	22000	0.6	1906	0.00591	22600
0.023	0.005553	0.00569	36900	37130	0.01327	31300	1.6	2708	0.0135	31000
0.031	0.012125	0.01203	43600	44150	0.0282	32000	2.9	2768	0.02865	33400
0.037	0.01803	0.01785	44800	45600	0.0426	33000	3.6	2858	0.0398	34500
0.047	0.02795	0.0276	51800	53300	0.0590	33000	5.7	2858	0.0621	36800
0.0555	0.03642	0.0358	56600	58700	0.0704	33700	7.6	2858	0.0766	38600
0.063	0.0450	0.0440			0.0839		8.6	2918	0.0946	
0.072	0.053 *	0.0516	58500	61600	0.1046	32000	9.6	2708	0.1123	38700
0.081	0.062	0.0601	60500	64300	0.1119	28880	10.9	2768	0.1249	40000
0.091	0.072	0.0695	64400	69000	0.1259	29220	12.4	2500	0.1423	40100
0.094	0.075	0.0724	64400	69250	0.1479	26160	13.6	2530	0.1583	40400
0.102	0.083	0.0797	64400	69700	0.1508	26160	14.7	2262	0.167	(39200)
0.110	0.091	0.0871	68400	74600	0.162	27840	15.7	2262	0.181	41100
0.116	0.097	0.0926			0.1806	26160	16.7	2412	0.1972	
0.118	0.099	0.0945			0.192**	28880	17.7	2262	0.2058	
0.125	0.106	0.1008	64400	71200	0.2025	28560	18.7	2500	0.2182	41000
0.1525	0.13	0.1223		72700	0.261		24.6		0.2743	

For No.2 Specimen

* : From the Relationship Between the Dial Gage Reading and Strain Gage Reading, Fig.3.11(b)
** : From the Relationship Between the Twisting Angle Reading and Strain Gage Reading, Fig.3.12(a)

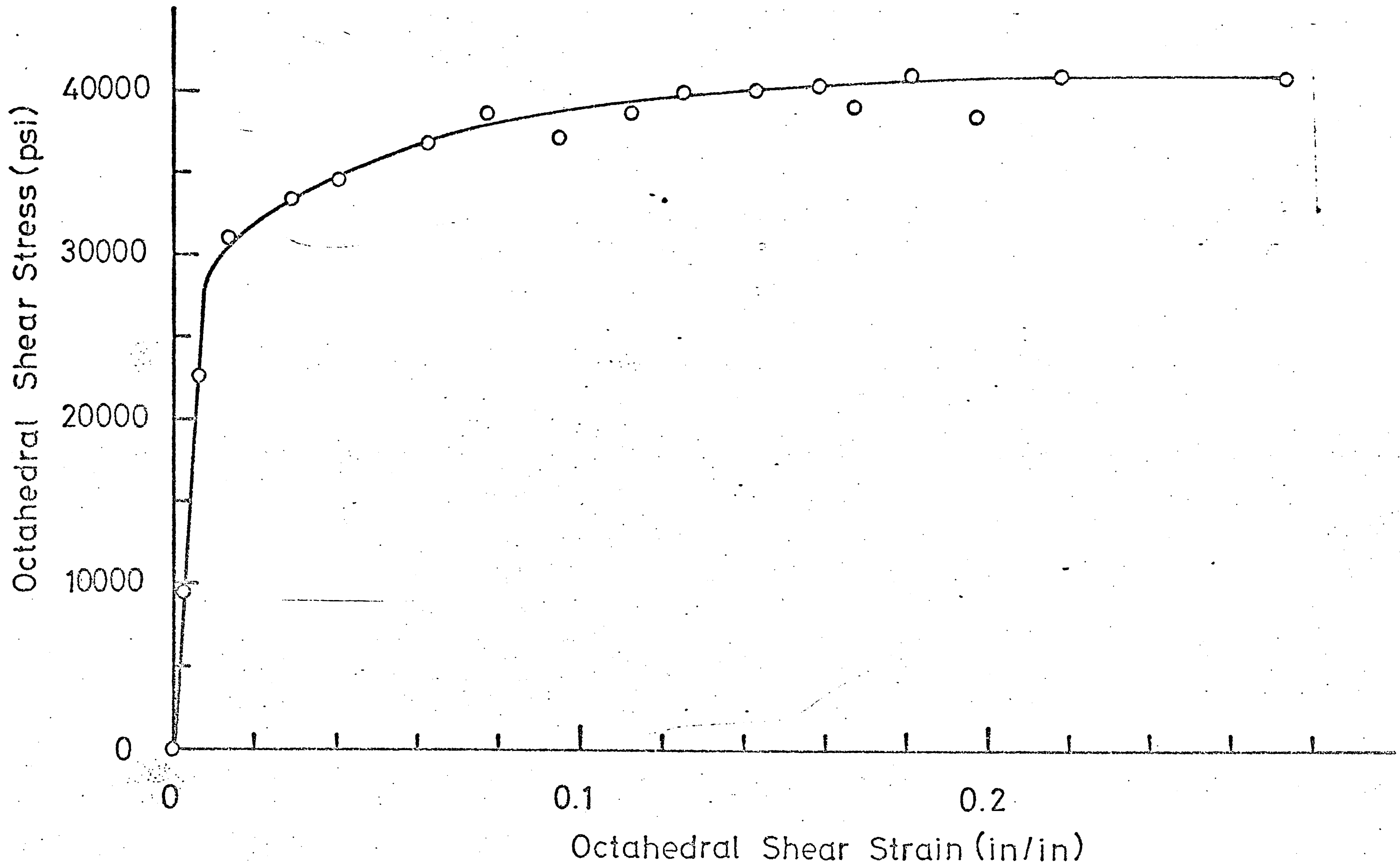

Fig. 4.9 Octahedral Shear Stress-Strain Curve for the Combined Static Test of No.1.

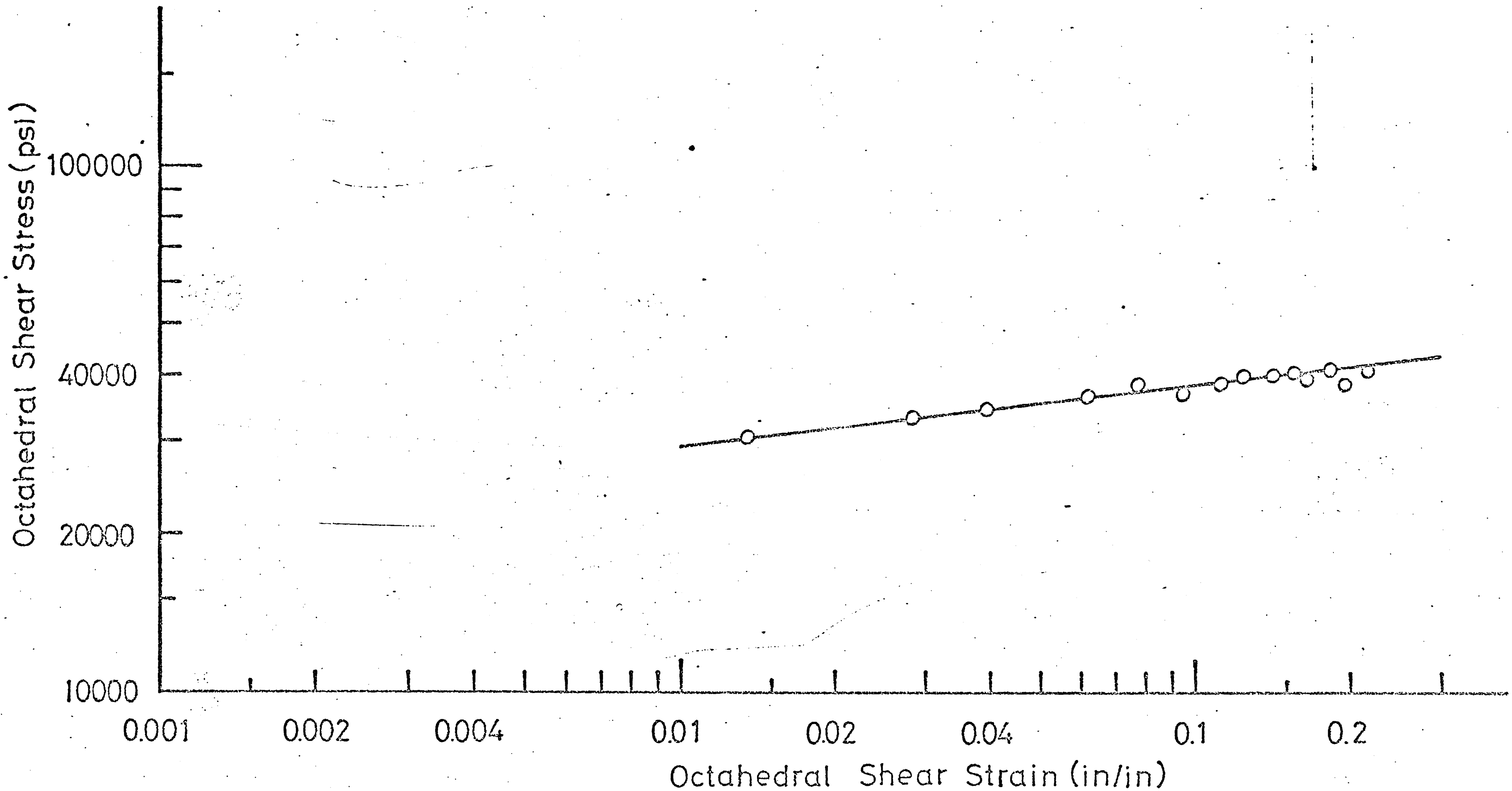

Fig. 4.10 Logarithmic Octahedral Shear Stress-Strain Relation for the Combined Static Test of No.1.

obtaining the strain from the die-set movement in the combined fatigue test. On the other hand, regarding the relationship between the angle of twist and the shear strain, the theoretical curve was used, because the theoretical and experimental lines coincide.

The failure lines on the specimen in these tests were seen to have the larger angle from the axis of the specimen for the smaller strain ratio, that is the larger axial strain.

(2) Fatigue Tests with the Strain Ratio A of 2:1

Ten available tests including two static tests were conducted. One of the two static test could not reach fracture because of unexpectable electric power break, but it went beyond the strain gage ability. Results of these ten tests were plotted on the log-log graph paper in Figs.4.11 and 4.13 to show the relationship between the octahedral shear strain range and the number of cycles to fracture. The relationship between the maximum principal strain range and the number of cycles to fracture are also shown in Fig.4.12. The numerical data are listed in Table 4.6.

The principal and octahedral shear strain ranges were calculated from the axial and torsional strain ranges by using the expressions (4.15), (4.19), (4.34), and (4.37). The axial and torsional shear strain ranges were obtained from the diagrams between the die-set movement and the strain and between the angle of twist and the shear strain, respectively.

Both in Figs.4.11 and 4.12, the octahedral shear strain ranges vs. the number of cycles to fracture for the tension test and the torsion test were also plotted to compare the effect of strain state. Goto's data for the rhombic specimens [87] and Shewchuk's data for the oval plate specimens [86] were also plotted in Fig.4.11.

Table 4.6

Results of the Combined Fatigue Test of $A=\frac{\Delta\gamma_{xy}}{\Delta\varepsilon_x}=2$, $\phi=0°$

Run No.	No. of Cycles to Fracture N	Die-Set Movement ΔD_i in	Conv. Axial Strain Range $\Delta\varepsilon_x$ in/in	True Axial Strain Range $\Delta\delta$ in/in	Angle of Twist $\Delta\theta$ degree	Shear Strain Range $\Delta\gamma_{xy}$ in/in	Strain Ratio A	Oct. Shear Strain R. $\Delta\gamma$ oct in/in	Max. Principal Strain Range $\Delta\varepsilon$ oct in/in
1	1/4								
2	1/4	0.305	0.26	0.2446	49.2	0.522	2.0	0.5486	0.37812
3	4	0.090	0.052						
4	5	0.0875	0.0467	0.0456	8.3	0.0760	1.63	0.0895	0.0626
5	5	0.084	0.046						
6	138	0.056	0.018	0.01784	4.7	0.0431	2.4	0.0433	0.02982
7	98	0.058	0.020	0.0198	4.7	0.0431	2.16	0.0449	0.03112
8	26	0.068	0.030	0.0296	5.6	0.0513	1.71	0.0591	0.0413
9	42	0.066	0.028	0.0276	5.1	0.0467	1.67	0.0545	0.0381
10	1144	0.048	0.012	0.01192	2.5	0.0229	1.91	0.02518	0.0175
11	661	0.0503	0.0138	0.01368	2.8	0.0257	1.86	0.02852	0.01986
12	330	0.053	0.016	0.01586	3.25	0.0298	1.86	0.0331	0.02307

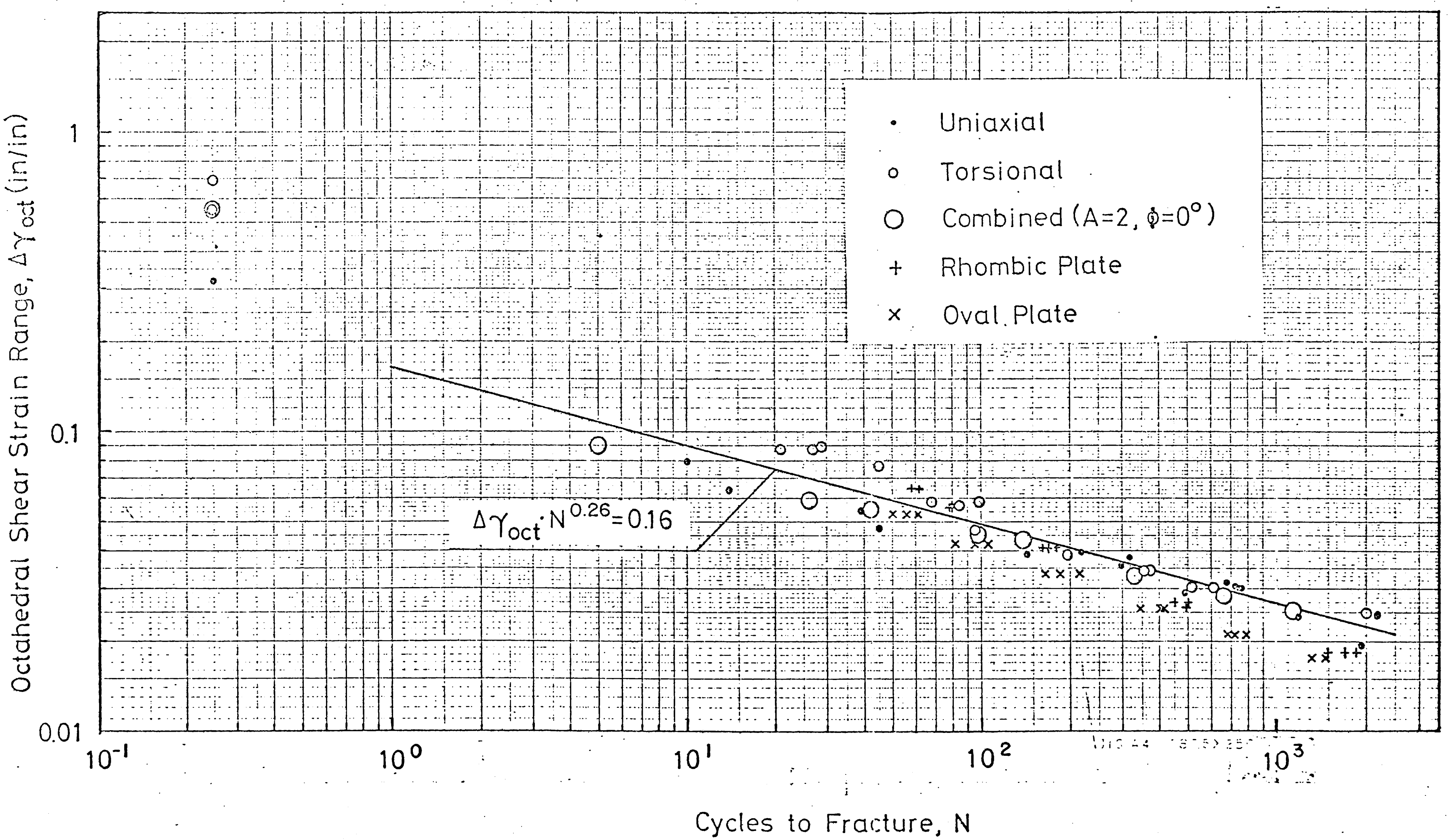

Fig. 4.11 Relationship between Octahedral Shear Strain Range and Number of Cycles to Fracture for Uniaxial, Torsional, Combined Synchronous(A=2), and Other Multiaxial Fatigue Tests.

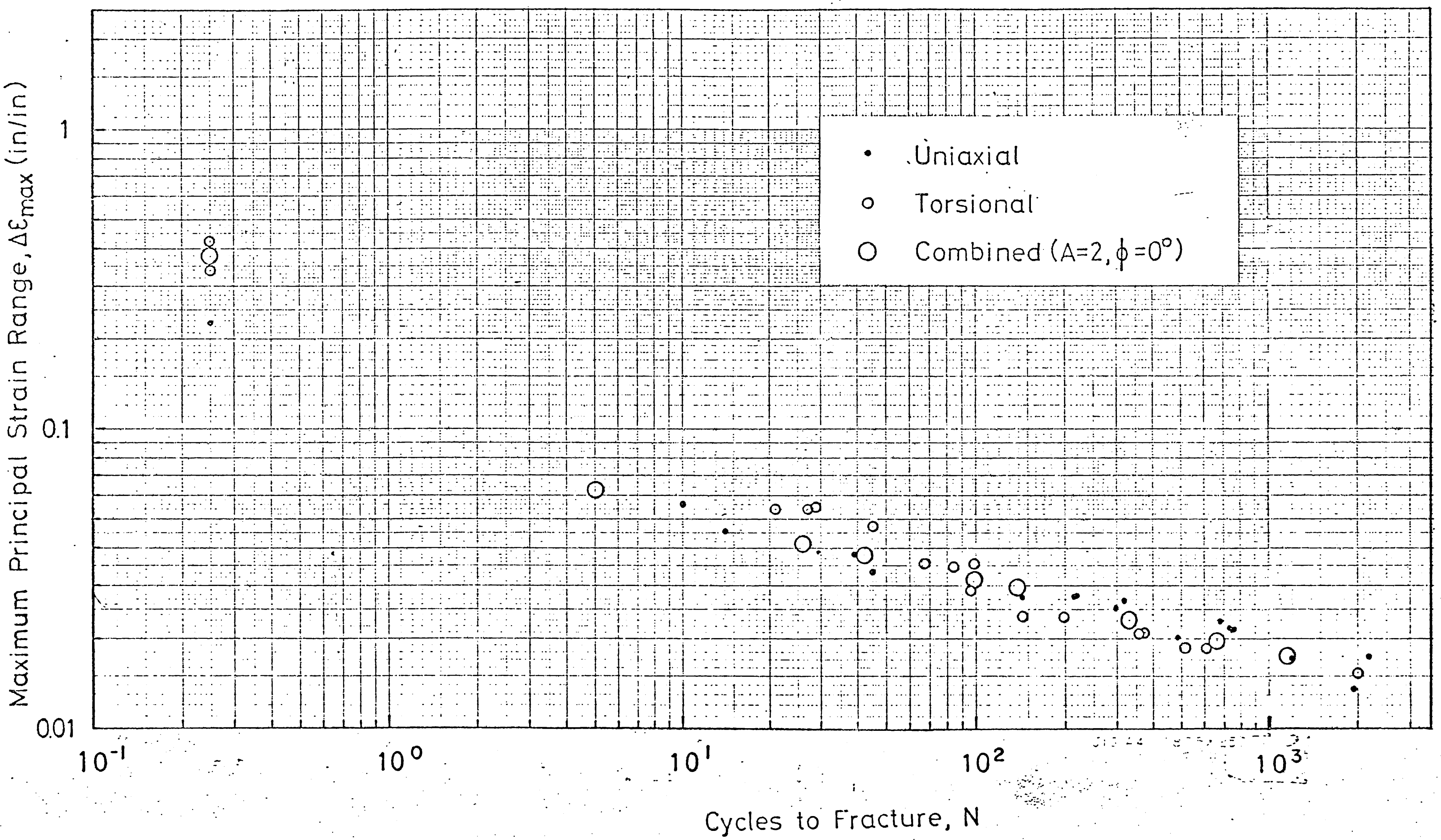

Fig. 4.12 Relationship between Maximum Principal Strain Range and Number of Cycles to Fracture for Uniaxial, Torsional, and Combined Synchronous(A=2) Fatigue Tests.

For the combined case, the octahedral shear strain range vs. the number of cycles to fracture appeared a straight line with the slope α_{oct} of 0.23, and C_{oct}=0.13. While for the axial fatigue tests, the slope α_t was 0.24 and for the torsion fatigue test, the slope α_s was 0.34. These discrepancies of the slopes for three tests were found larger for lower than about 100 cycles than for higher cycles. This may be because of complexity of the fracture mode in the lower cycles that is, for the combined case in the low cycle range, fracture initiated at the crossing points of two hills of buckling in the compressive direction, when it was applied by tension. Therefore, the local strain seemed to be much larger than the average strain calculated from the die-set movement and the twisting angle or the strain gage with length of 1/4 inch. This may be one of the reasons why the maximum principal strain range has less scatter than the octahedral shear strain range does. Another reason of the discrepancy is the definition of the axial true strain like as in the tesion test.

After the crack initiated, the specimens were torn obliquely.

Fracture was determined when the stress reduced considerably. This occurred at the same time as the specimen was torn.

The results of the reversed bending fatigue tests of rhombic plates by Goto and those of the bending fatigue tests of oval plates by Shewchuk were plotted together in Fig.4.11. These results drop exactly on the torsion fatigue data in this study.

(3) Fatigue Tests with the Strain Ratio A of 1:1 and 3:1

For each strain ratio, four fatigue tests including one static test were conducted. The results were plotted on the log-log graph paper in Fig.4.13 to show the relationship between the octahedral

Table 4.7

Results of the Combined Fatigue Tests of $A=\frac{\Delta\gamma_{xy}}{\Delta\varepsilon_x}=1$ & 3, $\phi=0°$.

Run No.	No. of Cycles to Fracture N	Die Set Movement ΔD in	Conv. Axial Strain Range $\Delta\varepsilon_x$ in/in	True Axial Strain Range $\Delta\delta$ in/in	Angle of Twist $\Delta\theta$ degree	Shear Strain Range $\Delta\gamma_{xy}$ in/in	Strain Ratio A	Oct. Shear Strain Range $\Delta\gamma$ oct in/in	Max. Princ. Strain Range $\Delta\varepsilon$ max. in/in
1'	1/4	0.266	0.228	0.216	20.4	0.187	0.82	0.3416	0.241
3'	90	0.074	0.0275	0.03515	3.2	0.0293	1.07	0.0452	0.0319
4'	37	0.081	0.02982	0.0421	3.8	0.0348	1.17	0.0503	0.0354
5'	308	0.064	0.0208	0.02567	2.4	0.02199	1.06	0.0342	0.0241
2"	1/4	0.310	0.272	0.255	56.6	0.528	1.94	0.562	0.3897
6"	18	0.061	0.0273	0.02263	7.8	0.07147	2.62	0.0697	0.0478
7"	311	0.052	0.0155	0.0149	4.1	0.03756	2.42	0.0377	0.0259
8"	58	0.056	0.0210	0.0208	5.2	0.04764	2.27	0.0488	0.0337

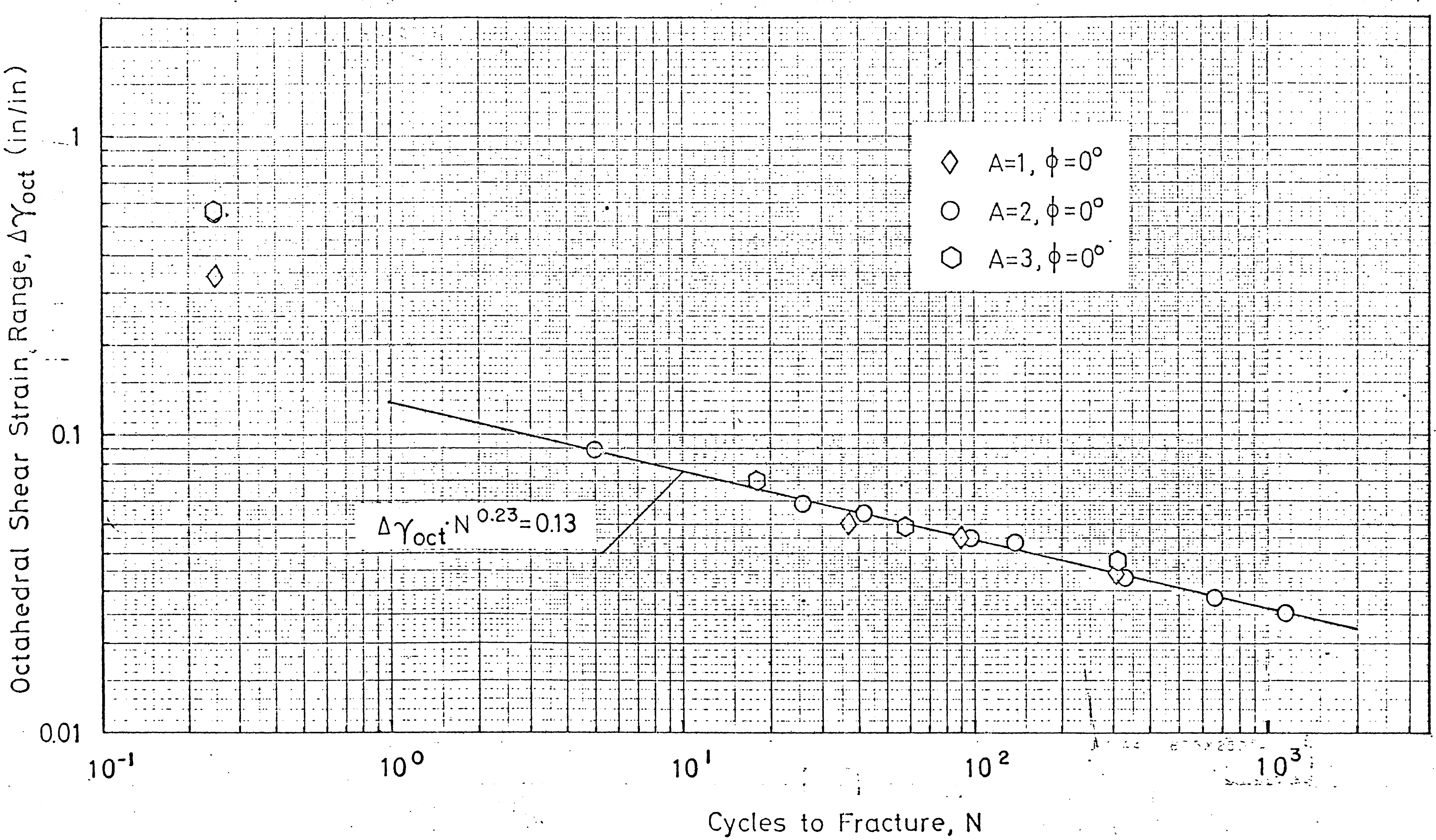

Fig. 4.13 Relationship between Octahedral Shear Strain Range and Number of Cycles to Fracture for All Combined Synchronous Tests of A=1, 2, and 3.

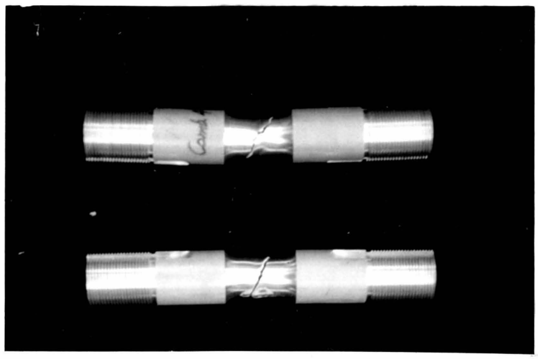

Combined Test No.4, A=2, $\phi=0°$, N=5

Combined Test No.3, A=2, $\phi=0°$, N=4

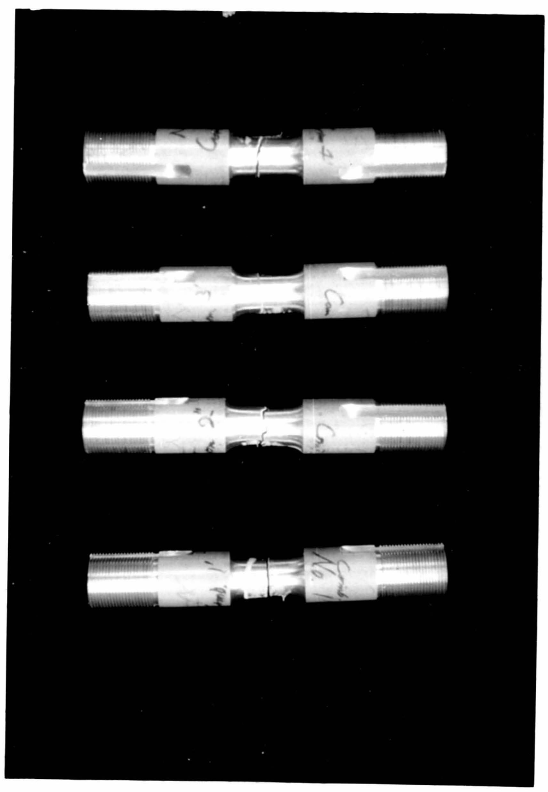

Combined Test No.4', A=1, $\phi=0°$, N=37

Combined Test No.3', A=1, $\phi=0°$, N=90

Combined Test No.2'', A=3, $\phi=0°$, N=1/4

Combined Test No.1'', A=1, $\phi=0°$, N=1/4

Photo. 4.3 Specimens after Synchronous Combined Tests shear strain range and the number of cycles to fracture for both strain ratios. The numerical data were listed in Table 4.7. The process dealing with the experimental data was the same as in the case of the strain ratio of 2:1. In Fig.4.13 the log-log plots of the octahedral shear strain range vs. the number of cycles to fracture for both cases appear straight lines with almost the same slopes, 0.19 for A=1 and 0.22 for A=3.

Comparing these two lines with the line for the strain ratio of 2:1, the lines for the ratios of 1:1 and 3:1 almost coincide with the line for the ratio of 2:1. Consequently, the effect of strain ratio is found to be negligible, if one uses the octahedral shear strain range. The slopes obrained in this study are smaller than the slope of 0.41 obtained by Taira et al.[83].

Variation of the principal strain state for the combined axial and torsional case is from 1:-1/2:-1/2 for the uniaxial case to 1:-1:0 for the torsional case and it is not so large.

The modes of fracture for three different strain ratios of the torsional and axial strains were naturally different. For smaller value of the strain ratio, the fracture line is almost the same as the uniaxial case where it is parpendicular to the axis of the cylinder. (See Photo.4.3) For larger value of the strain ratio, the main crack was similar to the torsional case and the subsequent crack appeared oblique. The two crossing hills by compressive strains were also observed.

§4.6 Nonsynchronous Fatigue Tests with the Strain Ratio A of 2:1

The phase difference ϕ means that the twisting angle is ahead the zero axial deformation by the angle of ϕ.

Two phase differences ϕ of 45° and 90° were chosen. Since there is no difference in the biaxial behavior between clockwise and anticlockwise twisting, the phase difference of 180° gives the same effect as that of 360° does. In the beginning of the fatigue test, the static angle of twist of ϕ was given the speciemn.

Eight fatigue tests were done for each phase difference. The results were plotted in the log-log graph paper in Fig.4.14 to show the relationship between the octahedral shear strain ranges and the number of cycles to fracture. In Fig.4.14, the results for the phase difference of zero which is the synchronous case were also plotted for the purpose of comparison.

The octahedral shear strain range was calculated from the axial strain range and the torsional shear strain range by using the expression (4.31).

In Fig.4.14, the plots were connected into straight lines for both cases. However, some discrepancy can be seen among three lines. The slopes are measured to be 0.18 for 45° and 0.21 for 90°, which are compared with the slope of 0.23 for the synchronous tests. The line for 45° lies below that for the synchronous case and further the line for 90° lines below that for 45° if one takes the $\Delta\gamma_{oct}$ calculated by Eq. (4.31) along the ordinates. As far as one uses $\Delta\gamma_{oct}$ as an index one can not neglect the effect of the phase difference. This conclusion is different from the conclusion by Taira et al.[115] as stated in CHAPTER II.

On the other hand, if the total energy to fracture vs. number of cycles to fracture were plotted on log-log graph paper as shown in Fig.4.15, for all the phase differences of 0°, 45°, and 90°, this diagram shows no distinct discrepancy caused by the phase difference, although scatter is pretty large. In this case, the energy was obtained by adding the areas of both the axial and the torsional shear stress-strain hysteresis loops which were recorded by the strain gages on the load cell and the specimen. In this case, the steady hysteresis loop was selected. The area inside the hysteresis loop, i.e., the dissipated energy, can be an index, but the reason can not be explained theoretically yet.

Regarding the mode of fracture, the crack initiated parpendiculat to the axis of the specimen and then the crack propatated in zig-zag way, that is, the crack parpendiculat to the axis first, the oblique crack subsequently. In some specimens for $\phi=45^o$ the cracks were seen everywhere on the gage length.

Table 4.8

Results of the Combined Fatigue Tests of $A=\frac{\Delta\gamma_{xy}}{\Delta\varepsilon_x}=2$, $\phi=90°$

Run No.	No. of Cycles to Fracture N	Die Set Movement ΔD in	Conv. Axial Strain Range $\Delta\varepsilon_x$ in/in	True Axial Strain Range $\Delta\delta$ in/in	Angle of Twist $\Delta\theta$ Degree	Shear Strain Range $\Delta\gamma_{xy}$	Strain Ratio A	Oct. Shear Strain Range $\Delta\gamma$ oct	Max. Princ. Strain Range $\Delta\varepsilon$ max.
1	31	0.075	0.0246	0.0242	5.5	0.050	2.03	0.0408	0.025
3	1034	0.0525	0.0105	0.0104	2.4	0.02199	2.10	0.0180	0.0160
4	1747	0.051	0.0096	0.0096	2.3	0.02107	2.20	0.0172	0.0105
5	45	0.0752	0.0248	0.0245	5	0.0458	1.85	0.0374	0.0245
6	366	0.060	0.0152	0.0151	3.7	0.0339	2.23	0.0277	0.0170
7	294	0.061	0.0159	0.0158	3.6	0.0330	2.08	0.0270	0.0165
8	13	0.088	0.0328	0.0323	6.1	0.0559	1.70	0.0457	0.0323
9	8	0.084	0.0342	0.0336	7	0.0641	1.87	0.0524	0.0336

Table 4.9

Results of the Combined Fatigue Tests of $A=\frac{\Delta\gamma_{xy}}{\Delta\varepsilon_x}=2$, $\phi=45°$

Run No.	No. of Cycles to Fracture N	Die Set Movement ΔD in	Conv. Axial Strain Range $\Delta\varepsilon_x$ in/in	True Axial Strain Range $\Delta\delta$ in/in	Angle of Twist $\Delta\theta$ degree	Shear Strain Range $\Delta\gamma_{xy}$	Strain Ratio A	Oct. Shear Strain Range $\Delta\gamma$ oct	Max. Princ. Strain Range $\Delta\varepsilon$ max.
1	21	0.074	0.0275	0.0271	6	0.0550	2.0	0.0547	0.0379
2	20	0.073	0.0269	0.0265	5.8	0.05314	1.98	0.0531	0.0368
3	1660	0.0525	0.0137	0.0136	2.6	0.02382	1.74	0.0253	0.0176
4	1229	0.0515	0.013	0.0129	2.7	0.02474	1.90	0.0252	0.0175
5	165	0.0675	0.0233	0.0230	3.8	0.03782	1.62	0.0400	0.0281
6	72	0.0660	0.0224	0.0222	4.2	0.03848	1.72	0.0410	0.0286
7	404	0.0570	0.0166	0.0165	3.2	0.02932	1.77	0.0309	0.0215
8	636	0.0574	0.0168	0.0167	3.2	0.02932	1.74	0.0310	0.0216

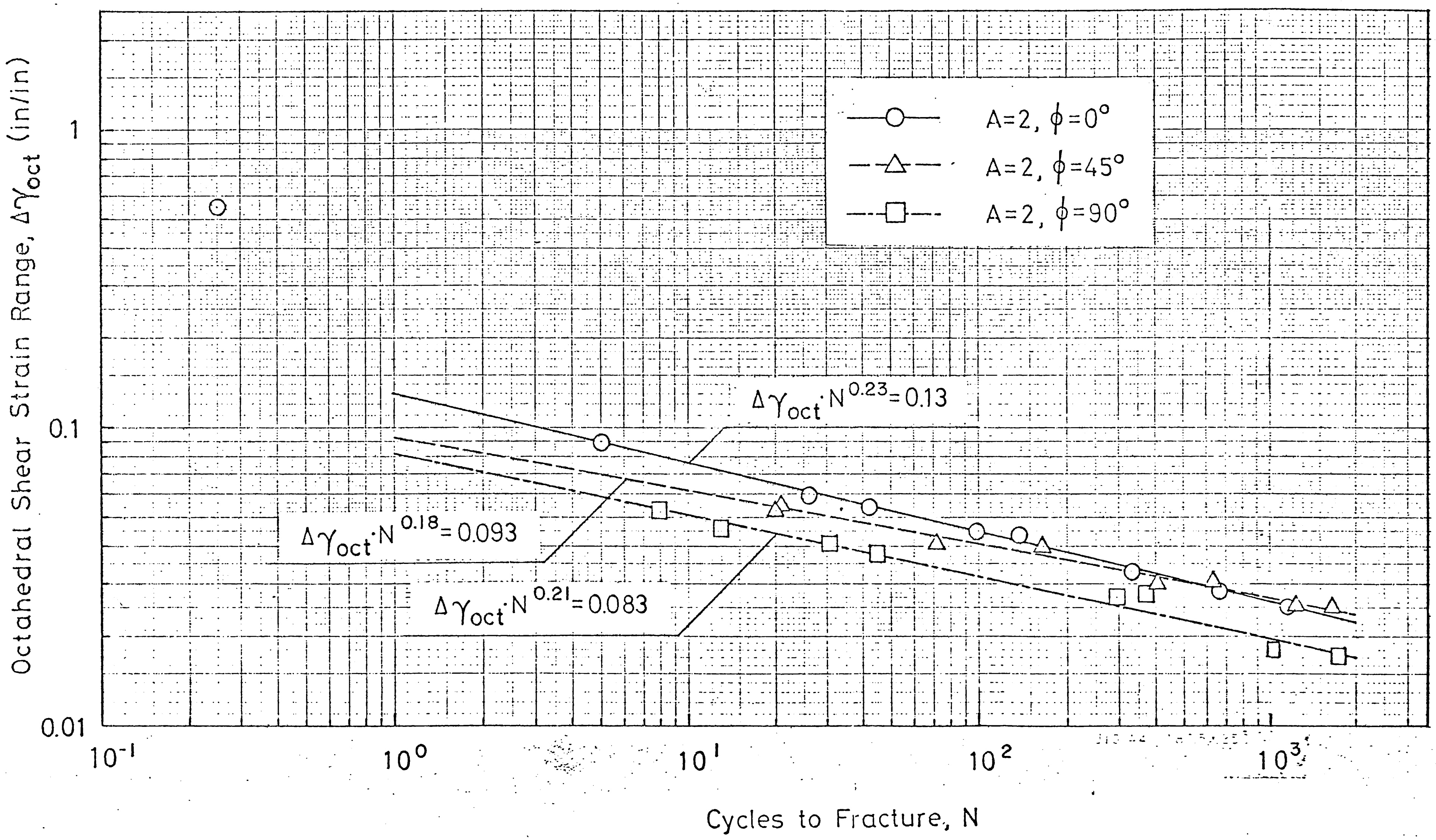

Fig. 4.14 Relationship between Octahedral Shear Strain Range and Number of Cycles to Fracture for All Combined Tests of A=2 and $\phi=0°$, 45°, and 90°.

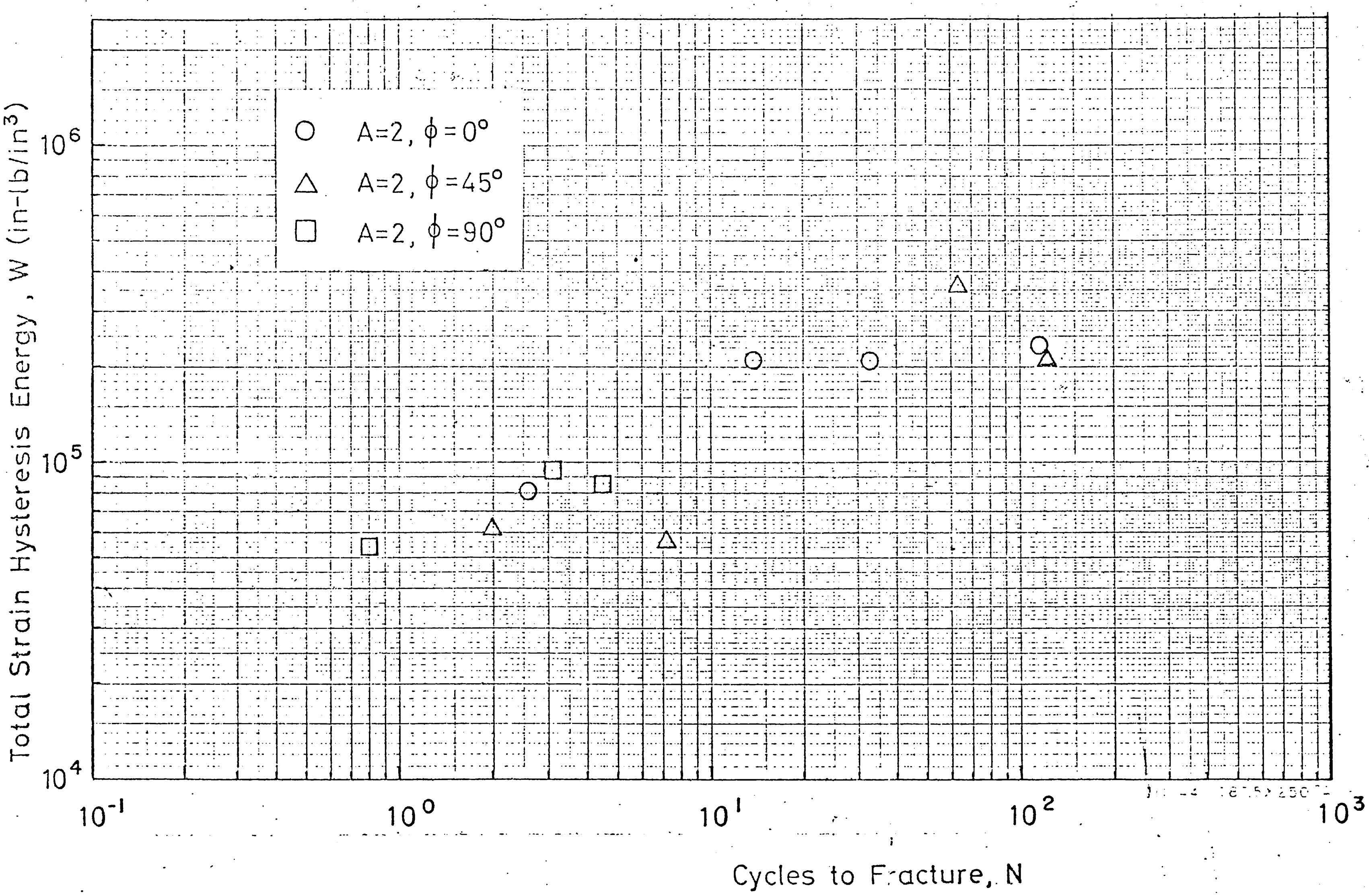

Fig. 4.15 Relationship between Total Hysteresis Strain Energy and Number of Cycles to Fracture for All Combined Tests of A=2 and ϕ=0°, 45°, and 90°.

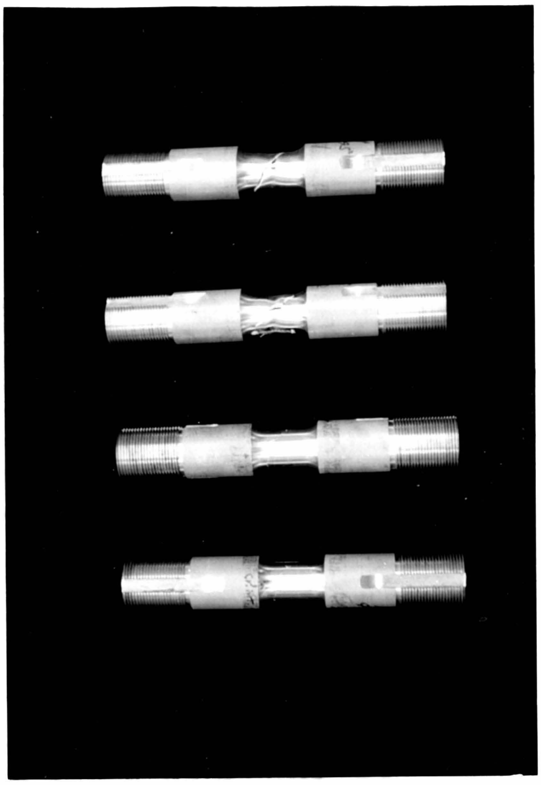

Combined Test No.1, A=2, ϕ=45°, N=21

Combined Test No.2, A=2, ϕ=45°, N=20

Combined Test No.3, A=2, ϕ=45°, N=1660

Combined Test No.4, A=2, ϕ=45°, N=1229

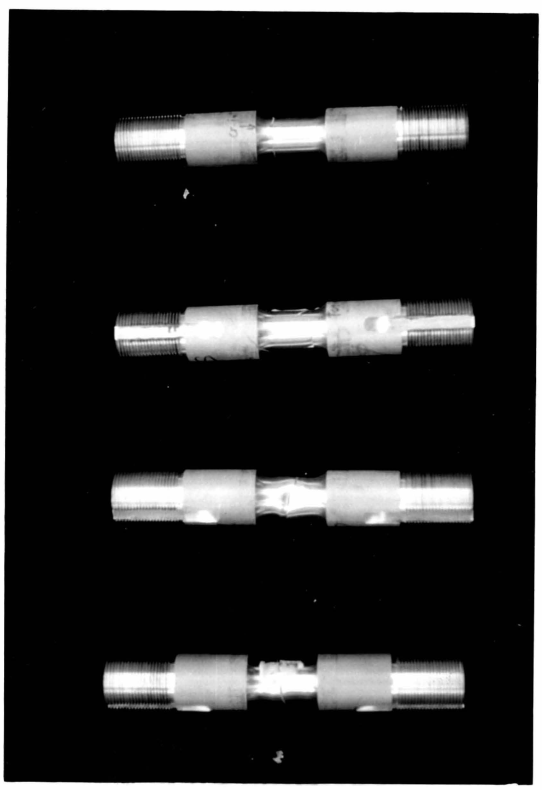

Combined Test No.6, A=2, ϕ=90°, N=366

Combined Test No.7, A=2, ϕ=90°, N=294

Combined Test No.8, A=2, ϕ=90°, N=13

Combined Test No.9, A=2, ϕ=90°, N=8

Photo. 4.4 Specimens after Nonsynchronous Combined Tests

CHAPTER V APPLICATIONS OF THE LOW CYCLE FATIGUE THEORY TO STRUCTURAL PROBLEM

§5.1 Introduction

In this chapter, it is considered how to apply or relate the low cycle fatigue theories of materials to the structural ploblems. As mentioned in CHAPTER I, low cycle fatigue in structural problems occurs when the building is subjected to large earthquakes and typhoons. In the past, because of restriction of experimental method that low cycle fatigue need large loads, quasi-static repeated loads were applied on the structural model. From the vibrational point of veiw, because there are many questionable points on the restoring force characteristics in the elastic-plastic region, rough assumptions were made on the structural model in the analysis. Further, in the vibrational analysis, interests are in the quantities of responses, and the total number of cycles to failure is not a question. Actually, however, the structure fails due to deterioration of consisting materials caused by large dynamic loads, which are mostly randomly varying loads. In the following, low cycle fatigue of structures due to randomly varying loads is considered.

Purpose of the study in this chapter is to estimate the life of the metallic structure due to randomly varying large loads expressed by $\varepsilon_{eq} \sim t$ from the results of the simple tension test and of the strain-controlled test of constant amplitude of the material. For the purpose of simplicity of explanation, only the earthquake load is taken up as the varying load. However, when other randomly varying large loads are applied, similar treatice will be available.

When the structure is subjected to a large earthquake, the random loads on the structural member is not earhquake motion itself, but response of the vibrating system with such restoring force characteristics as related to the hysteresis curve of the material. Therefore, the analysis of randomness should be made about the response. Although the restoring force characteristics of structres are not always the same as the hysteresis curve of the material, the theories about material may be applied to the structure, if the structure is fabicated so as to avoid buckling and backlash, for instance, in rivetted structures. For example, in Ref. [109], horizontal load-deflection curves of a single spanned and single storied frame are obtained theoretically from the stress-strain curve of material of bilinear type. Further, Igarashi [110] showed experimentally that in welded structures cyclic load deflection curves are steady except first several cycles. On the other hand, however, Nakamura [114] indicated that local buckling occurs in cyclic bending tests of I-beams.

§5.2 Low Cycle Fatigue of Structural Elements due to Random Vibrations

Up to the present, there are pretty many studies on high cycle fatigue under randomly varying loads [111], but only a few on low cycle fatigue [110]. In order to apply the random fatigue theory for high cycle fatigue to low cycle fatigue, the stress range in high cycle fatigue has to be rewritten into the strain range in low cycle fatigue.

With the above-mentioned in mind, the following assumptions are laid in the application of random fatigue theory to the earthquake resistant problem:

(1) The linear damage hypothesis is approximately applicable.

(2) During cycling, an almost steady stress-strain hysteresis curve is hold, in other words, the mechanical properties of material is not much changed.

(3) Effects of cycling rate and temperature are small in low cycle fatigue.

Kato [114] obtained analytically maximum strain rate of 1.2/min in a five storied braced steel structure subjected to El Centro earthquake (1940 NS) and showed experimentally that in this strain rate yield stress and ultimate stress on the member increase by about 10 %.

(4) When multiaxial stress conditions appear in the member, the octahedral shear strain theory is applicable.

(5) It is assumed that the random process is stationary and statistical quantities do not vary. If catastrophic mean strains which are non-stationary, appear, damages caused by these strains should be added to those by stationary strains. Damages by mean strains are expressed by

$$D_m = \frac{|\varepsilon_p| \max}{\varepsilon_f} \tag{5.1}$$

according to Kikukawa [112], where $|\varepsilon_p| \max$ is the absolute value of maximum plastic strain and ε_f is the fracture strain. For the non-stationary process, damages in the non-stationary process can be obtained by adding damages in each stationary process.

Each of the above assumptions except (5) have been already discussed in CHAPTER II.

To analyse the random process, the following methods were proposed [113]:

(1) Counting Methods.

(2) Power Spectral Analysis.

The first methods are ones to count the numbers of peaks and of ranges and of the points at a certain strain level in the whole process. By this method, the effect of the strain rate can not be considered. In Ref. [111], the following seven kinds of counting methods are compared and related to the power spectral analysis.

(a) Peak Count Method

(b) Mean-Crossing Peak Count Method

(c) Range Count Method

(d) Range-Mean Count Method

(e) Range-Pair Count Method

(f) Level-Crossing Count Method

(g) Fatiguemeter Count Method

The power spectral analysis can take into account the effect of the strain rate. By the power spectral analysis, the statistical density function of Δp(=peak value minus mean value) $f(\Delta p)$ is expressed for the stationary Gaussion process as

$$s_1 f(\Delta_p)=\frac{\sqrt{k^2-1}}{k\sqrt{2\pi}}\exp[-(\frac{\Delta p}{s_1})^2]\{\frac{k^2}{2(k^2-1)}\}$$

$$+\frac{1}{2k}\frac{\Delta p}{s_1}\exp[-\frac{1}{2}(\frac{\Delta p}{s_1})^2[1+\text{erf}\{\frac{\Delta p/s_1}{\sqrt{2(k^2-1)}}\} \qquad (5.2)$$

where

$$s_1{}^2=\int_0^\infty \Phi(\omega)\, d\omega$$

$$k=\frac{N_1}{No}=\frac{s_1 s_3}{s_2{}^2} \qquad (5.3)$$

$$s_2{}^2=\int_0^\infty \omega^2\Phi(\omega)d\omega$$

$$s_3{}^2=\int_0^\infty \omega^4\Phi(\omega)d\omega$$

and N_1 is number of peak values per second and N_o is the number of mean crossings per second and $\Phi(\omega)$ is the power spectral density. [113]

For the randomly varying strain, the linear damage hypothesis is expressed by

$$D_v=\int\frac{dn}{N}=1 \qquad (5.4)$$

where dn is the number of cycles at a strain level between ε_{eq} and $\varepsilon_{eq}+d\varepsilon_{eq}$, ε_{eq} is the equivalent strain based on the octahedral shear strain theory. Let $f(\varepsilon_{eq})d\varepsilon_{eq}$ be the probability that a given strain cycle will have an amplitude between ε_{eq} and $\varepsilon_{eq}+d\varepsilon_{eq}$. This probability will be obtained by using one of the above-mentioned counting methods from $\varepsilon_{eq}\sim t$ curve. Then, the number of cycles dn will be given in terms of the total number of cycles N_t by

$$dn=N_t f(\varepsilon_{eq})d\varepsilon_{eq} \tag{5.5}$$

Substituting Eq. (5.5) into Eq. (5.4), one obtain

$$\int_{\varepsilon_{eq,\ mim}}^{\varepsilon_{eq,\ max}} \frac{N_t f(\varepsilon_{eq})d\varepsilon_{eq}}{N}=1 \tag{5.6}$$

By the linear relationship of $\varepsilon_{eq}\sim N$ on the log-log paper, one has

$$\Delta\varepsilon_{eq}N^{\alpha}=\Delta\varepsilon_{eq,1}N_1^{\ \alpha} \tag{5.7}$$

with the known strain range $\Delta\varepsilon_{eq,1}$ and the number of cycles to failure N_1. Substituting N of Eq. (5.7) into Eq. (5.6) and rewriting $\Delta\varepsilon_{eq}$ into ε_{eq}, one obtains

$$N_t\int_{\varepsilon_{eq,\ mim}}^{\varepsilon_{eq,\ max}} \frac{f(\varepsilon_{eq})}{N_1}\left(\frac{\varepsilon_{eq}}{\varepsilon_{eq,1}}\right)^{\frac{1}{\alpha}}d\varepsilon_{eq}=1 \tag{5.8}$$

If the $\varepsilon_{eq}\sim N$ relationship can be extended to the static test, Eq. (5.8) turns out as

$$4N_t\int_{\varepsilon_{eq,\ mim}}^{\varepsilon_{eq,\ max}} f(\varepsilon_{eq})\left(\frac{\varepsilon_{eq}}{2\varepsilon_{eq,f}}\right)d\varepsilon_{eq}=1 \tag{5.9}$$

where $\varepsilon_{eq,f}$ is the fracture equivalent strain. With Eqs. (5.8) and (5.9), one can estimate the total number of cycles N_t. The experimental varification is not done yet.

§5.3 Example

As an example, a five-storied structure in Fig.5.1 is taken up. This structure is assumed to have the following natures as usually treated in the dynamic seismic analysis.

(1) Floor slabs and beams are infinitely rigid,

(2) Vibration of the structure is of shear type,

(3) Axial deformation of columns is negligible,

(4) Base of the structure is rigidly connected to the gound, and

(5) Horizontal restoring force characteristics are of bilinear type shown in Fig.5.2. According to Ref.[109] the horizontal load-deflection curve of the structure whose material has a stress-strain relation of bilinear type appears also bilinear. The fact that a steady hysteresis loop may be obtained during cycling was explained for material in CHAPTER II and for structures in Ref. [110]. Validity of bilinear type of stress-strain relation was explained by Martin. [31]

When the above-mentioned structure is subjected to an artificial earthquake as shown in Pen 1 of Fig.5.3, response (horizontal displacement, shear force, and acceleration, etc.) of each floor can be obtained by solving the differential equations by means of either analog or digiral computer. For example, by connecting each parts of an analog computer according to the block diagram shown in Fig.5.4, the relative displacements between two adjacent floors can be obtained continuously with time as shown in Fig.5.3. Strain in each members seems to appear like these curves.

For more complex structures, strain variation with time in each members can be obtained by digital computer.

Life of structures against cyclic loads should be estimated on the basis of such varying strain for the first approximate estimation.

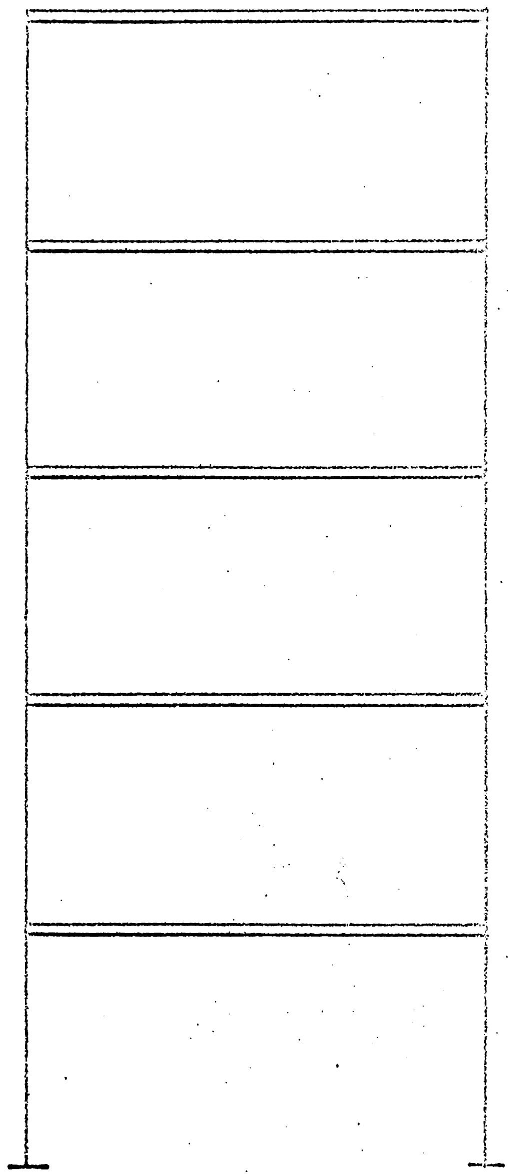

Fig. 5.1 Idealized Five Storied Structure

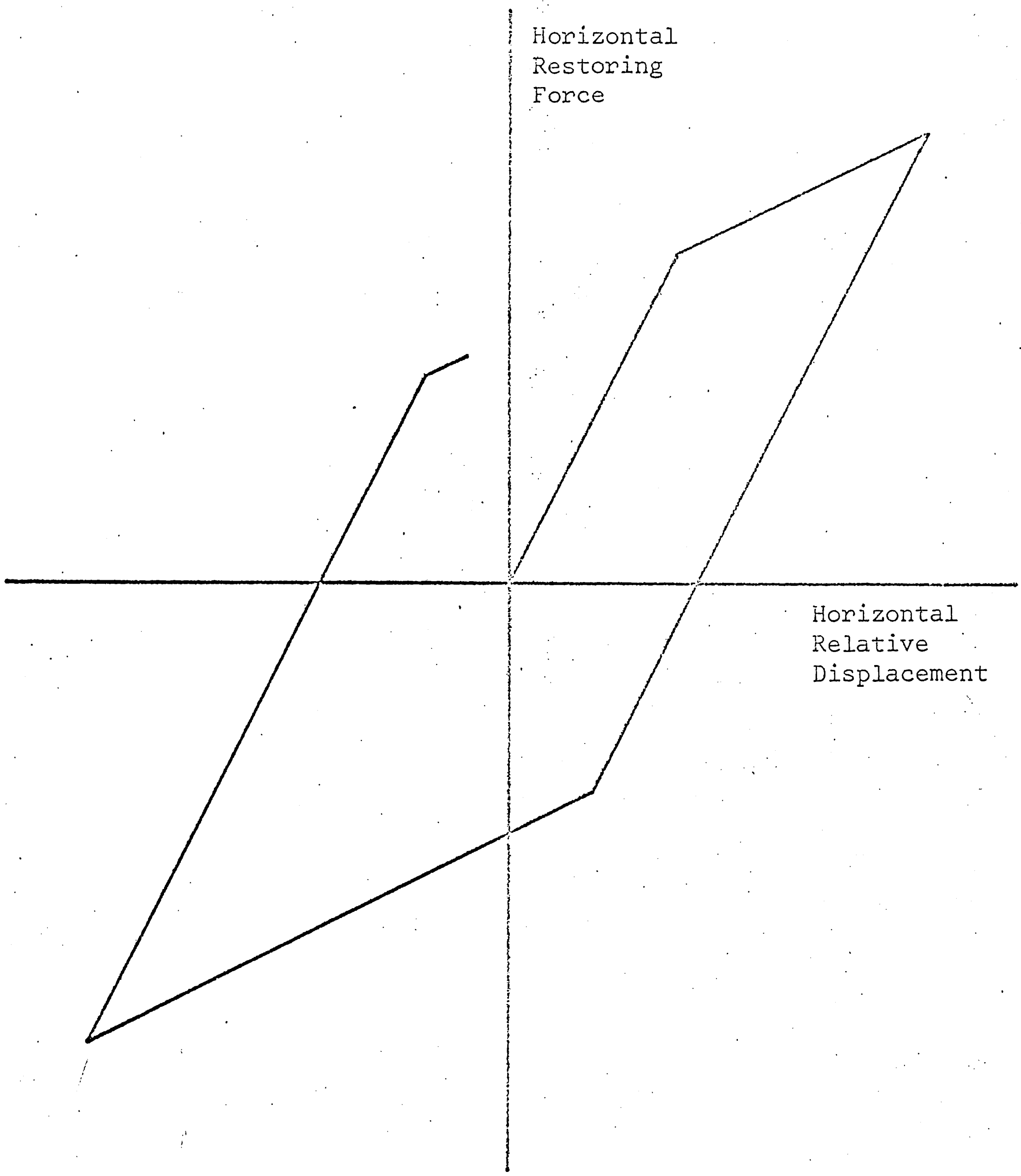

Fig. 5.2 Idealized Horizontal Restoring Force Characteristics

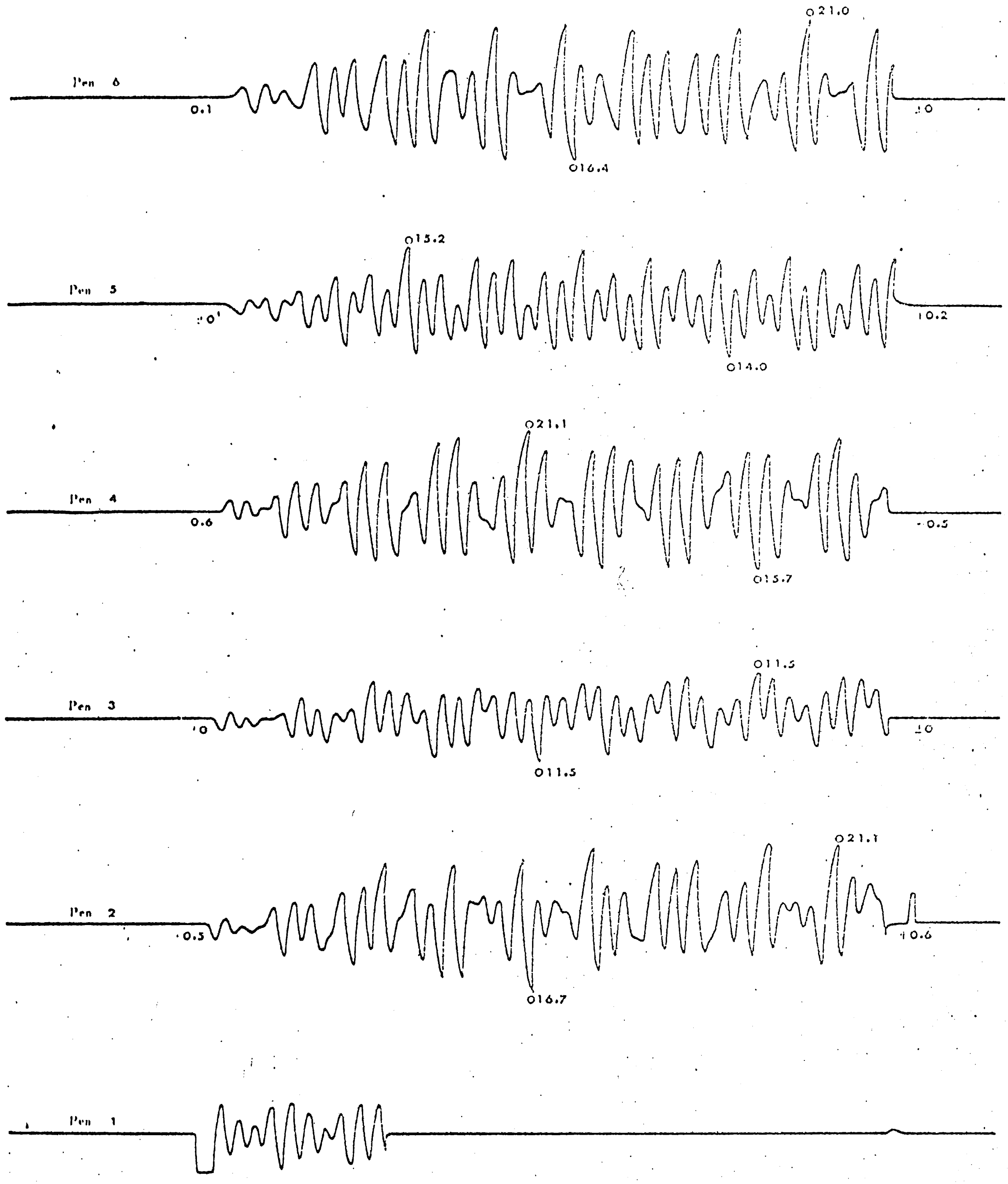

Fig. 5.3 Horizontal Relative Displacements with Time (Pens 2~6) Subjected to an Artificial Earthquake (Pen 1)

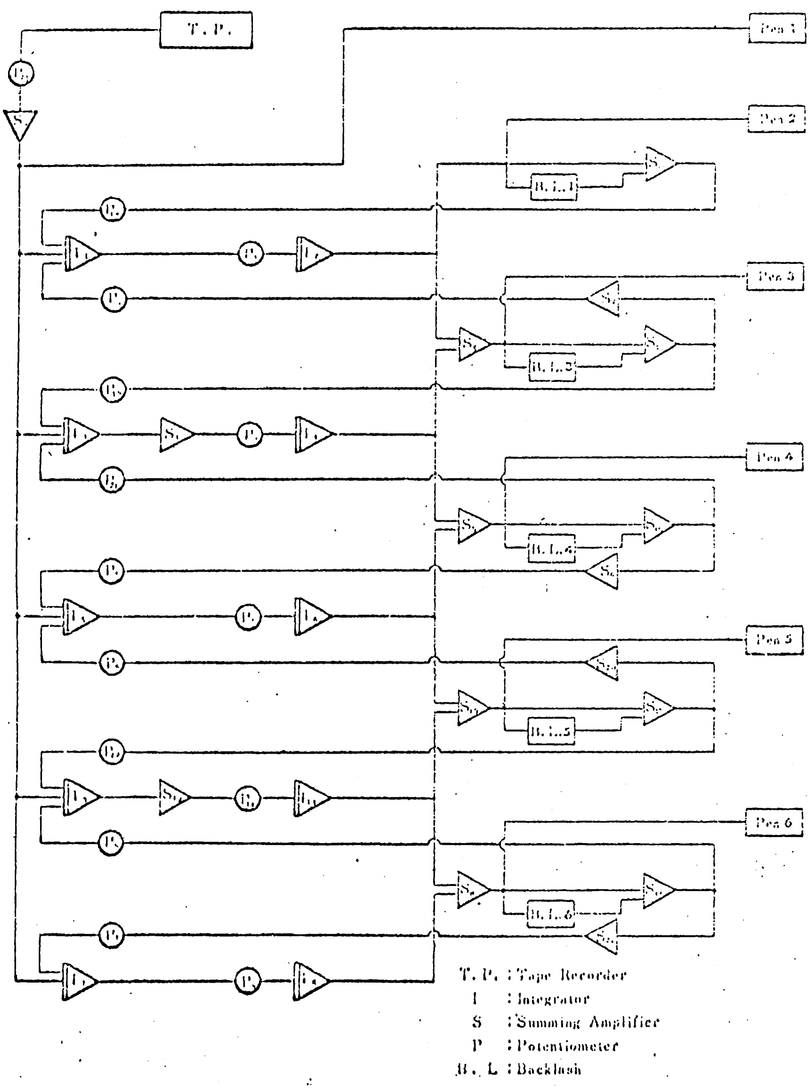

Fig. 5.4 Block Diagram of an Analog Computer for Solving Earthquake Responses

§5.4 Comments on Experimental Method

It may be very difficult to conduct experiments on low cycle fatigue of full scale structures due to earthquake-like random loads because randomly varying large loads must be generated. When the smaller model of structures is used, the following two methods may be availabe:

(1) Vibration test by means of a vibration table.

(2) Fatigue test of members and connections by means of a fatigue testing machine.

Both methods should be used in the experiments. In the first method, the input load is an original earthquake record or an artificial earthquake-like random load whose power spectrum is specified, but it is still very large in order to break the model. In the second method, the input load is an response of the model subjected to earthquake whose power spectral density is also specified. In this method, the load is reasonably large. In either method, a testing machine of electrohydraulic type is recommended, because the lower frequency range which is important for structural tests can be generated beautifully. An example of the block diagram of a random fatigue testing machine is shown in Fig.5.5.

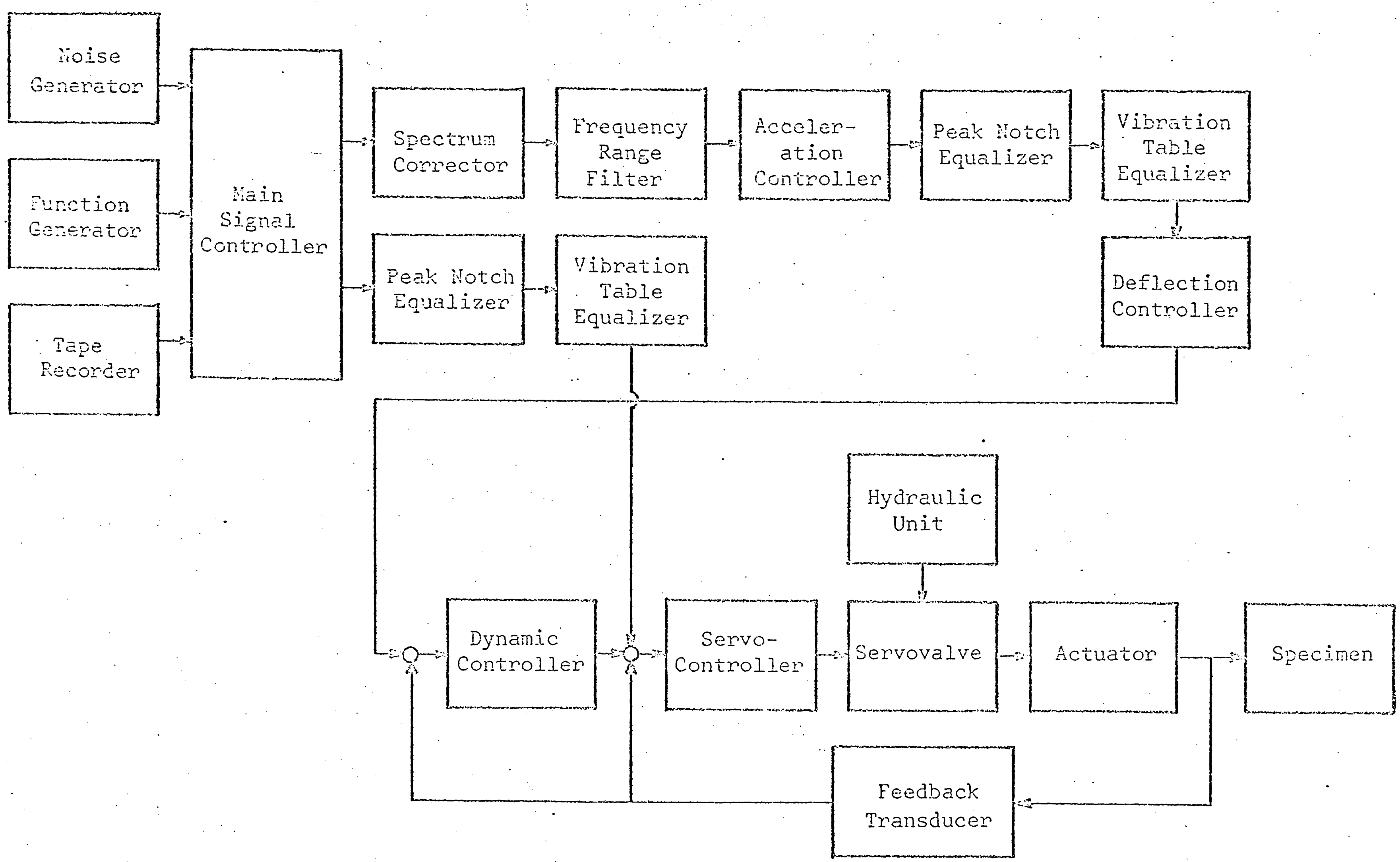

Fig. 5.5 Block Diagram of a Random Vibration Fatigue Test Equipment

CHAPTER VI SUMMARY AND CONCLUSTIONS

§6.1 Summary

For the uniaxial low cycle fatigue, since Manson-Coffin's formula $\Delta\varepsilon_p N^{\alpha}=C$ was proposed in 1953, a lot of studies have been done and almost steady conclusions were obtained. For the multiaxial low cycle fatigue, however, a limited number of experiments have been conducted. In this study, the combined axial and torsional load was applied on the thin-walled cylinder of aluminum alloy and its applications to the earthquake resistant design of structures have been considered.

In the experiment, a fatigue machine with two channels utilizing the electrohyraulic servomechanism was constructed and the following seventy-three tests were done: (1) Twenty-one uniaxial fatigue tests, (2) Nineteen torsional fatigue tests, (3) Nine combined axial and torsional fatigue tests with the strain ratio $A=\Delta\gamma_{xy}/\Delta\varepsilon_x=2$ and the phase difference $\phi=0°$, (4) Four combined fatigue tests with A=1 and $\phi=0°$, (5) Four combined fatigue tests with A=3 and $\phi=0°$, (6) Eight combined fatigue tests with A=2 and $\phi=45°$, and (7) Eight combined fatigue tests with A=2 and $\phi=90°$. Through the whole tests, the strain was controlled and the mean strain was zero. The number of cycles to fracture converd from 1/4 to 2000. The strain rate was 8 cycles per minute. The input signal was of sinusoidal type. In order to obtain the dissipated energy, both the stress and the strain were recorded continuously with time for some typical tests. The strain range was determined by the calibration curves between each strain and the dial gage and the potentiometer readings. Fracture was defined by the abrupt stress reduction. The tests were conducted in room temperature.

In order to compare all series of tests on one diagram, the total octahedral shear strain range was calculated and plotted on log-log graph paper vs. the number of cycles to fracture N. Under the condition of incompressibility, the octahedral shear strain appears as

$$\gamma_{oct}=\frac{2\sqrt{6}}{3}(\varepsilon_1{}^2+\varepsilon_1\varepsilon_2+\varepsilon_2{}^2)^{1/2}=\frac{\sqrt{6}}{3}[\ \Delta\varepsilon_x{}^2\ \sin^2\omega t+\Delta\gamma^2{}_{xy}\ \sin^2(\omega t+\phi)]^{1/2},$$

where $\varepsilon_{1,2}$: principal strains, $\Delta\varepsilon_x$: axial strain range, and $\Delta\gamma_{xy}$: shear strain range. When there is the phase difference between the axial and torsional strains, the extreme value was obtained by differentiating γ_{oct} wrt. time. For the cases (1)~(5), only $\Delta\varepsilon_x$, $\Delta\gamma_{xy}$, or $\Delta\gamma_{oct}$~N relationships were compared with the results in the previous studies, while for the other cases the dissipated energy was calculated by measuring the areas of both the axial and torsional hysteresis loops by a planimeter and then it has been shown that the relationship between the energy and the number of cycles to fracture is not affected by the strain ratio and the phase difference.

The experimental results fell along straight lines on a log-log paper expressed by $\Delta\varepsilon_x N^{\alpha_t}=C_t$ for the uniaxial case, $\Delta\gamma_{xy}N^{\alpha_s}=C_s$ for the torsional case, and $\Delta\gamma_{oct}N^{\alpha_{oct}}=C_{oct}$ for the combined case. However, the slope was more gentle than in the previous studies. This may be caused by the mode of fracture and the method of measurements, that is, the average strain instead of local strains was measured. The effect of the strain ratio was found to be negligible, while discrepancy due to the phase difference was observed. However, if the energy vs. the number of cycles to fracture was plotted, the effect of the phase difference has become smaller.

Application of the low cycle fatigue theory to the earthquake resistant design of structures was also considered.

§6.2 Conclusions

The following conclusions have been obtained in this study:

(1) The testing machine worked satisfactorily for this kind of experiment.

(2) The experimental results showed the linear relationship $\Delta\delta N^{0.24}=0.10$, for the uniaxial case, $\Delta\gamma_{xy}N^{0.34}=0.32$ for the torsional case, and $\Delta\gamma_{oct}N^{0.23}=0.13$ for the combined synchronous case on the log-log paper. However, the slopes of these lines were found to be more gentle than that by Coffin. The discrepancy may be because rather averaged strain was measured in this study.

(3) In the range of the number of cycles to fracture of more than one hundred, $\Delta\gamma_{oct}\sim N$ relationship was found to coincide for all the test except the nonsynchronous test. In the cycle range lower than one hundred, the mode of fracture was different from that for the higher cycle range and it is so complicated that the above mentioned discrepancy may have appeared. For the lower cycle range, the data of the torsion test drop a little above those for other tests.

(4) The results of torsion test coincided with those of the bending test of oval plates and of the anticlastic bending test of rhombic plates.

(5) For the nonsynchronous test, it is suggested that other kind of parameter such as hysteresis energy per cycle should be used, because if one takes the maximum octahedral shear strain range $\Delta\gamma_{oct}$ calculated by Eq. (4.31) along the ordinates, the $\Delta\gamma_{oct}\sim N$ line for $\phi=45°$ lies below that for the synchronous case and further the line for $\phi=90°$ lies below that for $\phi=45°$, though the slopes are almost the same.

(6) In the cyclic tension-compression test, the fracture line was observed in the circular direction of the specimen. In the cyclic

torsion test, crack initiated at the crossing point of two hills caused by the compressive principal stress for large strain and the fracture line appeared in the direction of axis in all torsional tests. In the combined synchronous test, for the smaller value of the strain ratio $A=\frac{\Delta\gamma_{xy}}{\Delta\varepsilon_x}$, the fracture line was almost the same as in the tension-compression test, while for the larger value of the strain ratio, the main crack was similar to the torsional case and the subsequent crack appeared oblique. Two crossing hills by compressive strains were also observed in the combined test. In the nonsynchronous case, crack initiated perpendicular to the axis of the specimen and then crack propagaged in zig-zag way. In some specimens, cracks were observed everywhere on the gage length.

(7) For the random fatigue caused by earthquakes, it may be possible to calculate the probability density $f(\varepsilon_{eq})$ and then to determine the total number of cycles N_t by Eq. (5.8) or Eq. (5.9).

§6.3 Suggestions for Further Studies

The following studies are suggested in the future.

From the material mechanics' point of view, discrepancies of the linear relationship between the octahedral shear strain and the number of cycles to fracture for different strain states should be investigaged, especially for the cyclic range lower than one hundred.

For the nonsynchronous case, other theories, such as the effective mean strain range recently developed by Taira et al., and the modified octahedral shear theory by Miller should be applied to the results in this study.

Confirmation of the conclusions in this thesis should be made by using other kind of materials. Especially for the structural engineer, behavior of structural steel may be more important than of aluminum alloy.

Although the simple sine wave was used for the input signal in this study, behavior of materials under more complicated load appearing in random vibrations should be studied both theoretically and experimentally in an other chance. For this purpose, some fundamental items, such as the effects of strain rate and of mean strain, may have to be clearified.

From the structural point of view, the study on low cycle fatigue seems to be still at the starting point. In recent big earthquakes, damages by low cycle fatigue were observed. First of all, the previous studies should be reviewed in detail and then the future studies should be planned carefully. On the other hand, the testing machine which can be used in the experiment of structural scale should be constructed. The buckling or instability problem under dynamic load should also be studied.

BIBLIOGRAPHY

1 Liu, S.I., J.J.Lynch, E.J.Ripling, and G.Sachs: "Low-Cycle Fatigue of the Aluminum Alloy 24S-T in Direct Stress", Metals Technol., Feb. 1948.

2 Manson,S.S: "Behavior of Materials under Conditions of Thermal Stress", NACA TN. 2933, 1953.

3 Coffin,L.F.Jr.: "Design for Low-Cycle Fatigue", SESA Design Clinics, Oct. 1959.

4 Benham,P.P.: "Fatigue of Metals Caused by a Relatively Few Cycles of High Load or Strain Amplitudes", Metallurgical Reviews, Vol.3, No.11, 1958.

5 Yao, J.T.P. and W.H.Munse: "Low-Cycle Fatigue of Metals, Literature Review", Welding Journal, Vol.41, 1962.

6 Coffin,L.F.Jr.: "Low Cycle Fatigue, A Review", Appilied Material Research, Vol.1, No.3, 1962.

7 Kawamoto,M. and K.Koibuchi: "On the Fatigue Phenomena in the Plastic Range", Journal of the Society of Material Science, Japan, Vol.12, No.194, 1963, and Vol.12, No.413, 1963.

8 Manson,S.S.: "Fatigue; A Complex Subject-Some Simple Approximations", Experimental Mechanics, Vol.5, No.7, 193, 1965.

9 Marin,J. and K.Ohji: "A Review of Research on Low Cycle Fatigue" The Pensylvania State University, Aug. 1965.

10 Ohji, K.: "Low Cycle Fatigue Under Multiaxial Stress Conditions", Journal of the Society of Material Science, Japan, Vol.12, No.194, 1968.

11 Gross,J.H. and R.D.Stout: "Plastic Fatigue Properties of High-Strength Pressure-Vessel Steels", Welding Journal, Vol.34, 1955. Research Suppl., pp. 161S-166S.

12 Low,A.C.: "The Bending Fatigue-Strength of Alminum Alloy MG 5 between 10 and 10 Million Cycles", J.Roy, Aeron. Soc., Vol.59, 1055, pp. 502 - 206.

13 Gucer,D.E.: "Cumulative Fatigue at High Plastic Strains", Trans, A.S.M., Vol.54, 1961, pp. 176 - 184.

14 Kikukawa,M. and K.Ohji, A.Sumiyoshi, and M.Asai: "On the Plastic Fatigue under Varying Strain Amplitude (I)", 21 st Annual Meeting of the Japan Soc. of Mech. Engineers, Ap.1964, Abstract of Papers, No.105, pp..167 - 170. (in Japanease)

15 Ohji,K., W.R.Miller, and J.Marin: "Cumulative Damage and Effect of Mean Strain in Low Cycle Fatigue of a 2024-T351 Aluminum Alloy", ASME Paper No.65-WA/Met-5.

16 Baldwin,E.E., G.Sokal, and L.F.Coffin, Jr.: "Cyclic Strain Fatigue Studies on AISI Type 347 Stainless Steel", Proc. ASTM, Vol.57, 1958, pp. 567 - 586.

17 Takenaka,Y.: "Fatigue of Metals under Repeated Finite Strain", Belletin of the Japan Soc. of Mechanical Eng., Vol.3, No.12, 1960, pp. 419 - 424.

18 D'Amato,R.: "A Study of the Strain Hardening and Cumulative Damage Behavior of 2024-T4 Aluminum Alloy in the Low-Cycle Fatigue Range", WADD.TR.60-175, April, 1960, Wright Air Development Division, Wright-Patterson Air Force Base, Ohio.

19 Wood,W.A., S.Mck. Consland, and K.R.Sargant: "Systematic Microstructural changes Peculier to Fatigue Deformation", Aeta Metallurgica, 11, 1963, pp. 643 - 652.

20 Forsyth,P.T.E.: "Fatigue Damage and Crack Growth in Aluminum Alloys", Acta Metallugica 11, 1963, p. 703.

21 Laird C. and G.C.Smith: "Crack Propagation in High Stress Fatigue", Philosophial Magazine 7, 1962, p. 847.

22 Larid C. and G.C.Smith: "Initial Stages of Damage in High Stress Fatigue in Some Pure Materials:, Philosophial Magazine, 8, 1963, 1945.

23 Avery,D.H., W.A.Backhofen: "Fatigue Hardening in Alloys of Low Stacking Fault Energy", Acta Metallurgica, 11, 1963, p. 653.

24 Grosskreutz, J.C.: "Fatigue-An Interdisciplinary Approach", Syracuse University Press, 1964, p.27.

25 Sinclair,G.M. and T.J.Dolan: Proc. of the First U.S. National Congress of Applied Mechanics, 1951, p. 647.

26 T.Yokobori: ASTM Bulletin, No.234, Dec. 1958, p.66, TP 278 - 279.

27 Thompson,N., N.Wadsworth, and N.Louat: "Origin of Fatigue Fracture in Copper", Philosophical Magazine, 1, 1956, p. 113.

28 Martin,D.E.: "Plastic Strain Fatigue in Air and Vacuum", Trans. ASME, Ser.D. 87 - 4, Dec. 1965, p.850.

29 Raymond,M.H. and L.F.Coffin,: "Geometrical Effects in Strain Cycled Alúminum", Trans, ASME, Ser. D. 85 - 4, Dec. 1963, p.548.

30 Miner,M.A.: "Cumulative Damage in Fatigue", Trans. ASME, 67, 1945, J.Appl. Mech. A.159.

31 Martin,D.E.: "An Energy Critecion for Low-Cycle Fatigue". Trans. ASME, Ser. D. 83 - 4, Dec. 1961, p.565.

32 Yao,J.T.P. and W.H.Munse: "Low-Cycle Axial Fatigue Behavior of Mild Steel", ASTM, STP. 338, 1963, p. 5.

33 Halford, G.R. and J.Morrow: "Low Cycle Fatigue in Torsion", Proc. ASTM, 62, 1963, p. 695.

34 Weiss,V.: "Fatigue-An Interdisciplinary Approach", Syracuse Univ., 1964, p.179.

35 Ohji,K.: "Discussion on the Cumulative Damage Hypothesis in Low Cycle Fatigue", Journal of JSME,, Vol.70, No.576, 1967 .

36 Pian T.H.H. and R.D'Amato: "Low Cycle Fatigue of Notched and Unnotched Specimens of 2024 Aluminum Alloy under Axial Loading", WADC. Technical Note 58 - 27, Feb. 1958, p.77, Wright Air Development Ceter, Ohio.

37 D'Amato,R. and R.de Boer,: "A Study of the Relationship between Notched and Unnotched Specimens of 2024 Aluminum Alloy in the Low Cycle Region", WADC. Technical Note 59 - 2, May 1959, p.69, Wright Air Development Center, Ohio.

38 Sachs,G., W.W.Gerberich, V.Weiss, and J.V.Latorre: "Low Cycle Fatigue of Pressure Vessel Materials", Proc. of ASTM, Vol.60, 1961, pp.512 - 529.

39 Sachs,G. and V.Weiss: "Beitrage zu Kurzzeitermüdung", Zeitschrift für Metallkunde, Vol.53, 1962, pp.37 - 47.

40 Sessler,J.G. and V.Weiss: "Low Cycle Fatigue Damage in Pressure Vessel Materials", Trans. ASME, Vol.85, 1963, Ser.D, pp.539 - 549.

41 Weiss,V., J.Sessler, and P.Packman,: "Effect of Several Parameters on Low Cycle Fatigue Behavior", Acta Metallurgica, Vol.11, No.7, 1963, pp.806 816.

42 Manson,S.S.: "Thermal Stresses in Design", Part 21-Effect of Mean Stress and Strain on Cycle Life. Machine Design, Vol.32, No.16, Aug.4. 1960, pp.129 - 135; Part 22-Cumulative Fatigue Damage, ibid., Vol.32, No.17, Aug.18. 1960, pp.160 - 166.

43 Shiratori,E. and Y.Obataya: "The Influence of Mean-Stress on the Low Cycle Fatigue Strength of Brass", Bulletin of the Tokyo Inst. of Tech., No.75, Sep. 1966.

44 Jahanson,A.: "Fatigue of Steel at Constant Static Amplitude and Elevated Temperature", Proc. of Colloquim on Fatigue, IUTAM, Stockholm, May 25- 27, 1955, Springer-Verlag, 1956, pp.112 - 122.

45 Swindeman,R.W. and D.A.Douglas: "The Failure of Structure Metals Subjected to Strain-Cycling Conditions," Trans. ASME. Vol.81,

1959, Sries D, pp.203 - 212.

46 Forrest,P.G. and K.B.Armstrong: "The Thermal Fatigue Resistance of Nickel Chromium Alloys", Proc. of Joint International Conference on Creep, New York, Aug.25 - 29, 1963, and London Sep.30 to Oct.4, 1963, Jointly sponsored by ASME, ASTM, and IME., The Institution of Mech. Eng. 1963, pp.3 - 1 to 3 - 7 (Paper 1).

47 Tavernelli,J.F. and L.F.Coffin, Jr.: "The Cyclic Strain Aging and Fatigue of a Low Carbon Steel", Proc. of Joint Int. Conference on Creep, New York, Aug.25 - 29, 1963, and London, Sep.30 to Oct.4, 1963, Jointly sponsored by ASME, ASTM, and IME. pp.3 - 63 to 3 - 70 (Paper 27).

48 Forrest,P.G. and H.J.Tapsell: "Some Experiments on the Alternating Stress Fatigue of a Mild Steel and on Aluminum Alloy at Elevated Temperatures with Special References to the Effect of Cyclic Speed", Proc. of Institution of Mech. Eng., Vol.168, 1964, pp.763 - 774.

49 Nishihara,T., S.Taira, K.Tanaka, and R.Koterazawa: "Fatigue of Low Carbon Steel at Elevated Temperature (Influence of Frequency of Stress Cycles on Fatigue at Elevated Temperature)", Proc. of the First Japan Congress on Testing Materials, Tokyo, Oct.28 - 29, 1957, Japan Society for Testing Materials, Kyoto, Japan, 1958.

50 Taira,S. and R.Koterazawa: "Influence of Frequency of Stress Cycles on Fatigue at Elevated Temperature", Bulletin of the Japan Society of Mechanical Engineers, Vol.3, No.10, 1960, pp.235 - 241.

51 Taira,S.: "Thermal Fatigue and its Relation to Creep Rupture and Mechanical Fatigue, High Temparature Structures and Materials", Proc. of the Third Symposium on Naval Structural Mechanics, Columbia University, New York, N.Y.Jan.23 - 25, 1963, Pergamon

Press, 1964, A.M.Freudenthal, B.A.Boley, and H.Liebowitz, editors, pp.187 - 213.

52 Taira,S.: "Lifetime of Structures Subjected to Varying Load and Temperature, Creep in Structures", IUTAM Colloquium, Stanford University, Calif., July 11 - 15, 1960. Academic Press, Inc., 1962, N.J.Hoff, editor, pp.96 - 124.

53 Smith,F.C., W.C.Brueggeman, and R.H.Harwell: "Comparison of Fatigue Strength of Bare and Alclad 24S-T3. Aluminum-Alloy Sheet Specimens. Tested at 12 and 1000 cycles per Minute", Notional Advisory Committee for Aeronautics, Tech. Note 2231, Dec. 1950, p.18.

54 Gohn,G.R. and W.C.Ellis: "Fatigue Test as Applied to Lead Cable Sheath", Proc. ASTM, Vol.51, 1952, pp.721 - 744.

55 Ekel,J.F.: "The Influence of Frequency on the Repeated Bending Life of Acid Lead", Proc. ASTM, Vol.51, 1952, pp.745 - 760.

56 Crum,R.G. and E.D'Appolonia: "Behavior of Ti-75A Titanium alloy under Repeated Load", Proc. ASTM, Vol.55, 1955, pp. 969 - 980.

57 Illg,W.: "Fatigue Tests on Notched and Unnotched Sheet Specimens of 2024-T3 and 7075-T6 Aluminum Alloys and of SAE4130 Steel with Special Consideration of the Life Range from 2 to 10000 Cycles, National Advisory Committee for Aeronautics, Tech Note 3866, Dec. 1956, p.40.

58 Swindeman,R.W.: "The Interrelation of Cyclic and Monotonic Creep Rupture", Proc. of Joint International Conference on Creep, New York, Aug. 25 - 29, 1963, and London, Sept 30 to Oct. 4 1963, Jointly sponsored by ASME, ASTM, and IME, pp.3 - 31 to 3 - 76 (Paper 32).

59 Benham,P.P. and H.Ford: "Low Endurance Fatigue of a Mild Steel and an Aluminum Alloy", Journal of Mechanical Engineering Science

(IME), Vol.3, No.2, 1961, pp.119 - 132.

60 Benham,P.P.: "Axial Load and Strain Cycling Fatigue of Copper at Low Endurance", Journal of the Institute of Metals, Vol.89, 196) - 61, pp.328 - 338.

61 Kawamoto,M. and T.Tanaka: "Completely Reversed Axial Fatigue Tests of Steel in the Plastic Range", Proc. of the Fifth Japan Congress on Testing Materials, Tokyo Univ., Tokyo, Japan, Sept. 7 - 8, 1961, (The Japan Society for Testing Materials, 1962) pp.36 - 40.

62 Kawamoto,M., K.Koibuchi, and Y.Yamaji: "Axial Fatigue Tests on Ni-Cr-Mo Steel in the Plastic Range", Proceedings of the Sixth Japan Congress on Testing Materials, Kyoto University, Kyoto Japan, Oct. 11 - 12, 1962 (The Japan Society for Testing Materials 1963) pp.18 - 21.

63 Kawamoto,M., K.Koibuchi, and Y.Yamaji: "Torsional Fatigue Test of Ni-Cr-Mo Steel at Room Temperature and High Temperature (350°C)", Transactions of the Japan Society of Mechanical Engineers, Vol.29, No.206, 1963, pp.1647 - 1652 (in Japanese with English Abstract).

64 Peterson,R.E.: "Fatigue of Metals in Engineering and Design", ASTM, 1962, Edgar Marburg Lecture, p.38; also see Materials Research and Standards, Vol.3, No.2, Feb.1963, pp.122 - 139.

65 Manson,S.S. and M.H.Hirschberg: "Crack Initiation and Propagation in Notched Fatigue Specimen", Technical Pre-Print prepared for International Conference on Fracture Sponsored by Tohoku Univ., Sendai, Japan, September 12 - 17, 1965.

66 Gross,J.H., S.Tsang, and R.D.Stout: "Factors Affecting Resistance of Pressure Vessel Steels to Repeated Overloading", Welding Journal, Vol.32, 1953, Research, Suppl. pp.23S - 30S.

67 Tor,S.S., M.Ruzek and R.D.Stout: "Repeated Load Tests on Welded and Prestrained Steels", Welding Journal, Vol.13, No.5, 1952, Research Suppl., pp.238S - 246S.

68 Gross,J.H. D.E.Gucer, and R.D.Stout: "The Plastic Fatigue Strength of Pressure Vessel Steels", Welding Journal, Vol.33, No.1. 1954, Research Suppl. pp.31S - 39S.

69 Blaser,R.V., J.T.Tucker, Jr., and L.F.Kooistra: "Biaxial Fatigue Tests on Flat Plate Specimens", Welding Journal, Vol.13, No.3, 1952, Research Suppl., pp.161S - 168S.

70 Bowman,C.E. and T.J.Dolan: "Biaxial Fatigue Properties of Pressure Vessel Steels", Welding Journal, Vol.32, No.11, 1953, Research Suppl., pp.529S - 537S.

71 Bowman,C.E. and T.J.Dolan: "Further Studies on the Biaxial Propertie of Pressure Vessel Steels", Welding Journal, Vol.34, No.1, 1955, Research Suppl., pp.51S - 59S.

72 Bowman,C.E. and T.J.Dolan: "Resistance of Low-Alloy Steel Plates to Biaxial Fatigue", Welding Journal, Vol.35, No.2, 1956, Research Suppl., pp.102S - 109S.

73 Kooistra,L.F.: "Effect of Plastic Fatigue on Pressure-Vessel Materials and Design", Welding Journal, Vol.36, No.3, 1957, Research Suppl., pp.120S - 130S.

74 Narduzzi,E.D. and G.Welter: "High-Pressure Vessels Subjected to Static and Dynamic Loads", Welding Journal, Vol.33, No.5, 1954, Research Suppl., pp.230S - 238S.

75 Dubuc,J. and G.Welter: "Investigation of Static and Fatigue Resistance of Model Pressure Vessels", Welding Journal, Vol.35, No.7, 1956, Research Suppl., pp.329S - 337S.

76 Kooistra,L.F. and M.M.Lemcoe: "Low Cycle Fatigue Research on Full Size Pressure Vessels", Welding Journal, Vol.41, No.7,

1962, Research Suppl., pp.297S - 306S.

77 Kooistra,L.F., E.A.Langer, and A.G.Pickelt: "Full-size Pressure Vessel Testing and its Application to Design", Trans. ASME, Vol.86, 1964, Series A. No.4, pp.419 - 428.

78 Benham,P.P.: "Torsional Strain Cycling Fatigue of Copper at Low Endurance", Journal of the Institute of Metals, 91, 404, 1962 - 63.

79 Kusumoto,S. and M.Takeuchi: "Comparison of Constant Strain Fatigue Tests by Torsion and by Tension-Compression", Journal of the Society of Material Science, Japan, Vol.13, No.131, Aug. 1964, p.613.

80 Kusumoto,S. and M.Takeuchi: Paper Presented to the Fifteenth Congress of the Society of Material Science, Japan, 1966, p.35.

81 Yokobori,T., H.Yamanouchi and S.Yamamoto: International Journal of Fracture Mechanics, No.1. 3, 1965.

82 Kikukawa,M., K.Ohji, S.Kotani, and T.Yokoi: Paper for the 42 nd Meeting of the Kansai Branch of the Japan Sec. of Mech. Engrs., 1967, No.2, p.49.

83 Taira,S., T.Inoue, and M.Takahashi: "Low Cycle Fatigue under Multiaxial Stress (In the Case of In-Phase Cyclic Tension-Compression and Cyclic Torsion at Elevated Temperature)", Trans. of the Japan Soc. of Mech. Engrs., Vol.32, 1966, p.1788.

84 Nakazawa,H. and H.Kiso: "On the Plastic Fatigue under Biaxial Stresses (Application for Closed-End Thin Walled Cylinder)", Trans. of the Jap. Soc. of Mech. Engrs., Vol.32, No.235, 1966, p.411.

85 Ives,K.D., L.F.Kooistra, and J.T.Tucker: "Equibiaxial Low Cycle Fatigue Properties of Typical Pressure Vessel Steels", Trans. ASME, Ser. D., 88, 745, 1966.

86 Shewchuk,J.: Ph D. Thesis, Dept. of Eng. Mech., The Penn State Univ., Aug., 1966.

87 Goto,T.: M.S.Thesis, Dept. of Eng. Mech., The Penn State Univ., Aug., 1966.

88 Kyriakakis,T.: "Low-Cycle Strain Behavior for Combined Stresses", M.S.Thesis, Dept. of Eng. Mech., The Penn State Univ., 1962.

89 Mullin,J.V.: "A Study of Biaxial Strain Cycling for Both Synchronous and Nonsynchronous Conditions", Ph. D. Thesis, Dept. of Eng. Mech., The Penn State Univ., June, 1964.

90 McClaren, S.W. and E.L.Terry: "Characteristics of Aerospace Materials Subjected to Biaxial Static and Fatigue Loading Conditions", ASME, Paper No.63-WA-315, 1963.

91 Welter,G. and J.A.Choquet: "Triaxial Tensile Stress Fatigue Testing", Welding Journal, 42, 565S, 1963.

92 Manson,S.S. and ,.H.Hirschberg: "Fatigue Behaivior in Strain Cycling in the Low and Intermediate Cycle Range", A paper presented at the 10th Sagamore Army Materials Research Conference, Aug. 13 - 16, 1963, Sagamore, N.Y.

93 Miller,W.R.: "Studies on Combined Stress and Strain Theories in Fatigue", Ph. D. Thesis, Dept. of Eng. Mechs., The Penn State Univ. March, 1965.

94 Pontzer,T.: "A Study on Low-Cycle Multiaxial Strain Cycling", M.S.Thesis, Dept. of Eng. Mech., The Penn State Univ., June, 1965.

95 Taira,S., R.Koterazawa, and M.Ohnami: "Relation between Thermal Fatigue and Cyclic Strain Fatigue at Elevated Temperature", Japan Soc. for Testing Materials, Vol.9, No.85, 1960, p.636.

96 Taira,S., M.Ohnami and T.Inoue: "Thermal Fatigue under Multiaxial Thermal Stresses", Proc. of the 8th Japan Congress on Testing Materials, 1965, p.40.

97 Taira,S., M.Ohnami, T.Inoue and F.Iori: "Thermal Fatigue under Multiaxial Thermal Stresses", Journal of the Soc. of Material Science, Japan, Vol.14, 1965, p.898.

98 Langer,B.F.: "Design of Pressure Vessels for Low-Cycle Fatigue", Trans. ASME, Series D., 84, 1962, 389.

99 Hagihara,S.: "Low Cycle Fatigue Tests of Rotating Disks", Trans. of the Japan Soc. of Mech. Engrs., Vol.31, No.222, 1965, p.173.

100 Hamada,M., S.Takezono, and T.Arita: "Strength of U-Shaped Bellows (5th Report, Fatigue Strength under Axial Loading)", Transactions of the Jap. Soc. of Mech. Engrs., Vol.32, No.243, 1966.

101 Hamada,M., S.Takezono, K.Okamoto, Y.Hiraishi, K.Matsumoto and N.Kashima: "Strength of U-Shaped Bellows (1st Report, The Case of Axial Loading), (2nd Report, The Case of Axial Loading-Continued), (3rd Report, The Case of Loading of Internal Pressure), Trans. of the Japan Soc. of Mech. Engrs.) Vol.31, No.231, 1965.

102 Hamada,M. and S.Takezono: "Strength of U-Shaped Bellows (4th Report, Limit Analysis under Axial Loading)", Trans. of the Japan Soc. of Mech. Engrs., Vol.32, No.236, 1966, p.569.

103 Richards,C.W.: "Engineering Materials Sirence", Wadsworth Publishing Company, Inc., 1961.

104 ASTM Standards, A 260

105 Moorse,A.C.: "Electrohydraulic Servomechanisms", McCraw-Hill Book Co., 1963.

106 Beckwith,T.G., N.L.Buck: "Mechanical Measurements", Addison-Wesley Publishing Company, Inc., 1961.

107 Marin,J.: "Mechanical Behavior of Engineering Metarials", Prentice-Hall, Inc., 1962.

108 Jo Dean Morrow: "Cyclic Plastic Strain Energy and Fatigue of Metals", ASTM, STP. 378, 1965.

109 Fujimoto,M., H.Hagura, and Y.Matsumoto: "Elasto-Plastic Analysis of Steel Frame Subjected to Alternative Loads, Using Strain

Hardening Models (I) & (II)", Trans. of the Arch. Inst. of Japan, Oct., 1967.

110 Igarashi,S.: "Plastic Behavior of the Steel Structure under Repeated Force", Thesis for 1968 Anual Awards of the Architectural Institute of Japan.

111 Crandall,S.H.: "Random Vibrations", Vol.1 and 2, John Willy and Sons, Inc., 1958 and 1963.

112 Committee on Fatigue, The Society of Material Science, Japan: Papers for Symposium on Fatigue Subjected to Actual Load, held in Osaka, Sep.22, 1967.

113 Schijve,J.: "Random Load-time Histories with Relation to Fatigue Tests", Fatigue of Aircraft Structures, W.Barrois and E.L.Ripley, editor, Pergamon Press, 1963.

114 Kato,T. and H.Aoki: "Effects of Strain Velocity on Mechanical Property of Steel", Trans. of the Arch. Inst. of Japan, Oct., 1967.

115 Taira,S., T.Inoue, and T.Yoshida: "Low Cycle Fatigue under Multiaxial Stresses (In the Case of Combined Cyclic Tension-Compression and Cyclic Torsion Out-of-Phase at Elevated Temperature)", Trans. of the Japan Soc. of Mech. Engrs., Vol.34, No.258, Feb., 1968, p.255.